Single Polymers at surfaces : Adsorption and Detachment

Dissertation
zur Erlangung des Grades

" Doktor der Naturwissenschaften"

am Fachbereich Physik
der Johannes Gutenberg-Universität
in Mainz

Swati Bhattacharya
geboren in Calcutta (Indien)
Mainz, Juli 2009

Datum der mündlichen Prüfung : 14. Juli 2009

To my family

Zusammenfassung

In dieser Arbeit befassen wir uns mit der Adsorption und dem Ablöseverhalten von Polymeren auf planaren, festen Oberflächen. Dazu wurden sowohl systematische analytische Untersuchungen, als auch detaillierte Monte-Carlo Simulationen durchgeführt. Für die Darstellung der Polymere verwendeten wir Kugel-Feder-Modelle. Zunächst wurde die Adsorption von einzelnen AB Multiblock-Copolymere auf festen Oberflächen mittels Skalenanalysen und Simulationen untersucht. Dabei konnte schlüssig gezeigt werden, dass dieses Problem auf die Adsorption entsprechendes Homopolymere abgebildet werden konnte. Somit konnte das Phasendiagramm berechnet und durch Simulationen bestätigt werden. Eine wichtige und neue Vorhersage war dabei das gegenläufige Verhalten von Blocklänge und kritischem Absorptionspotenzial. In diesem Zusammenhang wurden auch die Adsorption von Zufallscopolymeren untersucht. Deren Verhalten lässt sich mittels einer „annealed disorder approximation "verstehen. Auch dies konnte mit MC Simulationen gezeigt werden. Im nächsten Schritt wurde die Adsorptionskinetik detailliert betrachtet. Auf den Fall der „starken Adsorption "(Physiosorption) wurde dabei besonderes Augenmerk gelegt. Das physikalisch intuitive und durch Skalenargumente unterstrichene Strukturbild der sogenannten „stem-flower "(ein Teil der Polymerkette ist gestreckt, der restliche nicht) konnte sowohl mit der Herleitung und Lösung einer Fokker-Planck-Gleichung mit reflektierenden Randbedingungen, als auch mit de parallel dazu durchgeführten MC Simulationen bestätigt werden. Im Detail wurden dazu die zugehörigen Verteilungsfunktionen berechnet und durch Simulationen verglichen. Im dritten Teil der Arbeit wurde die Desorption der Polymere unter einer extern angelegten Kraft untersucht. Diese physikalischen Modelle sind vor allem für Experimente von gewisser Relevanz. Dabei zeigte sich, dass im Detail zwei verschiedene Ensembles wesentlich sind: kontante Kraft und fluktuierenden Höhe, sowie konstante Höhe fluktuierende Kraft, die sich mittels grokanonischen Theorien behandeln lassen. Dabei ist das Phasendiagramm eines adsorbierten Polymers unter einer konstanten Kraft auf einen neuartigen, dichotome Phasenübergang geführt worden, also einen Phasenübergang ohne Koexistenz. Im andern Fall, konstanter Abstand wurde das Phasendiagramm $h - \epsilon$ explizit berechnet und durch Simulationen bestätigt. Dabei konnte auch explizit gezeigt werden, dass sich in der Nähe des Desorptions übergangs die Fluktuationen in beiden Ensembles vollkommen verschieden verhalten.

Abstract

This thesis is concerned with the adsorption and detachment of polymers at planar, rigid surfaces. We have carried out a systematic investigation of adsorption of polymers using analytical techniques as well as Monte Carlo simulations with a coarse grained off-lattice bead spring model. The investigation was carried out in three stages. In the first stage the adsorption of a single multiblock AB copolymer on a solid surface was investigated by means of simulations and scaling analysis. It was shown that the problem could be mapped onto an effective homopolymer problem. Our main result was the phase diagram of regular multiblock copolymers which shows an increase in the critical adsorption potential of the substrate with decreasing size of blocks. We also considered the adsorption of random copolymers which was found to be well described within the annealed disorder approximation. In the next phase, we studied the adsorption kinetics of a single polymer on a flat, structureless surface in the regime of strong physisorption. The idea of a "stem-flower" polymer conformation and the mechanism of "zipping" during the adsorption process were used to derive a Fokker-Planck equation with reflecting boundary conditions for the time dependent probability distribution function (PDF) of the number of adsorbed monomers. The numerical solution of the time-dependent PDF obtained from a discrete set of coupled differential equations were shown to be in perfect agreement with Monte Carlo simulation results. Finally we studied force induced desorption of a polymer chain adsorbed on an attractive surface. We approached the problem within the framework of two different statistical ensembles; (i) by keeping the pulling force fixed while measuring the position of the polymer chain end, and (ii) by measuring the force necessary to keep the chain end at fixed distance above the adsorbing plane. In the first case we treated the problem within the framework of the Grand Canonical Ensemble approach and derived analytic expressions for the various conformational building blocks, characterizing the structure of an adsorbed linear polymer chain, subject to pulling force of fixed strength. The main result was the phase diagram of a polymer chain under pulling. We demonstrated a novel first order phase transformation which is dichotomic i.e. phase coexistence is not possible. In the second case, we carried out our study in the *fixed height* statistical ensemble where one measures the fluctuating force, exerted by the chain on the last monomer when a chain end is kept fixed at height h over the solid plane at different adsorption strengths. The phase diagram in the $h - \epsilon$ plane was calculated both analytically and by Monte Carlo simulations. We demonstrated that in the vicinity of the polymer desorption transition a number of proprties like fluctuations and probability distribution of various quantities behave differently, if h rather than f is used as an independent control parameter.

Contents

List of Figures

List of Tables

Chapter 1

Introduction

Polymer science has had a major impact on the way we live. People have used naturally occurring polymers such as shellac and amber for centuries without realizing their "polymeric" nature. Macromolecules such as nucleic acids and proteins play a crucial role in many biological processes [3]. Synthetic polymers are now ubiquitous in every sphere of modern life and are the basis of a burgeoning industry. Applications extend from adhesives, coatings, foams, and packaging materials to textile and industrial fibers, composites, electronic devices, biomedical devices, optical devices, and precursors for many newly developed high-tech ceramics.

In the middle of the nineteenth century, chemists started synthesizing polymeric substances but a proper understanding of the molecular structure was lacking until the work of Staudinger in the 1920s. Staudinger was the first to propose that polymers consisted of long chains of atoms held together by covalent bonds. There was an explosion of research in material sciences in the latter half of 20th century and polymer science was no exception. Kuhn, Flory, Huggins, Stockmayer and others developed the theories describing macromolecular sizes, self-avoidance and excluded volume effects, thermodynamics of mixing, polymer solutions etc. Rouse and Zimm developed the theories of the dynamics of single molecules. Subsequently Edwards, de Gennes, des Cloizeaux and others developed the modern principles of polymer physics. Today, polymer physics is a vast body of knowledge with challenging open problems both at the theoretical and the experimental ends.

A polymer is a giant molecule (macromolecule) made up of covalently bonded elementary units called monomers. The number of monomers in a molecule is called the degree of polymerization N. Macromolecules with only one type of repeating units are called homopolymers.

Polymers that contain different types of monomers are called heteropolymers. The properties of a heteropolymer is affected by the composition as well as the sequence of the monomers. Depending on the sequence, copolymers are classified as alternating,

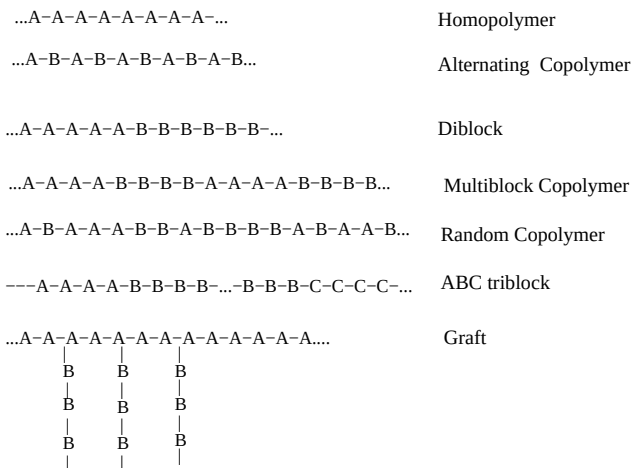

Figure 1.1: Different types of copolymers

random, block or graft. An important feature influencing the properties of a polymer is the architecture. Apart from single linear chains, polymers may have complex forms such as ring, star-branched, comb, ladder, dendrimer or randomly branched.

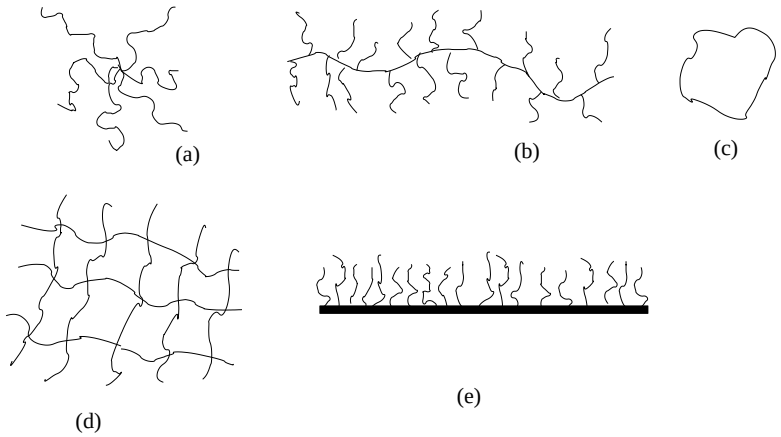

Figure 1.2: Different polymer topologies: (a) star polymer, (b) comb polymer, (c) ring polymer, (d) polymer network, (e) polymer brush

Another important property of a polymer is its configuration or spatial structure. The conformation of a polymer depends on its flexibility, the interaction of the monomers on the chain and the interaction of the monomers with the surroundings. Polymer systems can exist in many different macroscopic states. For instance, polymer liquids may exist as polymer melts or polymer solutions. If a polymer melt is cooled, it

can transform into a semicrystalline solid below its melting temperature or into a polymeric glass below its glass transition temperature. Polymer solutions may be classified as dilute or semidilute depending on the volume fractions of the polymer and solvent. The properties of a polymer depend strongly on the nature of the solvent. A solvent is referred to as 'good' if a polymer dissolves easily in it. The chain swells to maximize the number of polymer-fluid contacts. This gives rise to effective repulsive interactions between monomers and the chain assumes an expanded form. On the other hand, in a 'poor' solvent, the effective interaction between the beads is attractive and the polymer collapses to form a globule of high density. In between these two solvent conditions is the Θ regime which corresponds to a cancellation between the steric repulsion and the van der Waals attraction between the monomers. In a Θ solvent, a polymer behaves as an ideal chain. The quality of solvent depends also on temperature. For a flexible polymer, low temperature may correspond to poor quality and high temperature makes the same solvent good.

The adsorption of polymers on surfaces plays an important role in many industrial applications such as the stabilization of colloids, adhesion and chromatography [63, 75, 33]. Scientifically, the interplay of entropic and enthalpic effects lead to a rich variety of interesting static and dynamic phenomena. In addition to experimental techniques, theoretical models and computer simulations provide valuable insight into the subject [33, 14, 28]. The adsorption of polymers at an impenetrable surface has been an active field of research for over four decades. Consequently, the equilibrium properties of adsorption of homopolymers is now considered to be well understood. There are many open problems in this field. The adsorption of heteropolymers is one of the challenging issues. Recent advances in experimental techniques such as atomic force microscopy (AFM) and optical/magnetic tweezers which allow one to manipulate single polymer chains have triggered interest in the properties of single polymer chains at surfaces. The aim of this research is to explore some aspects of adsorption of polymers such as the adhesion of block copolymers and the force induced desorption of a polymer chain from a surface. The thesis is organized as follows:

- Chapter 2 gives an introduction to the theoretical concepts used to describe polymers. We begin with a description of an ideal polymer chain as a random walk. And then we describe real polymer chains and excluded volume effects. We discuss scaling aspects and the blob picture with regard to adsorption on rigid surfaces. We consider the force-extension relation of a real chain under tension and finally we briefly discuss the importance of computer simulations in the field of polymer physics.

- In Chapter 3 we present the simulation techniques that have been used in this study. We have carried out Monte Carlo simulations using a coarse grained ,off-

lattice, bead spring model. In this chapter, we give some general information about the model used. However, since the implementation of this method is different for each particular case we have studied, in each chapter we give a brief description of how the method has been adapted.

- Chapter 4 deals with the adsorption of regular multi-block and random copolymers at a rigid, flat surface. We are concerned with the case of a single polymer tethered at one end to a rigid substrate. Our system consists of copolymers composed of two kinds of monomers: type 'A' monomers which are attracted to the surface and experience an adsorption energy ϵ and type 'B' monomers which are neutral to the substrate. We have investigated the adsorption of regular multi-block copolymers by means of computer simulations and scaling analysis. In this chapter, we present a brief review of the scaling aspects of homopolymer adsorption before taking up the issue of block copolymers. We describe how the problem can be mapped onto an effective homopolymer adsorption problem. We are particularly interested in the critical adsorption point (CAP). We have discussed in detail, the methods used to locate the CAP and scaling behaviour of several quantities above, below and at the CAP. In particular we discuss how the critical adsorption energy and the fraction of adsorbed monomers depend on the block length M of sticking monomers A, and on the total length N of the polymer chains. The primary result of the study presented in this Chapter is the phase diagram of regular multiblock adsorption which gives the increase of the critical adsorption potential ϵ_c^M with decreasing length M of the adsorbing blocks. We also briefly discuss the adsorption of the random copolymers and show that the system is well described within the framework of the annealed approximation. Special interest has been paid to the determination of the so called *crossover exponent* ϕ which is known to govern the fraction of adsorbed monomers at the CAP. Our results show that the crossover exponent is unchanged for multi-block and random copolymers. Thus the universality class of the adsorption transition of a heteropolymer is the same as that of a homopolymer. In this chapter, we confine ourselves to the equilibrium aspects of adsorption phenomena.

- In Chapter 5, we turn our attention to the kinetics of adsorption. There are two broad classes of adsorption described in literature: chemisorption and physisorption. Chemisorption is characterized by a small monomer sticking rate, usually due to a large activation barrier and generally

  occurs due to covalent bonds between the monomers and the surface. We examine the adsorption kinetics of a single polymer chain on a flat surface in the strong physisorption regime. Based on the idea of a "stem-flower" polymer conform-

ation, and assuming that the segment attachment process follows a "zipping" mechanism, we develop a scaling theory which describes the time evolution of the fraction of adsorbed monomers for polymer chains of arbitrary length N at adsorption strength of the surface ϵ/k_BT. We derive a Master Equation as well as the corresponding Fokker-Planck equation for the time-dependent probability distribution function (PDF) of the number of adsorbed monomers and for the complementary PDF of tails with appropriate reflecting boundary conditions. We have used a kinetic Monte Carlo algorithm to study the system. The MC results are then compared to the theoretical predictions. Our focus is primarily on homopolymers although we briefly discuss the case of regular multiblock and random copolymers.

- In Chapter 6 we consider the force induced desorption of a polymer in contact with an attractive substrate. This study is motivated by single macromolecule experiments which involve the manipulation of individual polymer chains and biological macromolecules such as proteins and DNA. The system consists of a tethered homopolymer chain adsorbing at a flat surface with an external pulling force applied at its free end in the direction perpendicular to the surface. Once again, we have carried out extensive Monte Carlo simulations to probe the system. There is a close analogy between the forced detachment of an adsorbed polymer chain adhering to a solid surface , when the chain is pulled by the end monomer, and the unzipping of homogeneous double-stranded DNA. We use the analogy to treat the system within a Grand Canonical Ensemble (GCE) approach as previously done for the case of DNA unzipping. We derive theoretical expressions for the mean size of loops, trains, and tails of an adsorbed chain under pulling as well as values for the universal exponents which describe their probability distribution functions. We present the adsorption-desorption phase diagram of a polymer chain under pulling and demonstrate that the relevant phase transformation becomes first order. This is in contrast to the case of adsorptive transition in the absence of any external force where it is known to be a continuous one. In this chapter, we carry out our investigations in the "fixed force"- ensemble.

- In Chapter 7 we consider the detachment of a polymer chain at an attractive surface by an external force applied to a free end. However, in contrast to Chapter 6, our investigations are carried out in the "constant height ensemble". In many experiments using Atomic Force Microscopes (AFM), it is customary to anchor a polymer molecule at one end to a substrate while the other end is fixed to the cantilever. It is common to prescribe the height of the cantilever from the surface and to measure the corresponding force. In this chapter, we discuss the

adsorption-desorption of a single self-avoiding polymer chain keeping the distance h between the free end of the chain and the surface fixed as a control parameter. The phase diagram in the $\epsilon - h$ plane is obtained analytically as well as by Monte Carlo simulations. We demonstrate that in the vicinity of the desorption transition, many properties are different if h is used as the control parameter instead of the force f.

- Finally, the conclusions are drawn in Chapter 9.

Chapter 2

Basic Concepts in Polymer Physics

2.1 The Ideal Chain

We begin with a description of a polymer as an ideal chain in which there are no interactions between monomers far apart on the chain [39]. This situation is rare for real chains in which monomers interact with the solvent and with other monomers. The relative strength of these interactions determine if the monomers effectively attract or repel each other. At low temperatures, the effective interaction between monomers is attractive and the chain collapses into a globule. At high temperatures the chain swells due to the dominance of repulsive interaction. At a special intermediate temperature called the Θ temperature, the chains assume ideal conformation due to cancellation of repulsive and attractive parts of monomer-monomer interactions.

The starting point of the description of an ideal chain is a random walk [90]. Assuming there is no correlation between the directions of the bonds of the chain, and if all directions have the same probability, an ideal chain chain may be considered as a random walk on a lattice. A simple random walk (RW) is a succession of N steps starting from one lattice point and reaching another arbitrary point on the lattice. A step is considered to be a jump from a lattice site to a randomly chosen nearest neighbour. The statistical weight of all possible jumps to nearest neighbours are equal. To calculate the entropy, one needs to calculate the total number of distinct walks $Z(\mathbf{r})$ starting from $\mathbf{r} = 0$ and ending at a latice point $\mathbf{r}$ in N steps. The total number of $Z(\mathbf{r})$ is

$$\mathcal{Z}_N(tot) = \sum Z(\mathbf{r}) = z^N$$

where z is the number of nearest neighbours on a lattice. The entropy is $S(\mathbf{r}) = k_B \ln(Z(\mathbf{r}))$ where k_B is the Boltzmann constant.

Another simple model of an ideal polymer is the freely jointed chain model in which the chain consists of N bonds each of length a and no correlations between the bond

vectors. Since the bond vector can point in any direction, it is an off-lattice model. The basic quantity characterizing the spatial size of a polymer is the root-mean square (rms) end-to-end distance. If $\mathbf{r}_n$ is the nth bond vector , we have

$$\mathbf{R}_e = \sum_{n=1}^{N} \mathbf{r}_n$$

Now $\langle \mathbf{R}_e \rangle = 0$.

$$\langle \mathbf{R}_e^2 \rangle = \sum_{n=1}^{N} \sum_{m=1}^{N} \langle \mathbf{r}_n . \mathbf{r}_m \rangle \tag{2.1}$$

Since $\langle \mathbf{r}_n . \mathbf{r}_m \rangle = \langle \mathbf{r}_n \rangle . \langle \mathbf{r}_m \rangle = \delta_{n,m} a^2$, we have

$$\langle \mathbf{R}_e^2 \rangle = Na^2. \tag{2.2}$$

Therefore, the root mean square end-to-end distance is proportional to $N^{1/2}$ for an ideal chain. The spatial size of the chain is not given by the contour length which is proportional to N, but by $\mathbf{R}_e$ which is proportional to $N^{1/2}$. This implies that the probability of a freely jointed chain to assume a stretched conformation is very small. The chain is coiled in thermal equilibrium to maximize entropy. It is pertinent to mention that the only relevant macroscopic length scale of a polymer is the rms end-to-end distance. All other measures of size such as the radius of gyration and the hydrodynamic radius are directly proportional to $\mathbf{R}_e$ and differ only in the proportionality constant. The radius of gyration is given by

$$R_g = \left(\frac{1}{2N} \sum_{n.m=1}^{N} \langle |\mathbf{R}_n - \mathbf{R}_m|^2 \rangle \right)^{1/2} = \left(\frac{1}{N} \sum_{n=1}^{N} \langle |\mathbf{R}_{CM} - \mathbf{R}_n|^2 \rangle \right)^{1/2} \tag{2.3}$$

where $\mathbf{R}_{CM}$ denotes the centre of mass of the chain. It can be measured by small angle neutron scattering or light scattering [72]. For an ideal chain, the radius of gyration is related to the rms end-to-end distance as

$$R_g^2 = R_e^2/6$$

Another important feature of a polymer is its flexibility. In a freely jointed chain, there is no correlation between the orientations of bonds, which causes the chain to be very flexible. In more complicated models of polymers, the intrinsic stiffness is determined by the orientational correlations along the backbone of the chain. These correlations are usually short ranged and decouple on a length scale called the persistence length l_p of the chain. If the persistence length is much smaller than the size of the chain, the chain appears to be flexible. All sufficiently long polymer chains are flexible because of their length. Persistence lengths of real polymers can vary greatly.

A simple flexible polystyrene chain can have $l_p \simeq 1.0 - 1.4$nm which corresponds to 4 or 5 chain bonds. A double helix DNA can have $l_p \simeq 50$ nm corresponding to 150 base pairs [39].

The statistical distribution of the end-to-end vector of an ideal chain is Gaussian and is given by

$$P_n(\mathbf{R}_e) = \left(2\pi N a^2/3\right)^{-3/2} \exp\left(-3\mathbf{R}_e^2/2Na^2\right) \tag{2.4}$$

Therefore the ideal chain is also called the Gaussian chain. The distance between any two not-so-close points on an ideal chain obeys the Gaussian distribution.

The Gaussian chain has a single macroscopic spatial scale. As mentioned earlier, the radius of gyration, the hydrodynamic radius and the rms end-to-end distance are of the same order of magnitude.

The entropy of a Gaussian chain is defined as follows

$$S(R_e) = k_B \ln(P(\mathbf{R}_e)) + S_0 = -\frac{3k_B R_e^2}{2Na^2} + S_0$$

where S_0 is a constant. Typically we are interested in the change in entropy. Therefore the constant S_0 is trivial. The corresponding free energy is a quadratic function of the rms end-to-end distance.

$$F = \frac{3k_B T R_e^2}{2Na^2} \tag{2.5}$$

This implies that there is a linear relationship between the force and the rms end-to-end vector , *i.e.* the chain behaves as a spring with a restoring force $f(R_e)$ that is entropic in origin.

$$|f(R_e)| = T\frac{dS(R_e)}{dR_e} = \frac{3k_B T R_e}{Na^2}$$

for $|\mathbf{R}_e| \ll Na$. The chain acts as an entropic spring with spring constant $3k_BT/Na^2$.

Now, in all ideal chain models, the statistical properties of the chain do not depend on the specifics of the model for large N. Therefore , to study the properties of an ideal chain, it is convenient to use a model that is mathematically tractable [26] . The simplest is the Gaussian model in which the bond vector is flexible and follows a Gaussian distribution

$$p(\mathbf{r}) = \left(3/2\pi a^2\right)^{3/2} \exp\left(-3\mathbf{r}^2/2a^2\right)$$

. The Gaussian equivalent chain has N links each of average length a. If the position of the nth segment is $\mathbf{R}_n$ and the nth bond vector is $\mathbf{r}_n$, the conformational distribution function of the Gaussian chain is

$$\begin{aligned} P(\{\mathbf{r}_n\}) &= \prod_{n=1}^{N} \left(\frac{3}{2\pi a^2}\right)^{3/2} \exp\left(-\frac{3(\mathbf{R}_n - \mathbf{R}_{n-1})^2}{2a^2}\right) \\ &= \left(\frac{3}{2\pi a^2}\right)^{3N/2} \exp\left(\sum_{n=1}^{N} -\frac{3(\mathbf{R}_n - \mathbf{R}_{n-1})^2}{2a^2}\right) \end{aligned} \tag{2.6}$$

Such a model is microscopically unrealistic but can reproduce macroscopic properties quite well. The Gaussian chain is often represented as a mechanical model of $N+1$ beads connected by N harmonic springs. The energy of the chain is

$$U = \frac{1}{2}k\sum_{n=1}^{N}\left(\mathbf{R}_n - \mathbf{R}_{n-1}\right)^2 \tag{2.7}$$

where the spring constant $k = 3k_BT/a^2$. The equilibrium distribution of the rms end-to-end distance is the same as Eq. 2.4.

It is illuminating to take the continuous chain limit

$$\begin{aligned}\mathbf{R}_n - \mathbf{R}_{n-1} &\rightarrow \frac{\partial \mathbf{R}(n)}{\partial n}\\ \sum_{n=1}^{N} &\rightarrow \int_0^N dn\end{aligned}$$

In the continuous limit the probability of the chain configuration is represented as

$$P[\mathbf{R}(n)]\delta\mathbf{R}(n) \propto \mathcal{D}[\mathbf{R}(n)]\exp\left(-\frac{3}{2a^2}\int_0^N dn\left(\frac{\partial \mathbf{R}(n)}{\partial n}\right)^2\right)$$

This is called a Wiener distribution [34]. In this formalism, some path integrals can be calculated efficiently using familiar means.

2.2 "Real" Chains (SAW)

We now turn to the case of real polymers in which the interactions bet ween monomers separated by many bonds along the chain are no longer ignored. Typically, the interaction between two monomers involve a hard-core barrier corresponding to the energy cost of steric repulsion between two overlapping monomers and long-range attractions. In the previous section we mentioned that an ideal polymer can be modelled as a random walk on a lattice. This model allows the chain to loop back on itself *i.e.* permits intersections. This is physically impossible in a real polymer. Hence a corresponding lattice model of a real polymer would have an additional condition preventing two monomers from occupying the same lattice site. This is called a *self-avoiding walk* or SAW. In general, this kind of a condition is called 'excluded volume effect'. The mathematical properties of SAWs are complex and requires numerical techniques. The total number of SAWs of N steps has the asymptotic form

$$\mathcal{Z}_N(tot) \propto \mu^N N^{\gamma-1} \tag{2.8}$$

This can be compared to the random walk 2.1. The factor μ depends on the lattice and dimensionality. The exponent γ depends only on the dimensionality d and is ,

hence, a universal exponent. For three dimensional lattices $\gamma = \gamma_3 \simeq 7/6$. The rms end-to-end distance R_e scales as

$$R_e \equiv aN^{\nu} \tag{2.9}$$

where ν is another universal exponent depending only on the dimension. For $d = 3$, $\nu \simeq 3/5$.This corresponds to swelling of the chain in good solvents.

In order to deal with interactions , it is convenient to consider the canonical partition function.

$$Z = \int \mathcal{D}[\mathbf{R}(n)] \exp -\beta H(\mathbf{R}(n)) \tag{2.10}$$

where $\beta = 1/k_B T$. The Hamiltonian, H_0 for a non-interacting polymer chain is given by

$$\beta H_0 = \frac{3}{2a} \int_0^N dn \left(\frac{\partial \mathbf{R}}{\partial n} \right)^2$$

To model good solvent conditions, it is sufficient to introduce a repulsive two-body interaction. In the simplest case this can be done by means of a point contact interaction

$$\beta H_{int} = \frac{v}{2} \int_0^N dn \int_0^N dm \delta(\mathbf{R}(n) - \mathbf{R}(m))$$

The interaction constant v which determines the strength of interaction is given by

$$v = a^3 \left(1 - \frac{\Theta}{T} \right) \equiv a^3 \tau$$

where a^3 is the volume of one segment and Θ is the temperature at which v vanishes. τ is the reduced temperature. $H = H_0 + H_{int}$ is called the Edwards Hamiltonian. In order to model poor solvent conditions a three-body interaction has to be introduced.

The conformations of a real chain in an athermal or a good solvent are determined by a balance of the effective repulsive excluded volume interaction and the elastic energy arising from entropic effects tending to shrink the polymer. The essence of this balance can be illustrated by the Flory theory th at uses rough estimates for the energetic and entropic effects to the free energy. We recall that in the absence of interactions, the free energy of an ideal polymer chain is given by

$$F(\mathbf{R}_e) = k_B T \frac{3R_e^2}{2Na^2}$$

The Flory theory assumes that the monomers are uniformly distributed in the volume R_e^3 without correlations. Hence the probability of a second monomer being within the excluded volume of a given monomer is the product of the excluded volume v and the density of monomers in the chain N/R_e^3. The energetic cost of being excluded from this volume is $k_B T$ per exclusion or $v k_B T N/R_e^3$ per monomer. Hence the energy cost is

$$F_{int} \simeq \frac{1}{2} v k_B T \frac{N^2}{R_e^3}.$$

Thus the free energy of a real chain in the Flory approximation is

$$\beta F(\mathbf{R}_e) \simeq k_B T \frac{3R_e^2}{2Na^2} + \frac{1}{2} v k_B T \frac{N^2}{R_e^3}. \tag{2.11}$$

Minimization of F with respect to $\mathbf{R}_e$ gives $\nu \sim 3/5$ which is very close to the value obtained from more sophisticated techniques such as perturbative methods, Renormalization group calculations and simulations. The current estimation of ν is 0.588 ± 0.001 based on renormalization group calculations and simulations [54].

2.3 Polymer dynamics

The first successful molecular model of polymer dynamics was the Rouse model. A polymer chain in the Rouse model is represented a N beads connected by springs of rms size a in a freely draining solvent. The beads interact with each other only via the springs. Each bead has a friction coefficient ζ. The total friction of the chain is the sum of the individual contributions of the beads.

$$\zeta_{\mathcal{R}} = N\zeta$$

The viscous drag experienced by the chain if it is pulled with a velocity $\mathbf{v}$ is $\mathbf{f} = -N\zeta_{\mathcal{R}}\mathbf{v}$ as per Stokes' law. The diffusion coefficient of the Rouse chain is given by Einstein relation

$$D_{\mathcal{R}} = \frac{k_B T}{\zeta_{\mathcal{R}}}$$

The polymer diffuses a distance of the order of its size during a characteristic time called the Rouse time $\tau_{\mathcal{R}}$ given by

$$\tau_{\mathbf{R}} \simeq \frac{R^2}{D_{\mathcal{R}}} \simeq \frac{\zeta N R^2}{k_B T} \tag{2.12}$$

where R is the size of the chain. On time scales shorter than the Rouse time, the chain exhibits viscoelastic modes. But on longer time scales the chain is diffusive. Since $R \simeq aN^{\nu}$, we can define a monomer relaxation time $\tau_0 \simeq \zeta a^2/k_B T$ so that

$$\tau_{\mathcal{R}} \simeq \tau_0 N^{1+2\nu}$$

Here τ_0 is the timescale of individual motion of monomers. At time scales smaller than τ_0, the chain essentially does not move and exhibits elastic response. For $\tau_0 < t < \tau_{\mathcal{R}}$, the chain exhibits viscoelastic response. When a particle moves through a fluid, it drags some of the solvent around it. The long range force acting on the solvent and other particles arising from the motion of one particle is called the hydrodynamic interaction. The Rouse model ignores hydrodynamic interaction of the beads. This issue is addressed in the Zimm model a discussion of which can be found in [26].

2.4 Adsorption and Scaling

A scaling theory is often the first step in understanding universal properties of polymers. In order to make a scaling analysis, it is necessary to first identify the macroscopically relevant length scales. The observables are then written as dimensionless combinations of these variables. Since this thesis is primarily concerned with adsorption of polymers on rigid surfaces, let us see how scaling laws can be applied to this particular system.

In the presence of an attractive surface, the properties of a polymer solution are very different from the bulk. Consider a polymer in a dilute solution near a weakly attractive surface. Let $-\epsilon k_B T$ be the energy gain for a monomer in contact with the surface. The chain would like to increase the number of surface contacts. But this results to a loss of conformational entropy due to confinement at the surface. If the gain in adsorption energy is sufficient to offset the loss the entropy, one observes an increase in the density of monomers on the surface. Hence, an adsorptive transition can occur only when the value of the adsorption energy parameter ϵ exceeds a certain critical value ϵ_c. The adsorptive transition can be interpreted as a second order phase transition at the critical point of adsorption in the thermodynamic limit $N \to \infty$. Close to the critical point the number of monomers on the surface scales as

$$N_s(\epsilon = \epsilon_c) \sim N^{\phi} \tag{2.13}$$

where ϕ is called the crossover exponent. The numerical value of ϕ is a matter of ongoing discussion in literature. It is estimated to lie between 0.59 [29] and 0.484 [37]. This issue is dealt in detail in Chapter 4 and Chapter 6 where we have attempted to explain the cause of the wide variation in reported values of ϕ

The thickness of the adsorbed layer defines the adsorption blob size. An adsorbed chain can be viewed as a string of blobs on the surface. The blob size is the length scale at which the total interaction energy of the monomers within the blob with the surface is of the order of $k_B T$ which is the thermal energy. A blob appears to be on the verge of adsorption. On length scales smaller than the blob size, the surface interaction is much smaller than the thermal energy and the section of the chain remains in unperturbed condition *i.e.* in swollen condition as a real chain. On length scales larger than the blob size, the surface interaction is larger than $k_B T$ and hence , each blob is forced to be in contact with the surface. Therefore the polymer chain forms an array of blobs on the surface. Consider a chain adsorbed on a surface. Let D be the thickness of the adsorbed layer. The fraction of monomers in contact with the surface is a/D where a is approximately the size of a monomer. The energetic gain from surface interactions is

$$F_{int}/k_B T \simeq -\epsilon N a/D$$

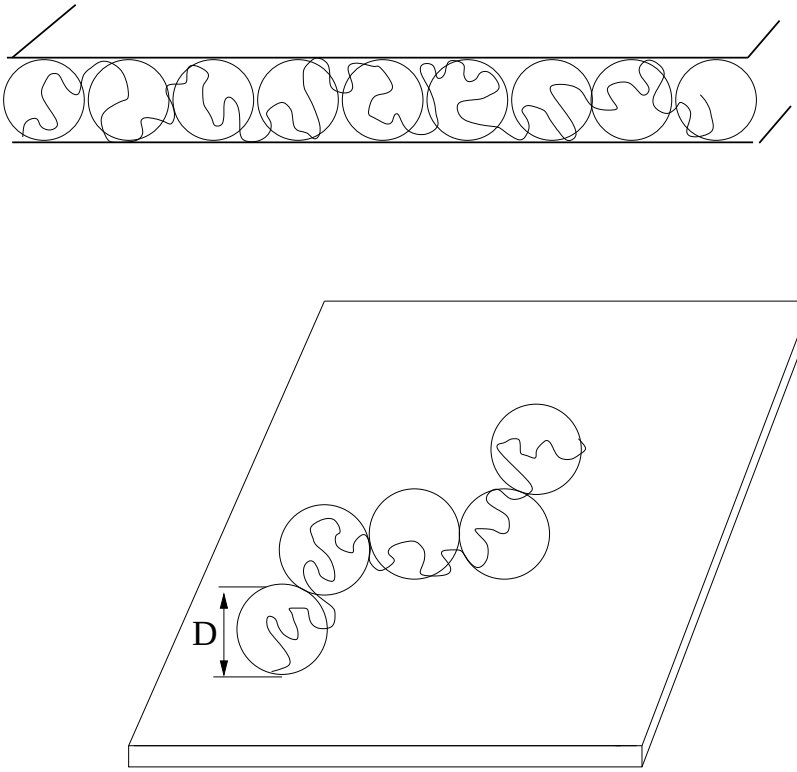

Figure 2.1: (a) Blob picture of a polymer confined in a slit, (b) Blob picture of a polymer weakly adsorbing on a planar surface. When seen from the top, the blobs appear to form a SAW in two dimensions with $R \sim n_b^{3/4} D = n_b^{\nu} D$ where n_b is the number of blobs.

In order to gain this energy the chain must pay the entropic confinement free energy. To calculate the confinement energy , consider a chain confined in a slit of size D. The chain can be viewed as a string of blobs . The diameter of the slit gives the size of the blob. On length scales smaller than D, the chain does not know that it is being compressed. The statistics in such length scales is the same as for unperturbed chains

$$D \simeq a g^{3/5}$$

where g is the average number of monomers in a blob of size D. The number of blobs is N/g. The confinement energy is of the order $k_B T$ for each blob. Hence, the confinement energy of the chain is

$$F_{conf}/k_B T \simeq N/g \simeq N \left(\frac{a}{D}\right)^{5/3}$$

Now, adding the adsorption and the confinement energies of the chain, we get

$$F/k_B T \simeq N \left(\frac{a}{D}\right)^{5/3} - \epsilon N a/D \tag{2.14}$$

Minimizing the free energy with respect to D we find

$$\begin{aligned} D &\sim a\epsilon^{-3/2} \\ F &\sim N\epsilon^{5/2}. \end{aligned}$$

2.5 Polymer under tension

Scaling arguments and the blob picture introduced in the previous section can also be used to describe the behaviour of a real chain under tension. Consider a force K applied to the ends of a polymer chain in a good solvent. There are two characteristic length scales associated with the system : $R_e \simeq aN^{\nu}$ and $\xi = k_BT/K$. The extension of the chain $R(K)$ is a function of K and the temperature and can be written as

$$R(K) \simeq R_e g_K\left(R_e/\xi\right)$$

Let $x = R_e/\xi$. There are different scenarios depending on the strength of the force. At very low force ($x < 1$) , the extension $R(K)|$ is linear in x, *i.e.* $g_K(x \to 0) \simeq x$. This gives

$$R(K) \simeq \beta R_e^2 K$$

for $KR_e < k_BT$.

At a larger force ($x \gg 1$), the chain breaks up into a series of blobs each of size ξ. At length scales smaller than the blob size, the chain is unperturbed and behaves as a self avoiding walk. At longer length scales, the chain behaves as an array of independent blobs. If the number of monomers within a blob is denoted by g,

$$\xi \simeq g^{\nu} a$$

or

$$g \simeq \left(\frac{k_BT}{aK}\right)^{1/\nu}.$$

The total chain extension is given by the product of the blob size and the number of blobs.

$$\begin{aligned} R(K) &\simeq \frac{N}{g}\xi \simeq Na(\beta Ka)^{\frac{1-\nu}{\nu}} \\ \text{or,} \quad K &\simeq \frac{1}{\beta a}\left(\frac{R}{Na}\right)^{\nu/(1-\nu)} \end{aligned} \tag{2.15}$$

Therefore the force-extension relationship for an ideal chain is 'Hookean' *i.e.* linear since $\nu = 1/2$. For a real chain, the dependence of the force K on the extension $R(K)$

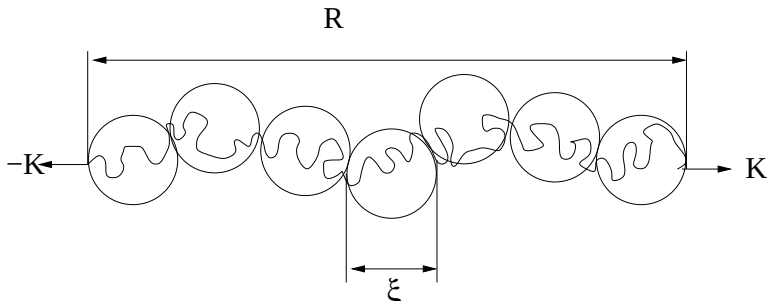

Figure 2.2: Blob picture of a polymer under tension

is a power law with exponent 3/2 for $\nu = 3/5$. This was first derived by Pincus and the tension blobs are often called Pincus blobs. This scaling approach is valid for relatively small extensions. The divergence of the force near maximal extension is not described by this method. We will consider the detachment of a chain at an attractive surface under the influence of a pulling force in Chapter 6 and 7.

2.6 Adsorption and Monte Carlo simulations

Computer simulations have been extremely useful in the field of polymer physics and chemistry and have been used extensively in our investigations. Polymers have special characteristics that make them an important class of physical systems. A single macromolecule exhibits different structure on different length scales ranging from that of a chemical bond to the persistence length to the total size. There are additional length scales for liquid crystalline polymers, polyelectrolytes, polyampholytes etc. The treatment of the full chemical detail of a polymer is a challenging task.

However, when one interested in global properties of a polymer system, it is often sufficient to work with a simplified coarse-grained model. Let us consider the two main commonly used techniques : molecular dynamics (MD) simulations and Monte Carlo (MC) methods. In MD, we consider a system of classical particles interacting through a set of forces. The equations of motion are numerically integrated and the averages of the state-variables are obtained as the time-averages over the trajectory of the system in phase space. In contrast, Monte Carlo methods attempt to simulate the distributions. A generic MC algorithm constructs a weighted walk in the configuration space of the system and samples different states according to their equilibrium probability distributions. MC can also be adapted to study time-dependent phenomena.

Polymer simulations took off with lattice models in the pioneering work of Wall *et.*

al [91]. The first off-lattice Monte Carlo simulations of single chains were later carried out by Lal [52]. An early molecular dynamics simulation of polythene using realistic interactions was done by Weber and Helfand [92]. The Monte Carlo techniques used in our investigations are described in the next chapter.

Chapter 3

Simulation Techniques

The simulation of polymers is a challenging task because of the complicated chemistry and the topology. However, simplified coarse grained models are an important tool in the study of universal properties of polymers [53]. The modelling leaves out the details of the chemical structure of the molecules but reduces the computational cost enormously. Monte Carlo simulations of coarse grained models provide valuable information about the physical properties of macromolecules.

We use an off-lattice bead spring model to study the static and dynamic properties of a single polymer chain tethered at one end to an attractive surface. The polymer chain is consists of coarse-grained monomers connected by coarse grained bonds. Each bond corresponds to 3-6 chemical bonds along the backbone of a polymer chain. Each coarse grained bond is described by the FENE potential (finitely extensible nonlinear elastic potential).

$$U_{FENE}(l) = -K(l_{max} - l_0)^2 ln \left[1 - \left(\frac{l - l_0}{l_{max} - l_0}\right)^2\right]$$

Here l_{max} is the maximum bond length. The minimum of this potential occurs at l_0 about which the potential is harmonic with K being the spring constant. The potential diverges to infinity for both $l \to l_{max}$ and $l \to l_{min} = 2l_0 - l_{max}$. We choose choose our length unit $l_{max} = 1$ and the other parameters as ;

$$l_0 = 0.7, \quad K/k_BT = 20, \quad l_{min} = 0.4$$

where T is the absolute temperature and k_B is the Boltzmann constant. The chains are flexible and there is no potential for bond angles. The non-bonded interactions between the effective monomers are described by a Morse-type potential.

$$U_M(r)/\epsilon_M = \exp[-2\alpha(r - r_{min})] - 2\exp[-\alpha(r - r_{min})]$$

where r is the distance between the beads. The parameters chosen are

$$\alpha = 24, \quad r_{min} = 0.8, \quad \epsilon_M/k_BT = 1$$

The Morse potential provides an impenetrable core and a weak attraction at somewhat long distances. It decays rapidly with $U_M \simeq 0$ for $r \simeq 1$ which allows the use of link-cell algorithm with a cell linear dimension of unity. The parameters of the potential are chosen so as to prevent the chain from crossing itself. The Morse potential is more suitable than the Lennard-Jones potential which has a slower decay of r^{-6} at long distances and requires a cutoff if one wishes to use the Linked-Cell methods. The polymer is tethered at one end to a flat structureless surface at $z = 0$. The surface interaction of the effective monomers are described by a square well potential $U_w(z) = -\varepsilon$ for $z < \delta = 0.125$ and $U_w = 0$ otherwise. ε/k_BT is varied between 1 and 10.

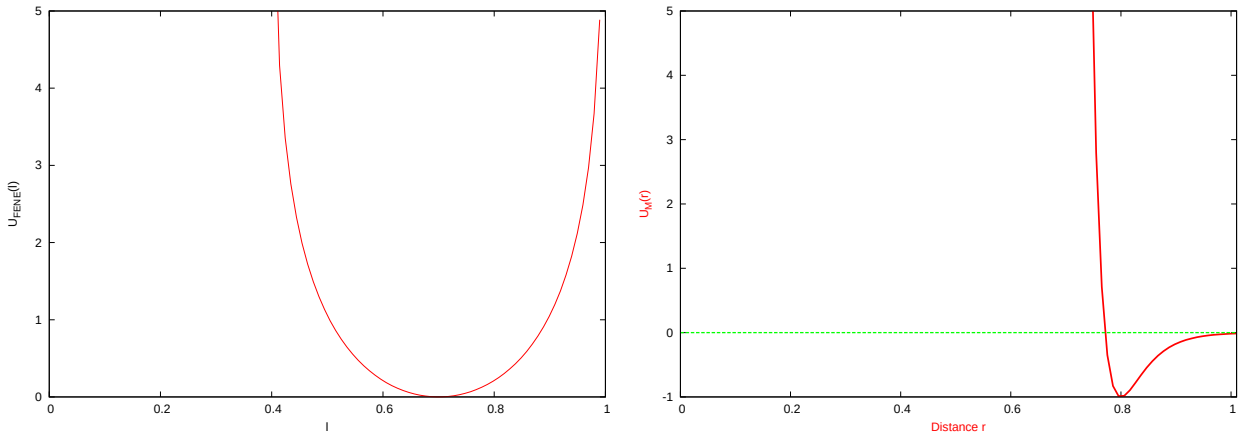

Figure 3.1: (a) The FENE potential $U_{FENE}(l)$ (b) The Morse potential $U_M(r)$

We use periodic boundary conditions in the xy direction and impenetrable walls in the $z-$direction. We have studied chain lengths between 32 and 512. The dimesions of the simulation box were chosen according to the chain length and the nature of the problem. While investigating the adsorption of polymers in the absence of a pulling force, the size of the box was $64 \times 64 \times 64$ for all chains except the longest. For the chain-length 512, a larger box size of $128 \times 128 \times 128$ was used. While investigating a chain under traction, we use a box size of $256 \times 256 \times 256$ for the longest chain (of length 128). The standard Metropolis algorithm was employed to govern the moves with self avoidance automatically incorporated in the potentials. In each Monte Carlo move, a monomer was chosen at random and a random displacement attempted. with Δx, Δy, and Δz chosen uniformly from the interval $-0.5 \leq \Delta x, \Delta y, \Delta z \leq 0.5$. The transition probability for the attempted move was calculated from the change ΔU of the potential energy because of the move as

$$\Omega = \min\{\exp[-\Delta U/k_BT], 1\}$$

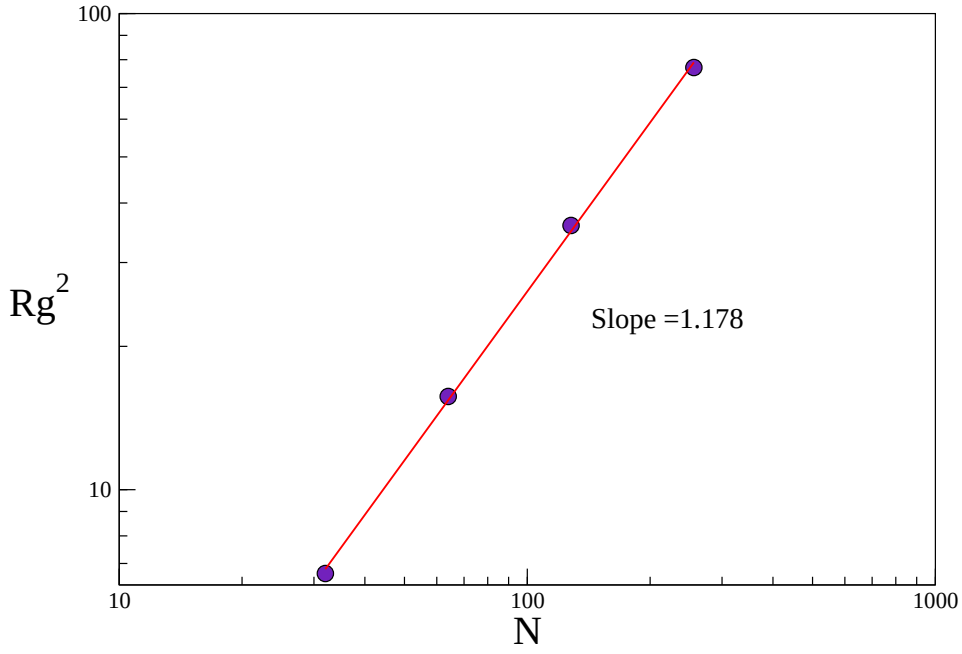

Figure 3.2: The square of the radius of gyration plotted against the chain length N in double logarithmic coordinates. The Flory constant which equals half the value of the slope is estimated to be 0.589.

As in the usual Metropolis algorithm, the attempted move was accepted if Ω exceeds a random number η uniformly distributed in the interval $[0, 1)$. For a chain of length N, one Monte Carlo move is completed after N attempts of elementary displacements of randomly selected monomeric units. As mentioned earlier, the potentials prevent self-intersection of the chain and one does not need to check for entanglement. This off-lattice algorithm is reasonably fast compared to most lattice models and suffers less from ergodicity problems. We have used the off-lattice algorithm to study both the statics and dynamics of polymer chains in the vicinity of an adsorbing surface. The code is implemented in ASCII C. We have run most of the simulations on an SGE cluster and some on PCs.

Chapter 4

Adsorption of Copolymers

4.1 Introduction

In this Chapter, we discuss the adsorption of multiblock and random copolymers on planar surfaces. We will consider the statics of adsorption with particular focus on the critical behaviour of the system. The next chapter deals with the time-dependent features of polymer adsorption.

As already mentioned in the introducton in Chapter 1, the adsorption of polymers on surfaces plays a critical role in numerous industrial applications such as adhesion, biocompatibility, colloidal stabilization, and chromatography. Block copolymers, in particular, play an important role as additives in many industrial products like paints, ink, lubricants, coatings, adhesives etc. They are effective in stabilizing colloidal suspensions and this has its origin in adsorbing properties. The adsorption of random copolymers merits attention because of its significance in biophysics. Random copolymers serve as pragmatic models to study the physics of proteins and other biomolecules.

The adsorption of homopolymers at an impenetrable surface has been the focus of many studies over four decades.

The theoretical studies of the behaviour of polymers interacting with solid substrate have been based predominantly on both scaling analysis à la de Gennes [15, 16, 17, 18, 29] as well as on the self-consistent field (SCF) approach à la Fleer *et. al* [33]. The close relationship between theory and computer experiments in this field [29, 58] has proved especially fruitful. As mentioned in Chapter 2, a polymer chain at an attractive surface can undergo adsorptive transition only when the value of the surface potential ϵ exceeds a certain critical value ϵ_c. Most of the studies on polymer adsorption in literature focus on the determination of the critical adsorption point (CAP) location and on the scaling behavior of a variety of quantities such as the radius of gyration below, above and at the CAP. The relation between polymer statistics and the corresponding correlation functions [29] in the n-vector model of magnets with a free surface in the limit $n \to 0$

has lead to a number of important results. Another important issue that has dominated the discussion of polymer adsorption is the determination of the so called *crossover exponent* ϕ which is known to govern the fraction of adsorbed monomers at the CAP. Close the critical point, the number of surface contacts of a polymer of length N is expected to obey $N_s \sim N^{\phi}$ where ϕ is a universal constant. The actual value of ϕ has been disputed in literature. A study by Eisenrigler, Binder and Kremer [29] suggests that ϕ is close to the Flory exponent ν in 3D. More recently, using a different algorithm, Hegger and Grassberger [43] determined ϕ to be close to 0.5, a result that is exact in 2D [11]. This subject is discussed in greater detail in Chapter 6, where we discuss the reasons for the different estimates of ϕ.

Recently the scaling relationship for a single chain adsorption has been tested by Monte Carlo (MC) simulation on a cubic lattice [20, 37] as well as by an off-lattice model [57, 58] and the adsorption transition of a homopolymer could be viewed nowadays as comparatively well understood.

Now, while the investigations mentioned above have been devoted almost exclusively to homopolymers, the adsorption of copolymers (e.g. multi-blocks or random copolymers) is still much less understood. Thus, for instance, the CAP dependence on block size M at fixed concentration of the sticking A-mers is still unknown as are the scaling properties of *regular multi-block copolymers* in the vicinity of the CAP. From the theoretical perspective, the case of diblock copolymers has been studied mainly within the SCF-approach [33, 31]. The case of *random copolymers* adsorption has gained comparatively more attention so far. The main variations to this problem are : a random copolymer adsorbing on a homogeneous surface, a homopolymer adsorbing on a random surface and a random heteropolymer adsorbing on random surface. It has been investigated by Whittington et al. [83, 61] using both the annealed and quenched models of randomness. The influence of sequence correlations on the adsorption of random copolymers has been studied by means of the variational and replica method approach [69]. Sumithra and Baumgaertner [87] examined the question of how the critical behavior of random copolymers differs from that of homopolymers by Monte Carlo simulations and scaling arguments. Thus, among a number of important conclusions, the results of Monte Carlo simulations demonstrated that the crossover exponent ϕ (see below) is independent of the fraction of attractive monomers p.

In this chapter, we use scaling analysis as well as Monte Carlo simulations to study the critical behavior of multi-block and random copolymers. It turns out that the critical behaviour of these two types of copolymers could be reduced to the behavior of an effective homopolymer chain with "renormalized" segments. For the multi-block copolymer this allows e.g. to explain how the critical attraction energy depends on the

block length M and to derive an adsorption phase diagram in terms of CAP against M. In the case of random copolymers the sequence of sticky and neutral (as regards the solid substrate) monomers within a particular chain is fixed which exemplifies a system with quenched randomness. Nevertheless, close to criticality the chain is still rather mobile, so that the sequence dependence is effectively averaged over the time of the experiment and the problem can be reduced to the case of annealed randomness. We show that our MC-findings close to criticality could be perfectly treated within the annealed randomness model. We start with a discussion of the simulation methods used in this study.

4.2 Monte Carlo Simulation Model

We have carried out extensive Monte Carlo simulations with a coarse grained, off-lattice bead spring model [58] to investigate the adsorption of homopolymer , multi-block copolymer and random copolymers on a flat surface. As already described in Chapter 3, our system consists of a single chain tethered at one end to a flat structureless surface. There are two kinds of monomers: "A" and "B", of which only the "A" type feels an attraction to the surface. The surface interaction of the "A" type monomers is described by a square well potential $U_w(z) = \epsilon$ for $z < \delta$ and $U_w(z) = 0$ otherwise. δ is chosen to be 0.125. ϵ is varied from 0.6 to 3.6. Here and in what follows ϵ is measured in units of the thermal energy k_BT (with k_B being the Boltzmann constant, and T - the temperature of the system). The effective bonded interaction is described by the FENE (finitely extensible nonlinear elastic) potential while the nonbonded interactions are described by the Morse potential.

We use periodic boundary conditions in the $x-y$ directions and impenetrable walls in the z direction. We have studied polymer chains of lengths 32, 64, 128, 256 and 512. We have also studied homopolymer chains and random copolymers (with a fraction of attractive monomers, $p = 0.25,\ 0.5,\ 0.75$). The size of the box was $64 \times 64 \times 64$ in all cases except for the 512 chains where a larger box size of $128 \times 128 \times 128$ was used. The standard Metropolis algorithm was employed to govern the moves with self avoidance automatically incorporated in the potentials. In each Monte Carlo update, a monomer was chosen at random and a random displacement attempted with $\Delta x,\ \Delta y,\ \Delta z$ chosen uniformly from the interval $-0.5 \leq \Delta x, \Delta y, \Delta z \leq 0.5$. The transition probability for the attempted move was calculated from the change ΔU of the potential energies before and after the move as $W = \exp(-\Delta U/k_BT)$. As for standard Metropolis algorithm, the attempted move was accepted if W exceeds a random number uniformly distributed in the interval $[0, 1]$. As a rule, the polymer chains have been originally equilibrated in the MC method for a period of about 10^6 MCS . Depending on degree of adsorption ϵ

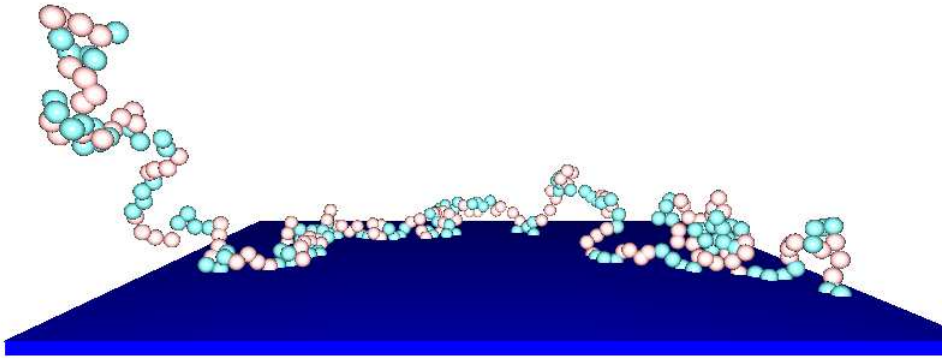

Figure 4.1: Snapshot of a chain with length $N = 256$ from the MC simulations and block size $M = 4$. The blue monomers adsorb on the surface while the pink ones are neutral to it.

and chain length N this period is varied. This was followed by 200 measurement runs, each of length 8×10^6 MCS. The values provided here are for the longest chain length , $N = 512$. In the case of random copolymers, for a given composition, i.e., percentage p of the $A-$monomers, a new polymer chain is created in the beginning of the simulation run by means of a randomly chosen sequence of segments. This chain is then sampled during the course of the run, and replaced by a new sequence in the beginning of the next run. Each new sequence is equilibriated for a while before the measurement run.

4.3 Theory: Scaling aspects of Homopolymer Adsorption

A scaling theory is often the first step in understanding universal properties of polymers. We start with a brief sketch of the scaling theory of homopolymer adsorption [29, 20, 57].

4.3.1 Order parameter

The process of adsorption is governed by a competition between the adsorption energy for a segment in contact with the surface and the loss in conformational entropy due to the confinement of the chain on the surface. It is well known that a single polymer chain undergoes a transition from a non-bound into an adsorbed state when the adsorption energy ϵ per monomer increases beyond a critical value ϵ_c. The adsorption transition can be interpreted as a second-order phase transition at the critical point (CAP) of adsorption $\epsilon = \epsilon_c$ in the thermodynamical limit, i.e. $N \to \infty$. Close to the CAP the number of surface contacts N_s scales as

$$N_s(\epsilon = \epsilon_c) \sim N^{\phi} \tag{4.1}$$

where the exponent ϕ is called the crossover exponent. The numerical value of ϕ is somewhat controversial and lies in a range between $\phi = 0.59$ (ref. [29]) and $\phi = 0.484$ (ref. [37]), we adopt however the value $\phi = 0.50 \pm 0.02$ which has been suggested as the most satisfactory [57] by comparison with comprehensive simulation results.

Consider a chain tethered to the surface at the one end. The fraction of monomers on the surface $n = N_s/N$ may be viewed as an order parameter measuring the degree of adsorption. Let us measure the distance from the CAP by the dimensionless quantity

$$\kappa = (\epsilon - \epsilon_c)/\epsilon_c \tag{4.2}$$

and also introduce the scaling variable $\eta \equiv \kappa N^{\phi}$. In the presence of an attractive surface, the following four cases can be distinguished.

- For $\epsilon << \epsilon_c$, in the thermodynamic limit $N \to \infty$, the fraction n goes to zero ($\approx \mathcal{O}(1/N)$). For very weak attractive potential , a tethered chain is in a mushroom like state.

- When κ is close to zero, $n \sim N^{\phi-1}$. This scaling behaviour of the order parameter is a signature of the critical threshold of adsorption. Now, the energy of adsorption is simply the product of the energy gain per monomer $\Delta\epsilon = \epsilon - \epsilon_c$ and the number of adsorbed monomers $N_s \sim N^{\phi}$. Therefore, near the critical point the energy gain of the chain is $N^{\phi}\Delta\epsilon$. This is balanced by the free energy due to loss of translation, which is of the order k_BT.

- For small κ but large η, *i.e.* $\kappa N^{\phi} \gg 1$, the chain is adsorbed as a whole , but the binding energy of each segment is small. The situation is called the weak coupling limit. The chain appears as a string of N/g blobs on the surface where g is the average number of segments in a blob. Each blob is considered to be on the threshold of adsorption. Each blob carries an adsorption energy of about k_BT. This is explained later.

- For $\epsilon \gg \epsilon_c$ (in the strong coupling limit) n is independent of N. Each segment is strongly attracted by the surface and the chain lies on the surface.

In this study, we focus on the critical adsorption point and will deal with the first three regimes described above. The scaling ansatz is then

$$n(\eta) = N^{\phi-1}\, G\,(\eta)\ . \tag{4.3}$$

with the scaling function

$$G(\eta) = \begin{cases} \text{const} & , \quad \text{for} \quad \eta \to 0 \\ \eta^{(1-\phi)/\phi} & , \quad \text{for} \quad \eta \gg 1 \end{cases} \tag{4.4}$$

The resulting scaling behavior of n follows as,

$$n \propto \begin{cases} 1/N & , \quad \text{for} \quad \kappa << 0 \\ N^{\phi-1} & , \quad \text{for} \quad \kappa \to 0 \\ \kappa^{(1-\phi)/\phi} & , \quad \text{for} \quad \kappa \gg 1 \end{cases} \tag{4.5}$$

4.3.2 Gyration radius

The two main quantities used to characterize the extension of the chain are the radius of gyration $\mathbf{R}_g$ and the end-to end distance $\mathbf{R}_e$ (see Chapter 2 eq. 2.3). The presence of a surface introduces an anisotropy in the system. In our analysis we have used the two components of $\mathbf{R}_g$: the component parallel to the surface $\mathbf{R}_{g||}$ and the component perpendicular to the surface $\mathbf{R}_{g\perp}$. These components are calculated in the simulations in the following way.

$$R_{g||}^2 = \langle \frac{1}{N} \sum_{i=0}^{N} \left((x_i - X)^2 + ((y_i - Y)^2 \right) \rangle \tag{4.6}$$

and

$$R_{g\perp}^2 = \langle \frac{1}{N} \sum_{i=0}^{N} (z_i - Z)^2 \rangle \tag{4.7}$$

where x_i, y_i and z_i denote the ith monomer's coordinates and X, Y and Z represent the coordinates of the centre of mass (COM).

$$\mathbf{R}_{COM} = \langle \frac{1}{N} \sum_{i=0}^{N} \mathbf{r}_i \rangle$$

Here, the $\langle ... \rangle$ denote the averages over the different realizations.

The gyration radius in direction perpendicular to the surface, $R_{g\perp}(\eta)$, has the form

$$R_{g\perp}(\eta) = aN^{\nu}\mathcal{G}_{g\perp}(\eta) \tag{4.8}$$

Here $\mathcal{G}_{g\perp}(\eta)$ is a dimensionless function. One may determine the form of the scaling function $\mathcal{G}_{g\perp}(\eta)$ from the following consideration. At $\kappa < 0$, the chain is not adsorbed, one has $R_{g\perp} \sim aN^{\nu}$, so that $\mathcal{G}_{g\perp} = \text{const}$. This is the regime in which the attraction is very small and the chain is practically unperturbed by the surface. In the opposite limit, $\eta \gg 0$ the N-dependence drops out and $\mathcal{G}_{g\perp}(\eta) \sim \eta^{-\nu/\phi}$. The chain is completely adsorbed on the surface and $R_{g\perp}$ is independent of the chain length. Thus

$$\mathcal{G}_{g\perp}(\eta) = \begin{cases} \text{const} & , \quad \text{for} \quad \eta \leq 0 \\ \eta^{-\nu/\phi} & , \quad \text{for} \quad \eta \gg 0 \end{cases} \tag{4.9}$$

As a result

$$R_{g\perp}(\eta) \propto \begin{cases} aN^{\nu} & , \quad \text{for} \quad \eta \leq 0 \\ \kappa^{-\nu/\phi} & , \quad \text{for} \quad \eta \gg 0 \end{cases} \tag{4.10}$$

The gyration radius in direction parallel to the surface has similar scaling representation:

$$R_{g\parallel}(\eta) = aN^{\nu}\mathcal{G}_{g\parallel}(\eta) \tag{4.11}$$

Again at $\kappa < 0$ the gyration radius $R_{g\parallel} \sim aN^{\nu}$ and $\mathcal{G}_{g\parallel} = \text{const}$. At $\eta \gg 0$ the chain behaves as a two-dimensional self-avoiding walk (SAW), i.e. $R_{g\parallel} \sim aN^{\nu_2}$, where $\nu_2 = 3/4$ denotes the Flory exponent in two dimensions. As a result, the scaling function behaves as

$$\mathcal{G}_{g\parallel}(\eta) = \begin{cases} \text{const} & , \quad \text{at} \quad \eta \leq 0 \\ \eta^{(\nu_2-\nu)/\phi} & , \quad \text{at} \quad \eta \gg 0 \end{cases} \tag{4.12}$$

Thus

$$R_{g\parallel}(\eta) \propto \begin{cases} aN^{\nu} & , \quad \text{at} \quad \eta \leq 0 \\ \kappa^{(\nu_2-\nu)/\phi}N^{\nu_2} & , \quad \text{at} \quad \eta \gg 0 \end{cases} \tag{4.13}$$

Blob picture

In the limit $\kappa N^{\phi} \gg 1$ the adsorbed chain can be visualized as a string of *adsorption blobs* which forms a pancake-like quasi-two-dimensional layer on the surface (see Chapter 2 Sec. 2.4). The blobs are defined to contain as many monomers g as necessary to be on the verge of being adsorbed and therefore carry an adsorption energy of

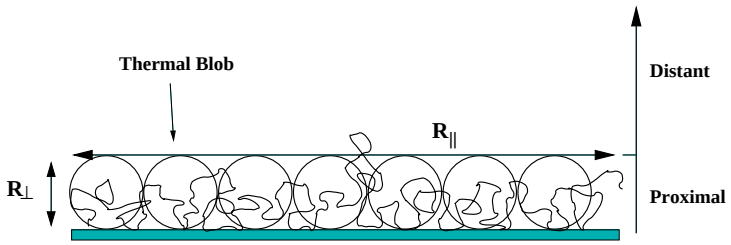

Figure 4.2: Blob picture of an adsorbed polymer chain.

the order of k_BT each. The thickness of the pancake $R_{g\perp}$ corresponds to the size of the blob and the chain conformation within a blob stays unperturbed (i.e. it is simply a SAW), thus $g \sim (R_{g\perp}/a)^{1/\nu} = \kappa^{-1/\phi}$ where we have used eq 4.10. The gyration radius can be represented thus as

$$R_{g\|} = R_{g\perp}\left(\frac{N}{g}\right)^{\nu_2} \propto \kappa^{(\nu_2-\nu)/\phi} N^{\nu_2} \tag{4.14}$$

and one goes back to eq 4.13 which proves the consistency of the adsorption blob picture. Generally speaking, the number of blobs, $N/g \sim \kappa^{1/\phi}N$, is essential for the main scaling argument in the above-mentioned scaling functions. For example we could recast the order parameter scaling behavior eq 4.3 as

$$n = N^{\phi-1} H\left(\frac{N}{g}\right) \tag{4.15}$$

where $H(x)$ denotes a new scaling function :

$$H(x) = \begin{cases} \text{const} & , \quad \text{for} \quad x \to 0 \\ x^{1-\phi} & , \quad \text{for} \quad x \gg 1 \end{cases} \tag{4.16}$$

Ratio of gyration radius components

The study of the ratio, $r(\eta) \equiv R_{g\perp}/R_{g\|}$, of gyration radius components is a convenient way to find the value of ϵ_c (see [20, 57]). In fact, from the previous scaling equations

$$r(\eta) \equiv \frac{R_{g\perp}(\eta)}{R_{g\|}(\eta)} = \frac{\mathcal{G}_{g\perp}(\eta)}{\mathcal{G}_{g\|}(\eta)} \tag{4.17}$$

Hence at the critical point, i.e. at $\eta \to 0$, the ratio $r(0) = const$ is independent of N. Thus by plotting r vs. ϵ for different N all such curves should intersect at a single point which gives ϵ_c.

Another way to fix ϵ_c is the following. Exactly at the critical point $n \sim N^{\phi-1}$, so that by plotting $nN^{1-\phi}$ vs. N at different values of ϵ one can determine the value $\epsilon \approx \epsilon_c$ under which $nN^{1-\phi}$ becomes independent of N.

4.3.3 Free energy of adsorption

The adsorption on a surface at $\kappa > 0$ is due to a free energy gain which is proportional to the number of blobs, i.e.,

$$\frac{F - F_{\text{bulk}}}{N} \propto -\frac{1}{g} \sim -\kappa^{1/\phi} \, . \tag{4.18}$$

The expression for the specific heat per monomer follows immediately from eq 4.18 as

$$C_V = -\frac{\partial^2 (F - F_{\text{bulk}})}{\partial^2 \kappa} \propto \kappa^{-\alpha} \tag{4.19}$$

where $\alpha = 2 - \phi^{-1}$. Note that a factor of $k_B T$ is absorbed in the free energy throughout the chapter.

For a chain (of the length N) on the verge of adsorption, the foregoing free energy gain, $F - F_{\text{bulk}}$, should be of the order of unity. In view of eq 4.18 this gives an estimate for the critical energy of adsorption - CAP,

$$\epsilon_c(N) = \epsilon_c(\infty) \left(1 + \frac{1}{N^{\phi}}\right), \tag{4.20}$$

where we have explicitly marked the CAP, $\epsilon_c(N)$ and $\epsilon_c(\infty)$, for finite and infinitely long chains respectively.

4.3.4 Polymer adsorption and the Landau theory of phase transitions

One of the simplest phenomenological theories of phase transition is the Landau theory which is based on the idea that the free energy of a system is analytic and obeys the symmetry of the Hamiltonian. With these two conditions, one can write the free energy as a Taylor expansion in the order parameter n. For the case of the adsorptive transition of a single polymer chain on a plane surface, the free energy is expanded in powers of the order parameter n in the vicinity of the critical adsorption potential.

$$F = F_0 + A(\epsilon_c - \epsilon) n^{\zeta} + B n^{2\zeta} \tag{4.21}$$

where A and B are positive coefficients and the exponent ζ is determined below by comparison to the scaling theory. For $\epsilon < \epsilon_c$ the minimization of the free energy with

respect to n gives the equilibrium value $n = 0$. When $\epsilon > \epsilon_c$, the free energy can be minimized

$$\left.\frac{\partial F}{\partial n}\right|_{n=0} = 0$$

to get

$$\zeta A(\epsilon_c - \epsilon) n_0^{\zeta-1} + 2\zeta B n_0^{2\zeta-1} = 0$$

or,

$$n_0^{\zeta} = \frac{A}{2B}|\epsilon_c - \epsilon|$$

Thus, above the threshold (CAP), the free energy minimum occurs for non-zero value of the order parameter. The order parameter scales as

$$n_0 \sim |\epsilon_c - \epsilon|^{\frac{1}{\zeta}} \sim |\epsilon_c - \epsilon|^{\frac{1}{\phi}-1} \tag{4.22}$$

see eq. 4.5. Therefore, we can now relate the exponent ξ with the crossover exponent ϕ as $\zeta = \phi/(1-\phi)$.

Consider the case of a Gaussian chain [79] where $\phi = 1/2$. Hence, $\zeta = 1$. Thus, for a Gaussian chain,

$$F = F_0 + A(\epsilon_c - \epsilon)n + Bn^2 \tag{4.23}$$

If we consider $\phi \simeq 0.59$ (see [29]), we obtain $\zeta \simeq 1.44$.

The phase transition corresponds to the disappearance of the minimum at $n = 0$ and the emergence of a lower minimum at a nonzero n. Since the value of n at the new minimum grows continuously from 0, the phase transition is said to be of second order.

Consider the PDF (probability distribution function) of the order parameter $P(n)$. This is related to the free energy of the chain as

$$F - F_0 = -\ln[P(n)/P(n_0)]$$

assuming $k_B T = 1$. Here n_0 is the reference value of the order parameter usually taken as $n_0 = 0$. However, since our simulations involve an anchored chain, we cannot obtain $n = 0$. We choose $n = 1/128$ as our reference point in our simulations for chains of length 128. The order parameter histogram obtained from the MC simulations can be used to calculate the free energy. The free energy, in this form, is plotted in Fig. 4.3 for several values of ϵ . This appears as a typical plot of Landau free energy for a second order phase transition. For $\epsilon < \epsilon_c$, there is a minimum at $n = n_0$. Since the fraction of adsorbed monomers cannot be negative, we restrict ourselves to $n \geq 0$. The value of the CAP of a homopolymer in the thermodynamic limit is determined to be

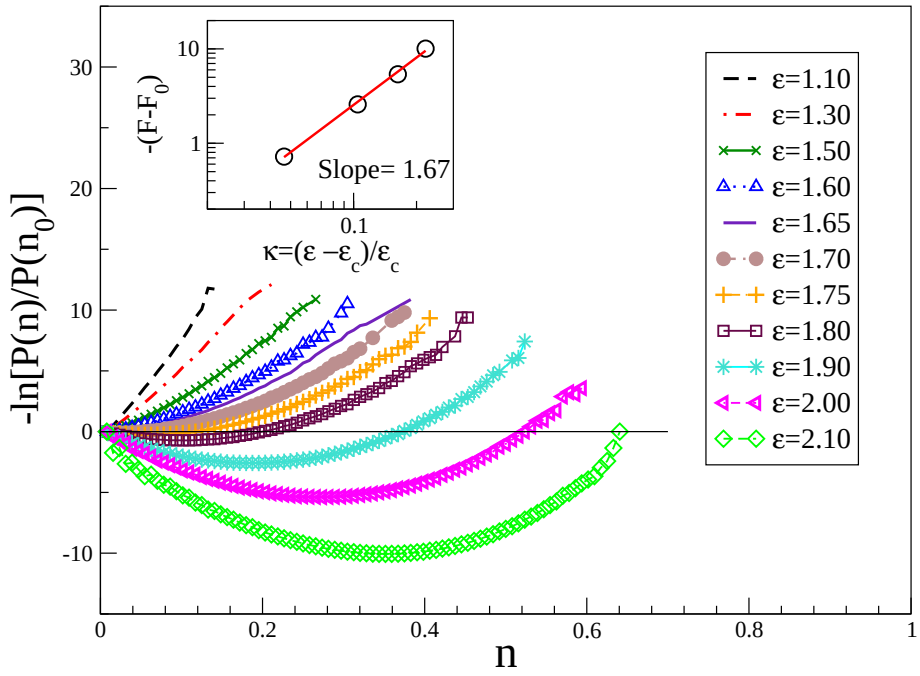

Figure 4.3: Landau free energy $F - F_0$ plotted against the order parameter for a polymer chain with $N = 128$ undergoing a phase transition of second order. The inset shows the free energy minima plotted against κ in double logarithmic coordinates. The inverse of the slope gives an estimate of ϕ.

$\epsilon_c(\infty) \simeq 1.72$ (see Sec. 4.6). For a chain of length $N = 128$, $\epsilon_c(N = 128) \simeq 1.66$. It is evident from Fig. 4.3, that for $\epsilon > 1.70$, the free energy shifts away from $n = 0$. Such behaviour is typical of second order phase transitions.

4.4 Scaling aspects of Multiblock Copolymer Adsorption

Consider now the adsorption of a regular multi-block copolymer which is built up from monomers A which attract (stick) to the substrate and monomers B which are neutral to the substrate. In order to treat the adsorption of a regular multi-block AB - copolymer we reduce the problem to that of a homopolymer which has been considered above. The idea is that a regular multi-block copolymer can be considered as a "homopolymer" where a single AB-diblock plays the role of an effective monomer [13]. For such a mapping we first estimate the effective energy of adsorption per diblock.

4.4.1 Effective energy of adsorption per diblock

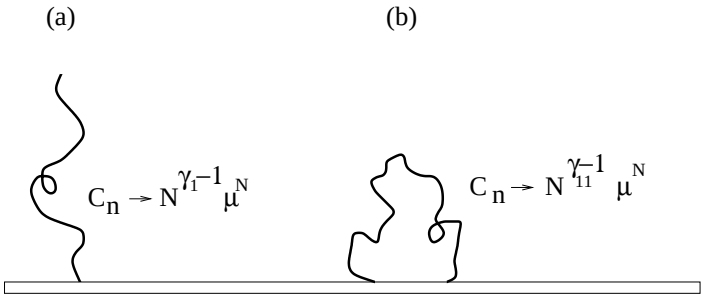

Figure 4.4: Polymer conformation with (a) one end and (b) both ends attached on the surface. The exponents γ_1 and γ_{11} correspond to the cases when one end is tethered to the surface (tail) or both ends are attached (loop) respectively.

Each individual diblock is made up of an attractive A-block of length M and a neutral B-block of the same length M. Upon adsorption the attractive A-block forms a string of blobs whereas the B-part forms a non-adsorbed tail (or loop) - (see Figure 4.5).

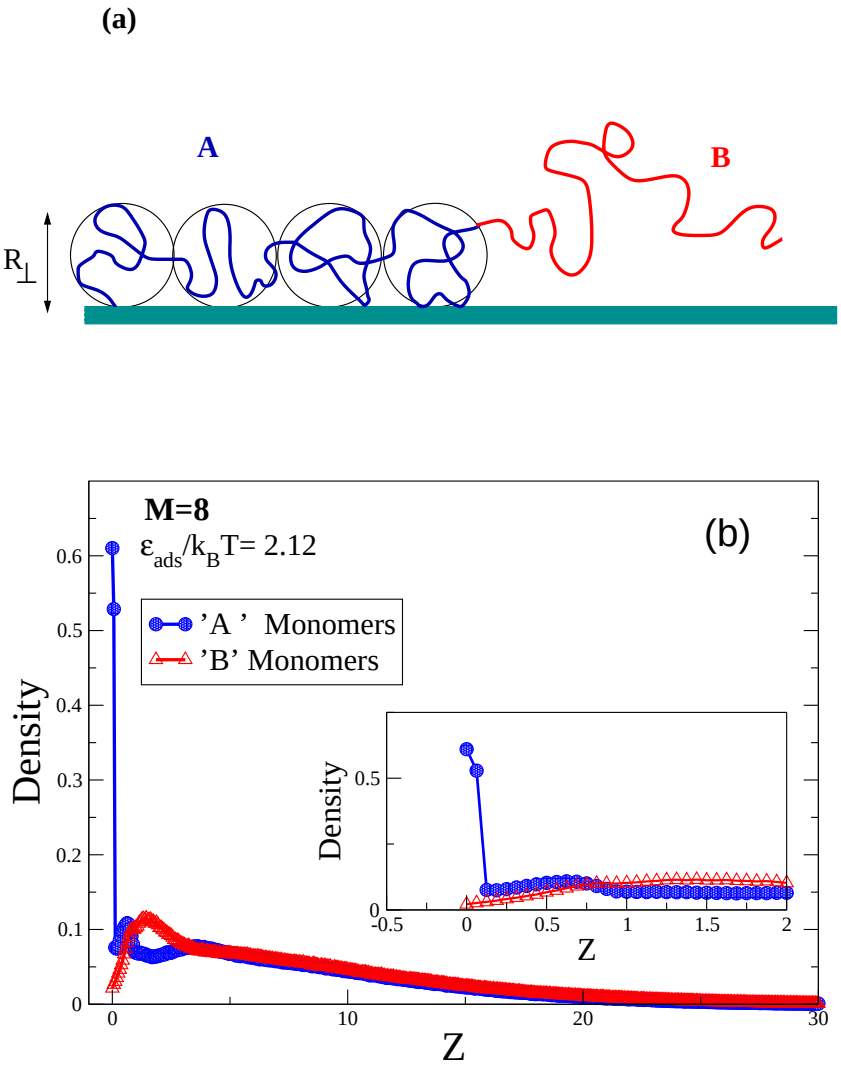

Figure 4.5: (a) Schematic representation of an individual adsorbed AB-diblock. The A - part forms a string of quasi-two dimensional blobs and the B-part is neutral regarding the substrate and its contribution to the free energy is of pure entropical nature. (b) Density profiles against distance z from the adsorbing plane of $A-$ and $B-$monomers at the CAP $\epsilon_{ads} = 2.12$ for a chain with $N = 256$ and block size $M = 8$. In the inset this is magnified for better visibility. The ratio of the number of $A-$ and $B-$monomers in the immediate vicinity of the attractive wall is about 30.

The free energy gain of the attractive block may be written according to eq 4.18 as

$$F_{\rm attr} = -\kappa^{1/\phi} M \tag{4.24}$$

where we measure the energy in units of $k_B T$ and $\kappa \equiv (\epsilon - \epsilon_c^h)/\epsilon_c^h$ measures the normalized distance from the CAP ϵ_c^h of a homopolymer. The neutral B-part which is most frequently a loop connecting adjacent A-blocks, but could also be a tail with the one end free, contributes only to the entropy loss. It is well known that the number of distinct configurations of a polymer of N links is given by $C_N \sim N^\gamma \mu^N$ where μ is a constant that depends on the model and γ is a universal constant [90]. In $3D$ - space $\gamma = 1.159$. The entropy associated with the conformations is $S \simeq \ln(C_N)$. For a chain tethered to a surface at one end or at both ends (see Fig. 4.4), the exponent γ is changed to $\gamma_1 = 0.679$ and $\gamma_{11} = -0.390$ respectively. Hence the free energy of a loop of length M that arises from the entropy loss when a polymer in bulk gets attached to a surface at both ends, is given by

$$F_{\rm rep} = (\gamma - \gamma_{11}) \ln M \tag{4.25}$$

In case that also the tails are involved, one should also use the exponent $\gamma_1 = 0.679$ albeit this does not change qualitatively the expression eq 4.25. They enter the partition function expressions for a free chain, a chain with both ends fixed at a two points, and for a chain, tethered by the one end [90]. Therefore the effective adsorption energy of a diblock is

$$E(M) = \kappa^{1/\phi} M - (\gamma - \gamma_{11}) \ln M \tag{4.26}$$

We may see from the MC simulations in Fig. 4.5b that the number of $A-$monomers in the immediate vicinity of the attractive wall substantially exceeds (by a factor of 30) the number of $B-$monomers although the chain is at the critical threshold for adsorption. The theoretical treatment which follows below takes this into account.

4.4.2 Order parameter

Now we consider a 'homopolymer' which is build up from effective units (diblocks), with the attractive energy given by eq 4.26. Let us denote the total number of such effective units by $\mathcal{N} = N/2M$. The fraction of effective units on the surface obeys then the same scaling law as given by eq 4.3, i.e.,

$$\frac{\mathcal{N}_s}{\mathcal{N}} = \mathcal{N}^{\phi-1} G\left(\Delta \mathcal{N}^\phi\right) \tag{4.27}$$

where now $\Delta \equiv (E - E_c^h)/E_c^h$ with the critical adsoption energy E_c^h of the renormalized homopolymer. Generally E_c^h is expected to be of the same order but different from ϵ_c^h

since these are model dependent parameters. Eq 4.27 is accurate if one require that (i) $\kappa \ll 1$ but $M \gg 1$ such that $\ln M \gg 1$ and $\kappa^{1/\phi} M \gg 1$, and (ii) $\mathcal{N} \gg 1$. The effective attraction E of a segment of the renormalized chain now depends on M according to eq 4.26.

Within each effective unit only M_s A-monomers will be adsorbed at criticality whereby this monomer number scales as

$$M_s = M^{\phi} G\left(\kappa M^{\phi}\right) \tag{4.28}$$

with $\kappa \equiv (\epsilon - \epsilon_c^h)/\epsilon_c^h$. The total number of adsorbed monomer is given by

$$N_s = \mathcal{N}_s M_s = \mathcal{N}_s M^{\phi} G\left(\kappa M^{\phi}\right) \tag{4.29}$$

It follows that the fraction

$$\begin{aligned} n \equiv \frac{N_s}{N} &= \frac{\mathcal{N}_s}{N} M^{\phi} G\left(\kappa M^{\phi}\right) = \frac{\mathcal{N}_s}{2\mathcal{N}} M^{\phi-1} G\left(\kappa M^{\phi}\right) \\ &= \frac{1}{2} M^{\phi-1} G\left(\kappa M^{\phi}\right) \left(\frac{N}{2M}\right)^{\phi-1} G\left(\Delta \left(\frac{N}{M}\right)^{\phi}\right) \quad , \end{aligned} \tag{4.30}$$

where we have used the scaling law, eq 4.27, for the effective units. Hence, the final expression for the order parameter can be written as follows:

$$n = \frac{1}{2^{\phi}} N^{\phi-1} G\left(\kappa M^{\phi}\right) G\left(\Delta \left(\frac{N}{M}\right)^{\phi}\right) \tag{4.31}$$

Thus we have expressed the order parameter n of a multi-block copolymer in terms of the chain length N, the block length M, the monomer attraction energy ϵ as well as the model-dependent homopolymer critical attraction energy ϵ_c^h. Let us consider now some limiting cases.

Close to criticality $\Delta = 0$

At the CAP of the multiblock chain one has $\Delta = 0$, thus one can estimate the deviation κ_c^M, of the corresponding critical energy of adsorption, ϵ_c^M, from that of a homopolymer, namely

$$\kappa_c^M \equiv \frac{\epsilon_c^M - \epsilon_c^h}{\epsilon_c^h} = \left(\frac{(\gamma - \gamma_{11}) \ln M + E_c^h}{M}\right)^{1/2} \tag{4.32}$$

where we have used eq 4.26 and set $\phi = 0.5$. Under this condition the second G - function in eq 4.31 is a constant, i.e., $G(0) = \text{const}$. On the other hand, with respect to a single effective unit the chain stays far from the criticality because of

$$\kappa_c^M \sqrt{M} = \sqrt{(\gamma - \gamma_{11}) \ln M + E_c^h} \gg 1. \tag{4.33}$$

Eq 4.33 reflects our simulation result, cf. Fig. 4.5b, and justifies the consideration of $A-$monomers as a string of blobs. In this case the first G - function in eq 4.31 behaves as $G(\kappa_c^M\sqrt{M}) \sim \kappa_c^M\sqrt{M}$ where κ_c^M now is fixed by eq 4.32. In result, eq 4.31 becomes

$$n \propto \left(\frac{(\gamma-\gamma_{11})\ln M + E_c^h}{N}\right)^{1/2} \tag{4.34}$$

State of the strong adsorption

In this regime $\kappa\sqrt{M} \gg 1$ and $\Delta\sqrt{N/M} \gg 1$ so that $n \simeq (1/\sqrt{N})G(\kappa\sqrt{M})G(\Delta\sqrt{N/M}) \sim \kappa\Delta$. Therefore,

$$n \simeq \frac{\kappa\left[\kappa^2 M - (\gamma-\gamma_{11})\ln M - E_c^h\right]}{E_c^h} \tag{4.35}$$

4.4.3 Gyration radius

The components of the gyration radius of a multi-block copolymer can be treated again by making use of the mapping on the homopolymer problem given by eqs 4.8 and 4.11. In doing so the mapping looks as follows:

$$\begin{aligned} a &\longrightarrow aM^\nu \\ \kappa &\longrightarrow \Delta = \frac{E-E_c^h}{E_c^h} \\ N &\longrightarrow \mathcal{N} = \frac{N}{2M} \end{aligned} \tag{4.36}$$

Thus the gyration radius component in direction perpendicular to the surface becomes

$$\mathcal{R}_{g\perp} = aN^\nu\,\mathcal{G}_{g\perp}\left(\Delta\left(\frac{N}{M}\right)^\phi\right) \tag{4.37}$$

In the strong adsorption limit $\Delta\sqrt{N/M} \gg 1$ and $\mathcal{R}_\perp \sim a\Delta^{-\nu/\phi}M^\nu$, which yields

$$\mathcal{R}_\perp \simeq \frac{aM^\nu {E_c^h}^{2\nu}}{\left[\kappa^2 M - (\gamma-\gamma_{11})\ln M - E_c^h\right]^{2\nu}} \tag{4.38}$$

In a similar manner, the gyration radius component parallel to the surface has the form

$$\mathcal{R}_{g\parallel} = aN^\nu\,\mathcal{G}_{g\parallel}\left(\Delta\left(\frac{N}{M}\right)^\phi\right) \tag{4.39}$$

which in the limit $\Delta\sqrt{N/M} \gg 1$ results in

$$\begin{aligned} \mathcal{R}_{g\parallel} &\simeq a\left(\frac{\Delta^{1/\phi}}{M}\right)^{\nu_2-\nu} N^{\nu_2} \\ &\simeq \frac{a\left[\kappa^2 M - (\gamma-\gamma_{11})\ln M - E_c^h\right]^{2(\nu_2-\nu)}}{M^{\nu_2-\nu}}\,N^{\nu_2} \end{aligned} \tag{4.40}$$

Like in the homopolymer case, one can define a blob length $g_{\rm eff} \sim (\mathcal{R}_\perp/a)^{1/\nu} \sim \Delta^{-1/\phi}\, M$ which in the strong adsorption limit, $\Delta \geq 1$, approaches the block length, $g_{\rm eff} \simeq M$, as it should be.

Also in the limit of strong adsorption, $\Delta\sqrt{N/M} \gg 1$, the ratio

$$\frac{\mathcal{R}_{g\|}}{\mathcal{R}_\perp} \simeq \left(\frac{\Delta^{1/\phi} N}{M}\right)^{\nu_2} \simeq \left(\frac{N}{g_{\rm eff}}\right)^{\nu_2} \tag{4.41}$$

leads to the correct scaling in terms of number of blobs, *i.e.* the 'effective homopolymer' built up of N/g_{eff} units behaves as a two dimensional SAW on the surface .

4.5 Random copolymer adsorption

Let us now turn to the case of random copolymers. Consider a random copolymer which is built up of N_p A-type and N_h B-type monomers. The sampled AB-sequences are frozen (i.e. a distinct sample does not change during the measurement) which corresponds to quenched disorder. The binary variable σ specifies the arrangement of monomers along the chain, so that $\sigma = 1$, if the monomer is of A-type (A-monomers attract to the surface) and $\sigma = 0$ otherwise (i.e. in case of neutral B-monomers). Let the fraction of attractive monomers (i.e., the composition) be $p = N_p/N$ and the fraction of neutral ones be $1-p = N_h/N$. We assume that the statistics of sequences is governed by the Bernoulli distribution [64], i.e., the corresponding distribution function looks like:

$$P\{\sigma\} = p\delta(1-\sigma) + (1-p)\delta(\sigma) \tag{4.42}$$

This distribution is a special case of the more general Markovian copolymers [64] when the "chemical correlation length" goes to zero. Two statistical moments , the mean and the variance, which correspond to the distribution eq 4.42 are

$$\begin{aligned} \langle\sigma\rangle &= p \\ \left\langle\theta^2\right\rangle &\equiv \left\langle[\sigma - \langle\sigma\rangle]^2\right\rangle = p(1-p) \end{aligned} \tag{4.43}$$

4.5.1 Composition and the critical ϵ_c

The adsorption of a random copolymer on a homogeneous surface has been studied by Whittington et al. [83, 61] within the framework of the annealed disorder approximation. Physically this means that during the measurements the chain touches the substrate at random in such a way that, as a matter of fact, one samples all possible distributions of monomers sequences along the backbone of the macromolecule. Following this assumption [83], let $c_N^+(n)$ be the number of polymer configurations such that

n units have contact with the surface simultaneously. The percentage of A-monomers (composition) is denoted by p. In the annealed approximation one then averages the partition function over the disorder distribution, i.e.,

$$\begin{aligned} Z(\epsilon) &= \sum_{n=1}^{N}\sum_{n_p=0}^{n} c_N^+(n)\binom{n}{n_p}p^{n_p}(1-p)^{n-n_p}\,\mathrm{e}^{\epsilon n_p} \\ &= \sum_{n=1}^{N} c_N^+(n)\;[p\mathrm{e}^{\epsilon}+1-p]^n = \sum_{n=1}^{N} c_N^+(n)\,\mathrm{e}^{n\,\epsilon_{\mathrm{eff}}^h} \end{aligned} \tag{4.44}$$

where $\epsilon_{\mathrm{eff}}^h$ is the attraction energy of an effective homopolymer. From eq 4.44 one can see that the annealed problem is reduced to that of a homopolymer where the effective attractive energy is defined as

$$\epsilon_{\mathrm{eff}}^h = \ln\left[p\mathrm{e}^{\epsilon}+1-p\right] \tag{4.45}$$

We know that at the critical point the homopolymer attraction energy, $\epsilon_{\mathrm{eff}}^h = \epsilon_c^h$, is model dependent. Then the critical attraction energy $\epsilon = \epsilon_c^p$ of a random copolymer reads

$$\epsilon_c^p = \ln\left[\frac{\exp\epsilon_c^h + p - 1}{p}\right] \geq \epsilon_c^h \tag{4.46}$$

where the composition $0 \leq p \leq 1$. At $p \to 0$ $\epsilon_c^p \to \infty$ whereas at $p = 1$ $\epsilon_c^p = \epsilon_c^h$. The relationship in eq 4.46 has been recently found to be confirmed by Monte Carlo simulations [95].

4.6 Results and Analysis

The determination of the critical adsorption point (CAP) is essential for testing the scaling results and for comparison with theory. We have determined the CAP from the analysis of different quantities: the order parameter n, and the gyration radius R_g based on scaling ideas. These methods are described as follows:

CAP from the order parameter

From the plots of the order parameter n against the adsorption energy ϵ, we determine the CAP as the point where the tangent taken at the inflexion point of the order parameter curve intersects the horizontal axis ϵ. This is shown in Fig 4.6(a), where the order parameter for a homopolymer chain of length $N = 256$ is plotted against the adsorption energy ϵ. Evidently, the order parameter n increases with growing

strength of the substrate potential ϵ. Thus the polymer chain undergoes a transition from a grafted, but otherwise detached state, to an adsorbed state whereby the chain lies flat on the surface plane - see Figure 4.1. In Fig 4.6(b), the order parameter is plotted against the adsorption energy for homopolymers of different lengths. The transition region narrows down as N increases, which is in good agreement with the scaling prediction of n, eq 4.20, in all cases. The corresponding critical adsorption potentials are plotted against the inverse chain lengths in the insert. Similar results are shown in Figure 4.7 for multi-block copolymer with block size $M = 2$. We observe that the corresponding plots for multiblock copolymers appear to be very similar to the homopolymers.

In the insets of Figures 4.6 and Figure 4.7, we see that the critical point $\epsilon_c^h(N)$ for homopolymers of chain length N as well as the critical points $\epsilon_c^M(N)$ for multi-block copolymers of chain length N with $M = 1$, $M = 2$, $M = 4$, $M = 8$, and $M = 16$, gradually increase as $N \to \infty$. By extrapolating the data to $1/N = 0$, one obtains the CAP values in the thermodynamic limit. Results for ϵ_c^h, obtained from the analysis of the order parameter are listed in Tables 4.1. In the last column of both tables we give the estimate from the intersection point of the respective R_g data which is described below.

Table 4.1: CAP

M/N	64	128	256	512	∞	R_g
1	2.47(3)	2.58(3)	2.63(3)	2.63(3)	2.672(30)	2.65(3)
2	2.32(3)	2.44(3)	2.47(3)	2.48(3)	2.52(2)	2.52(3)
4	2.13(3)	2.260(3)	2.29(3)	2.29(3)	2.34(2)	2.30(4)
8	1.93(3)	2.08(3)	2.12(3)	2.14(3)	2.19(3)	2.06(4)
16	1.76(3)	1.93(3)	2.00(3)	2.01(3)	2.06(3)	1.95(4)
p/N						
1.0	1.62(2)	1.66(2)	1.701(20)	1.698(25)	1.716(20)	1.718(20)
0.75	1.83(2)	1.89(2)	1.92(2)	1.946(20)	1.95(3)	1.95(3)
0.50	2.21(2)	2.25(2)	2.29(2)	2.32(2)	2.33(2)	2.38(5)
0.25	2.81(4)	2.97(4)	2.98(4)	3.02(4)	3.05(5)	2.91(6)

From the components of R_g

According to eqs 4.10, 4.13, and 4.17, one should expect that all curves of $R_{g\perp}^2/R_{g\parallel}^2$, for different chain length N intersect at a fixed point which gives the CAP in the limit

of $N \to \infty$. In Figure 4.8, we illustrate this method by plotting the ratio $R^2_{g\perp}/R^2_{g\parallel}$ vs ϵ for copolymers with block size $M = 2$. The curves for different N intersect nearly at a single intersection point. The CAP obtained from this method, $\epsilon_c^{M=2} = 2.52(3)$ is consistent with the estimate from the order parameter method where $\epsilon_c^{M=2} = 2.521(20)$. The CAPs $\epsilon_c(M)$ for homopolymers, multi-block copolymers with different block size M, and for random copolymers are listed in Table 4.1.

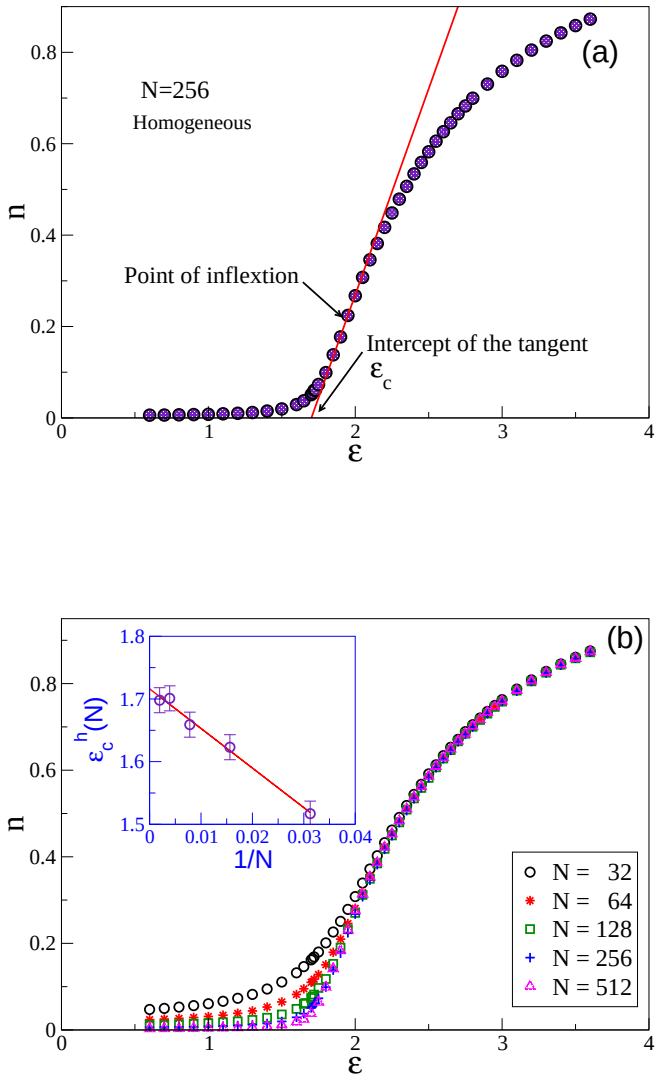

Figure 4.6: (a) The order parameter n is plotted against the ϵ for a chain of length $N = 64$ and with block size $M = 2$. The point where the tangent at the point of inflexion on the curve meets the abscissa is the CAP . (b) The order parameter n against the adsorption energy ϵ for homopolymers of different chain lengths N. The value of the CAP $\epsilon_c^h(N)$ for $N \to \infty$ is extrapolated from the log-log plot of $\epsilon_c^h(N)$ versus $1/N$ as shown in the insert. In the thermodynamic limit (a) $\epsilon_c^h \approx 1.716$.

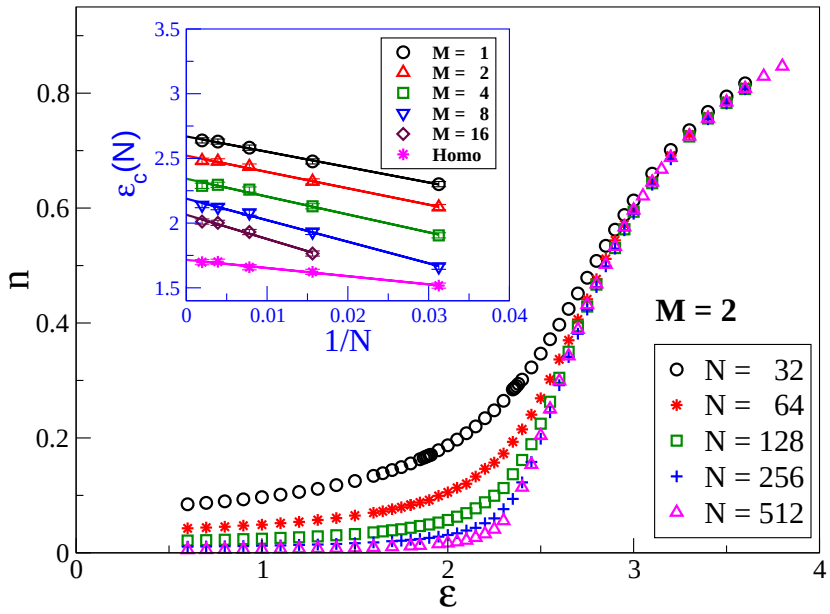

Figure 4.7: The order parameter n plotted as a function of attractive energy ϵ for copolymers with block size $M = 2$. The extrapolation plots for $\epsilon_c(N)$ versus $1/N$ for block sizes $M = 1$, 2, 4, 8, 16, and for the homopolymer, plotted versus $1/N$, are shown in the insert.

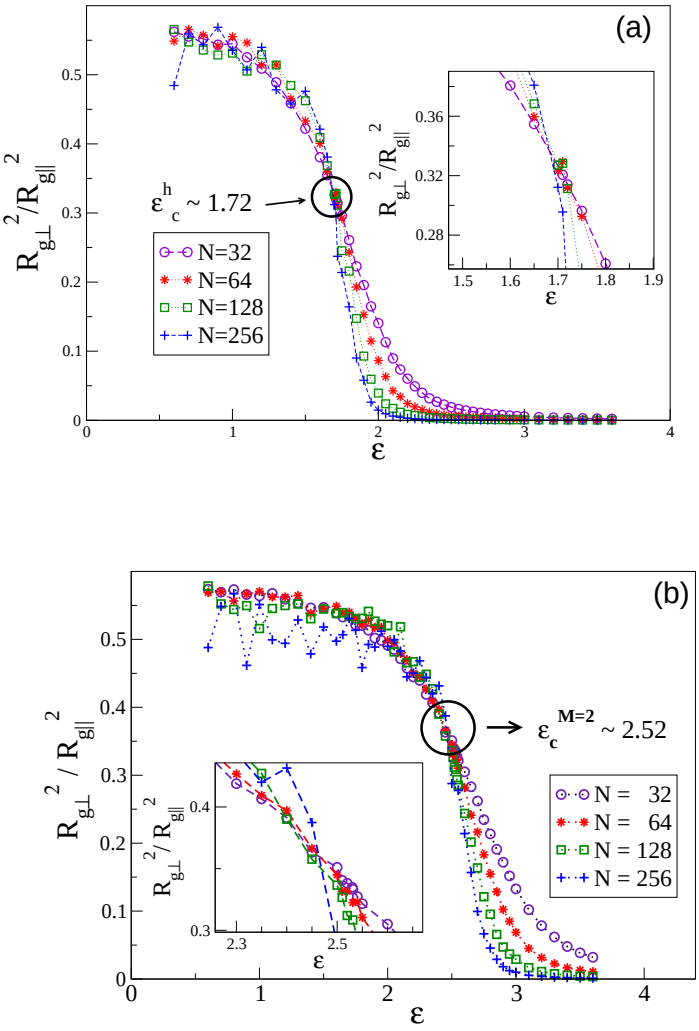

Figure 4.8: The ratio of $R_{g\perp}^2/R_{g\parallel}^2$ plotted as a function of ϵ for (a) homopolymers and (b)copolymers with block size $M = 2$. The critical point is determined by the intersection of all curves which are found to be at $\epsilon_c^h \approx 1.72$ for the homopolymers and $\epsilon_c^{(M=2)} \approx 2.52$ (M=2).

4.6.1 Scaling behavior

From the data for the CAP one may check the value of the crossover exponent $\phi = 0.50$ by plotting the order parameter n vs. N

Now , as mentioned before in eq 4.5, the scaling behaviour of the order paramenter goes as

$$n \propto \begin{cases} 1/N & , \quad \text{for} \quad \kappa << 0 \\ N^{\phi-1} & , \quad \text{for} \quad \kappa \to 0 \\ \kappa^{(1-\phi)/\phi} & , \quad \text{for} \quad \kappa \gg 1 \end{cases}$$

Therefore, in a double logarithmic plot of the order parameter n against N, the slope is expected to be $\phi - 1$.

This is illustrated in Figure 4.9 as a double logarithmic plot of n vs. N for the case of (a) homopolymers and (b) $M = 1$, i.e., regular alternating polymers. Figure 4.9 demonstrates clearly that the slope of the n vs N curves in logarithmic coordinates is nearly equal to $\phi - 1 = -0.5$ only in the cases where the strength of the substrate potential nearly equals the CAP value ϵ_c , in agreement with the relation $n \propto N^{\phi-1}$. As in the case of homopolymers (eq 4.5), Figure 4.9b shows that in the strongly adsorbed regime ($\epsilon = 3.40$ for $M = 1$) above the CAP the order parameter $n \propto N^0$ (independent of chain length). In contrast, far below the CAP, only the anchoring monomer is attached to the substrate, $n \sim N^{-1}$, as in the asymptotic limit $N \to \infty$ of homopolymers. This is observed for $\epsilon = 0.60$ for the alternating chains ($M = 1$).

In Figure 4.10, we consider the order parameter scaling behavior for two different block sizes $M = 8$ and $M = 1$. We see that the curves collapse to a master curve when scaled appropriately. The straight lines represent the predicted asymptotic behaviour. For small block size $M = 1$, we see that the curves follow the expected scaling predictions very well. However, for larger block size $M = 8$, there are clear deviations from the predictions.

Turning now to the scaling of the radius of gyrations, we present the results for $R_{g||}$ and $R_{g\perp}$ in a scaled form for different chain lengths. The straight lines indicate the theoretically predicted scaling behaviour. We observe that the curves fit well to a master curve and that the expected power law behaviour is very well obeyed by the perpendicular component $R_{g\perp}$.

In Figure 4.12 we present the corresponding results for the components of the mean square gyration radius, $R^2_{g||}$ and $R^2_{g\perp}$, in scaled form in terms of the parameter κN^ϕ for regular block-copolymers with block size $M = 1$ and $M = 8$. Generally, one observes a good agreement with the predictions of Section 4.3 for $M = 1$. Considerable deviations from the expected scaling behavior are observed only in Figure 4.12b where the effective

segment of a diblock with $M = 8$ is comparatively large for the simulated chain lengths $N \leq 512$, meaning *effective* chain lengths of $N_{eff} = N/16 \leq 32$ which are definitely too short for a well pronounced scaling behavior to be demonstrated. Simulations with much longer chain lengths is unfeasible by the method used in this study.

4.6.2 Phase diagram of multi-block copolymer adsorption

Using the values for the CAP, given in Table 4.1, one may construct a phase diagram showing the relative increase of the critical potential $\epsilon_c(M)$ compared to that of a homopolymer against (inverse) block size M. This is one of the central results of the present study. In Figure 4.13 one may see that the line of critical points, defining the region of adsorption, is a steadily growing function of the inverse block size M^{-1}. Evidently, the theoretical result, eq 4.32, appears to be in good qualitative agreement with simulation data . As far as eq 4.32 comes as a result of scaling analysis, it can be verified only up to a factor of proportionality. As mentioned in Section 4.3.1, the CAP of a homopolymer, ϵ_c^h, is of the same order as that of the "renormalized" chain consisting of diblocks, E_c^h. Thus from a fit of the data points with the expression eq 4.32 one may actually determine E_c^h. Therefore, one gets $E_c^h = 3.306$, that is, one gets values which are two to four times larger than the CAP values of a homopolymer.

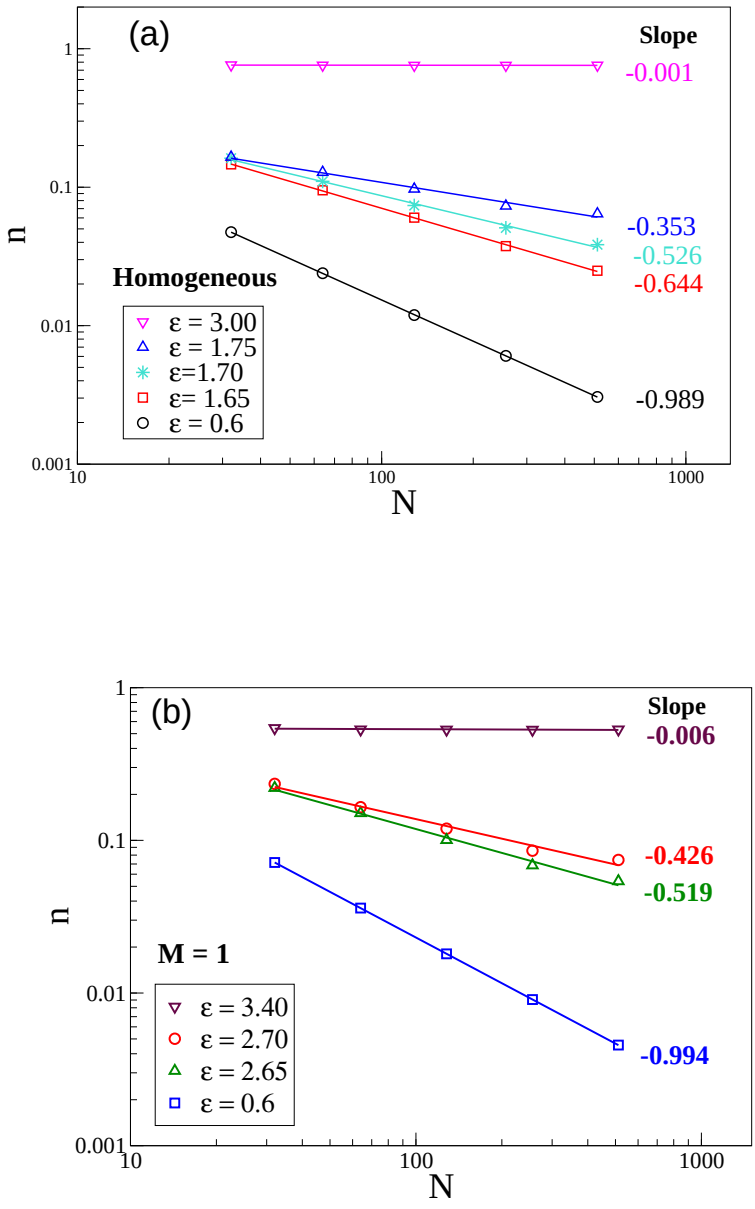

Figure 4.9: Log-log plot of the order parameter n vs N for (a) homopolymers and (b) block copolymers with block size ($M = 1$). The value of ϵ for each curve is given in the legend while the slope is also indicated. One may readily check that the straight lines with slope ~ 0.5 correspond to the corresponding values of ϵ_c ,

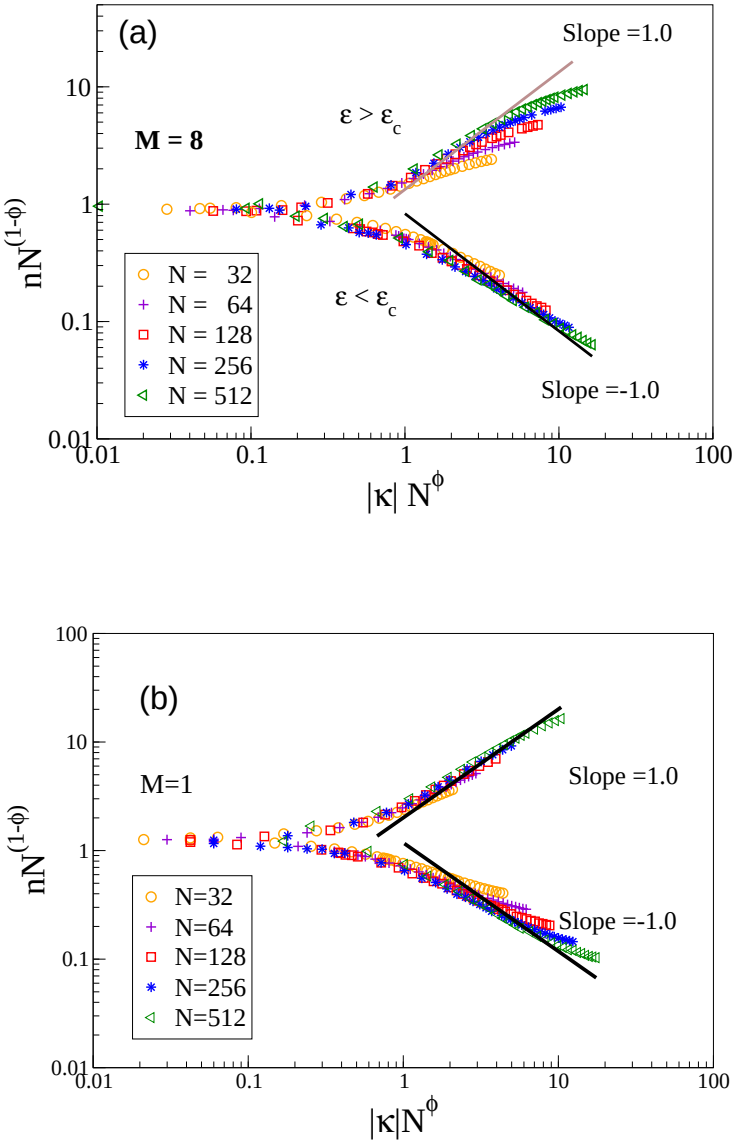

Figure 4.10: Log-log plots of the scaled order parameter $nN^{1-\phi}$ vs κN^{ϕ} for two different block sizes : (a) $M = 8$ and (b) $M = 1$. The straight lines indicate the asymptotic behavior of the scaling functions given by eq 4.31.

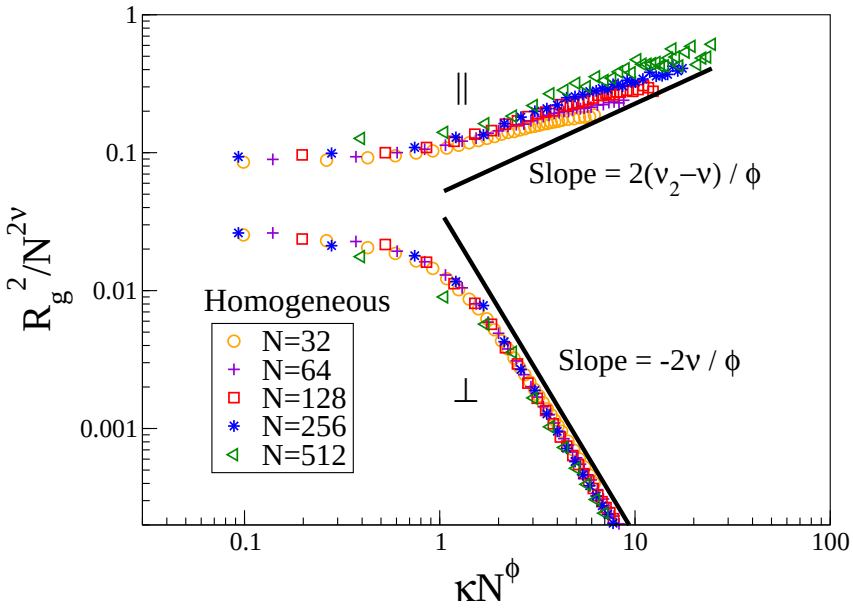

Figure 4.11: Log-log plots of the gyration radius components $R^2_{g\|}/N^{2\nu}$ and $R^2_{g\perp}/N^{2\nu}$ vs κN^{ϕ} with $\nu = 0.588$ and $\nu_2 = 3/4$ for homopolymers. The straight lines indicate the asymptotic behaviour of the scaling functions given by eq 4.10 and 4.13.

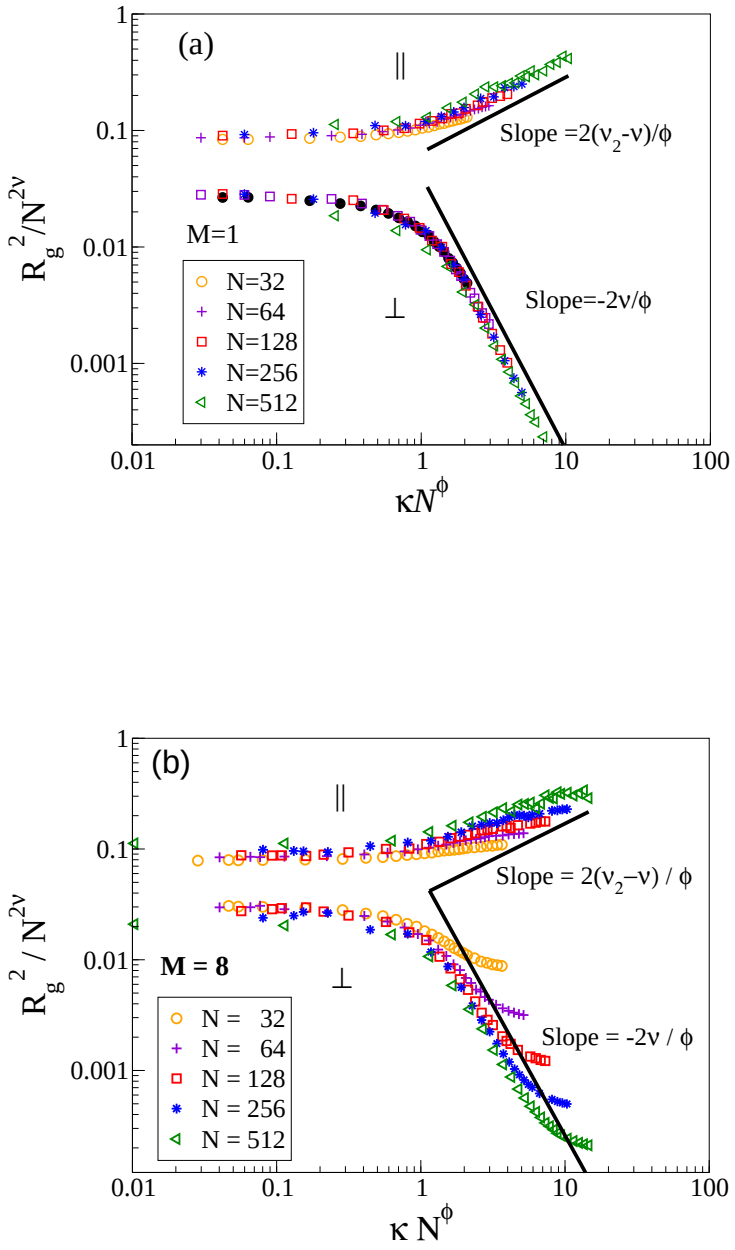

Figure 4.12: Log-log plots of the gyration radius components $R^2_{g\|}/N^{2\nu}$ and $R^2_{g\perp}/N^{2\nu}$ vs κN^{ϕ} with $\nu = 0.588$ and $\nu_2 = 3/4$ for Block copolymers with block size (a) $M = 1$ and (b) $M = 8$. The straight lines indicate the asymptotic behaviour of the scaling functions given by eq 4.31, 4.10 and 4.13.

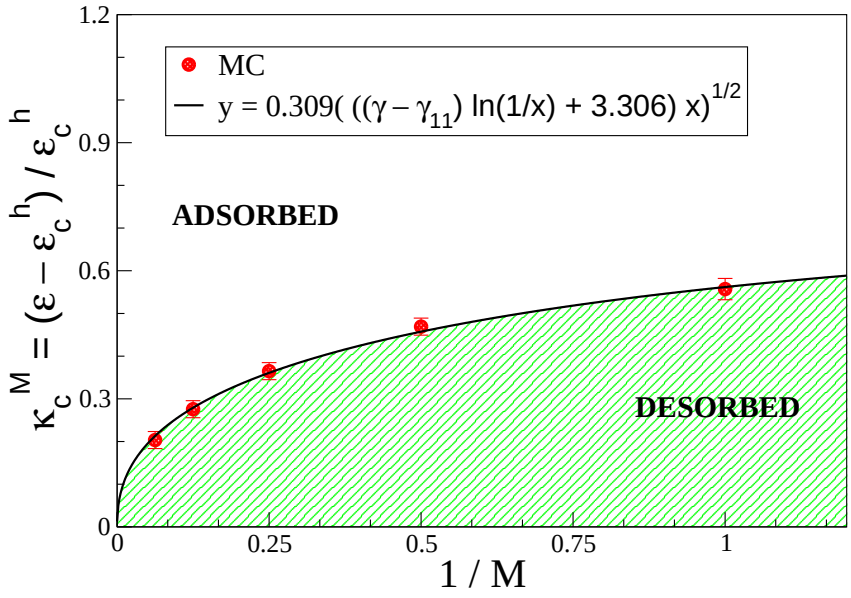

Figure 4.13: $\kappa_c^M = (\epsilon_c^M - \epsilon_c^h)/\epsilon_c^h$ plotted vs $1/M$ for multi-block copolymers with various values of M. The critical point of adsorption for homopolymers is $\epsilon_c^h = 1.72$. The red symbols denote the simulation results while the curve gives the best fit of eq 4.32, $\kappa \propto \left(\frac{(\gamma-\gamma_{11})ln(M)+E_c^h}{M}\right)^{1/2}$. Note that the block size $1 \leq M \leq 16$.

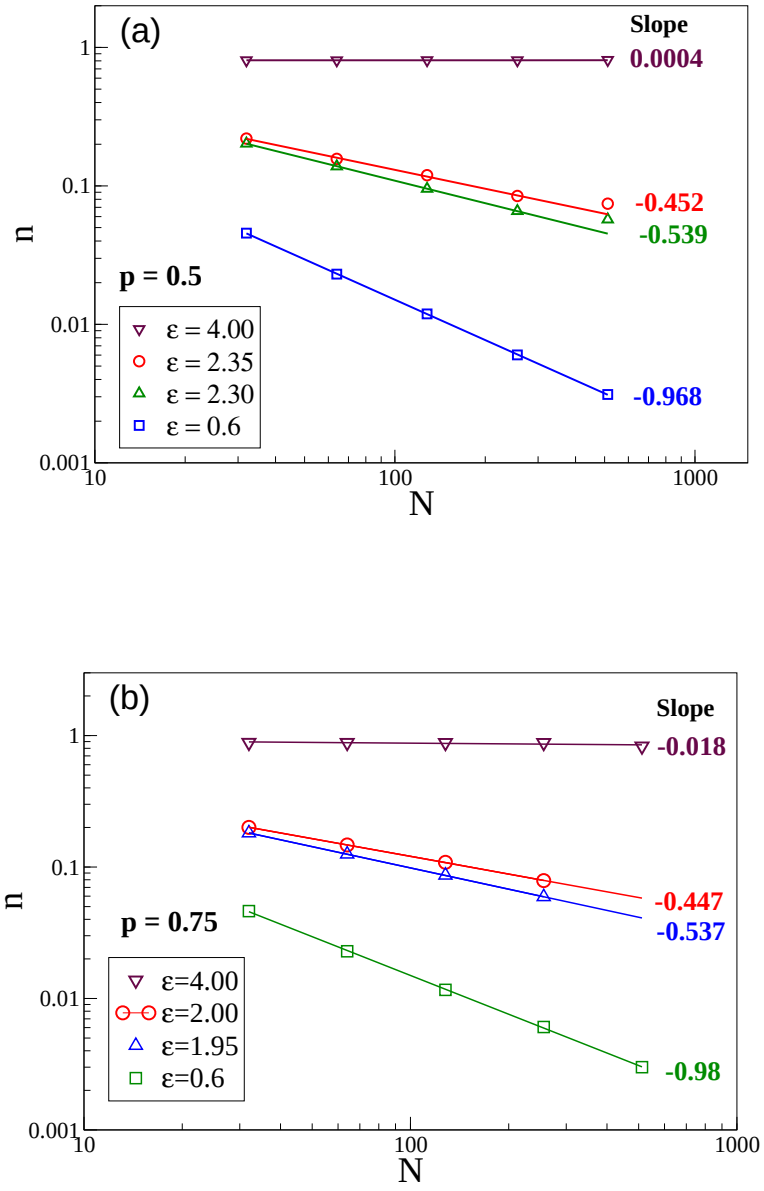

Figure 4.14: The same as in Figure 4.9 but for random copolymers with the composition (a) $p = 0.5$ where $\epsilon_c^p = 2.33$ and (b) $p = 0.75$ where $\epsilon_c^p = 1.95$.

4.6.3 Random Copolymers

In this section we examine the adsorption transition of random copolymers with quenched disorder and average percentage p of the A monomers. In addition to testing the scaling behavior, we also check to what extent one may employ the theory developed within approximation of "annealed disorder" for the description of the CAP properties. We performed Monte Carlo simulations for heterogeneous random copolymers of chains lengths $32, 64, 128, 256$ and 512 with different fraction of attractive monomers ($p = 0.125, 0.25, 0.50$ and 0.75).

It has been pointed out earlier [87, 60] that the crossover exponent stays the same, $\phi = 0.5$, also in the case of random copolymers. The simulations in the present study demonstrate this in Figure 4.14 where qualitatively the observed picture is similar to that of Figure 4.9 - small deviations in the attraction potential ϵ, which was used when sampling the values of the order parameter n, manifest themselves in significant changes of the log-log slope $1 - \phi$ from the expected value of -0.5.

In Figure 4.15 we demonstrate that the scaling of the mean square gyration radius components, which we discussed before with regard to the multiblock copolymers, holds also for random copolymers with different composition p. Again the value of $\phi = 0.5$ gives best scaling results. Thus it turns out that the composition affects only the value of the CAP ϵ_c^p.

In Figure 4.16 we present a plot of the critical point of adsorption against the fraction of attractive monomers. The full line corresponds to the theoretical prediction [83], eq 4.46. Given that there are no fitting parameters in this equation, one finds a very good agreement between theoretical predictions and simulation results as well as with very recent simulation results [95] which demonstrates that the adsorption of random copolymers can be properly described within the scope of the annealed approximation. This confirms an earlier theoretical result derived in a somewhat different context (heteropolymer coil-globule transition) by Grosberg and Shakhnovich [40]. Figure 4.16 also indicates that this approximation breaks down for chains which are not random [95] - at 50% composition the CAPs of regular block copolymers are clearly off the theoretical prediction, eq 4.46. As far as polymer adsorption is greatly facilitated by the formation of trains of monomers on the substrate [95], the larger the block size M, the lower the respective CAP ϵ_c^M under the line, eq 4.46. No monomer trains are possible in the case of alternating chains which results in an $\epsilon_c^{M=1} > \epsilon_c^p$. Thus from the position of the CAPs on Figure 4.16 one may conclude that the mean length of an A-train on the substrate at $p = 0.5$ is close to four.

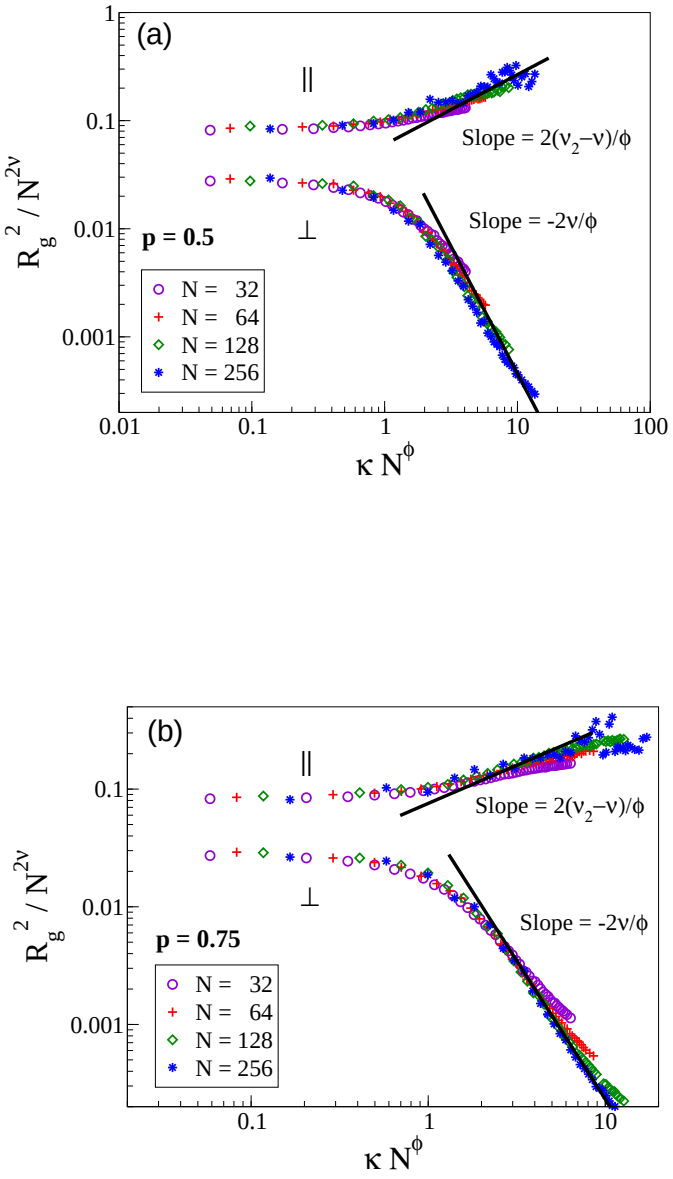

Figure 4.15: Log-log plots of the gyration radius components $R^2_{g\|}/N^{2\nu}$ and $R^2_{g\perp}/N^{2\nu}$ vs κN^{ϕ} with $\nu = 0.588$ and $\nu_2 = 3/4$ for random copolymers at different composition p.

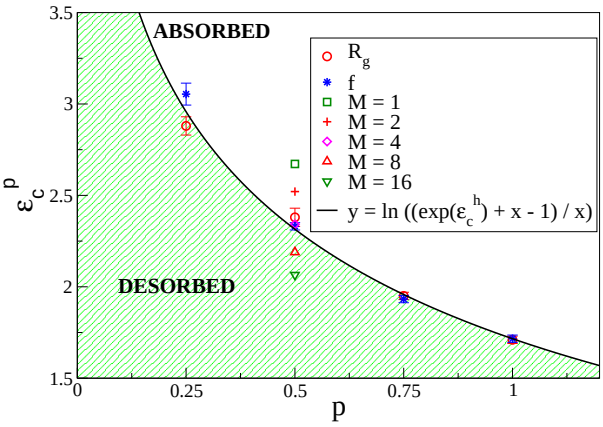

Figure 4.16: The CAP, ϵ_c^p, plotted vs the composition p for random copolymers. The curves give the best fit of eq 4.46, $\epsilon_c^p = \ln\left[\frac{\exp\epsilon_c^h + p - 1}{p}\right] \geq \epsilon_c^h$, The critical points of adsorption for homopolymers are $\epsilon_c^h = 1.716$. Symbols denote the CAP for multiblock copolymers with block size M.

4.7 Discussion

The main focus of this chapter has been the adsorption transition of random and regular multiblock copolymers on a rigid substrate. We have used Monte Carlo simulations to study the adsorption transition and to test scaling predictions at criticality. The simulation model used is an off-lattice coarse-grained bead-spring model of polymer chains which interact with a structureless surface by means of a contact potential when an A-monomer comes close enough to be captured by the adsorption potential. The simulation results are in good agreement with the scaling predictions.

The central result of the study presented in this Chapter is the phase diagram of regular multiblock adsorption which gives the increase of the critical adsorption potential ϵ_c^M with decreasing length M of the adsorbing blocks. For very large block length, $M^{-1} \to 0$, we find that the CAP approaches systematically that of a homogeneous polymer (see Fig. 4.13). We have demonstrated that the phase diagram, derived from computer experiment agrees well with the theoretical prediction based on scaling considerations.

The phase diagram for random copolymers with quenched disorder which gives the change in the critical adsorption potential, ϵ_c^p, with changing percentage of the sticking A-monomers, p, is also determined from extensive computer simulations. We observe perfect agreement with the theoretically predicted result which has been derived by treating the adsorption transition in terms of the "annealed disorder" approximation.

We show how some basic polymer chain properties of interest such as the gyration radius components perpendicular and parallel to the substrate, or the fraction of adsorbed monomers at criticality, scale when a chain undergoes an adsorption transition. An important conclusion concerns the value of the universal crossover exponent $\phi = 0.5$ which is found to remain unchanged, regardless whether homo-, regular multiblock-, or random polymers are concerned. Thus the universality class of the adsorption transition of a heteropolymer is the same as that of a homopolymer. Having studied the equilibrium behaviour of polymers at surfaces, the next step is to study the kinetics. The next Chapter deals with the kinetics of polymer adsorption at plane surfaces.

Chapter 5

Kinetics of adsorption

5.1 Introduction

Let us now consider the time dependent aspects of adsorption. The theory of the kinetics of polymer adsorption is less developed than that of equilibrium adsorption. In fact, the kinetics of adsorption of a single homopolymer chain is a non-trivial and challenging problem and is the focus of this chapter.

In this section, we briefly review some of the earlier numerical studies of the kinetics of adsorption of single polymer chains.

There are two broad classes of polymer-adsorption described in literature : chemisorption and physisorption. Chemisorption is characterized by a small local monomer sticking rate and usually occurs due to covalent bonds between the monomers and the surface. This is important in many technological applications. In such cases, the relaxation kinetics is slowed down sharply and the process may be considered to be irreversible on an experimental time scale. The monomer sticking energy is usually large (at least one or more orders of magnitude greater than k_BT) and there is usually a significant activation barrier associated with the adsorption of monomers. Physisorption , on the other hand, typically occurs at a much faster rate . It often arises from hydrogen bonding or other dipolar forces, dispersion forces or attractions between charged groups. The activation barrier associated with monomer adsorption in this case is often negligible. The monomer sticking energy can sometimes be large ($\epsilon > k_BT$). For example, oxidized metal or silicon based surfaces can form hydrogen bonds with many polymers. For strong sticking energies, the relaxation dynamics may become very slow leading to strong non-equilibrium effects.

Konstadinidis *et. al.* [49] carried out dynamical Monte Carlo simulations for single chains on a cubic lattice. They studied the configurational distribution after performing dynamic simulations with a completely irreversible adsorption model and a reversible one in which a move resulting in the desorption of a segment occurred with a probability

$\exp(\chi_s)$. They observed that for $\chi_s > 2k_BT$, the fraction of loop and train segments start to deviate from the equilibrium values and at $\chi_s \simeq 10k_BT$, the fraction of segments in loops and trains merges with the corresponding values of the totally irreversible model. Cosgrove *et al.* [46] have used Monte Carlo simulations of single chains on cubic lattices to study the evolution of structure of polymers undergoing adsorption in strong and weak adsorption regimes. Shaffer [77] has studied the problem using Monte Carlo simulations with the bond fluctuation model (BFM) for strong sticking energies. He investigated the time required for adsorption, τ_{ads}, as a function of the chain length and the chemical composition of the chains. He carried out simulations for homopolymers as well as diblock and random copolymers. The copolymers were composed of two kinds of monomer segments, one of which adsorbed strongly at the surface while the other was neutral to the surface. The relaxation function for the adsorption is defined as

$$q(t) = \frac{n(t) - n_{eq}}{n(0) - n_{eq}} \tag{5.1}$$

where $n(t)$ is the number of segments adsorbed at time t, $n(0)$ is the number of segments at time $t = 0$ and n_{eq} is the number of segments adsorbed at equilibrium. The relaxation function was found to have a simple exponential decay during most of the adsorption process. During the late stages, however, the relaxation function was found to deviate from an exponential. According to Shaffer, the late stage deviation might be due to artefacts of the lattice model. He defined the relaxation time as the time constant for the relaxation in the intermediate region. This time constant was found to have a power law dependence on the chain length. The main result of Shaffer [77] is that $\tau_{ads} \sim N^{1.58}$ with excluded volume and $\tau_{ads} \sim N^{1.50}$ without excluded volume for homopolymers. For diblock copolymers, the adsorption time of single chains was found to be almost independent of the non-adsorbing block length. Since there was no activation barrier for monomer adsorption, these results correspond to physisorption.

The same scaling for homopolymers has been found by Ponomarev *et al.*[70] who also used the BFM for $N \leq 100$. Apart from the energy gain (per segment) of ϵ_s, an additional activation barrier ϵ_b for a segment to access the surface was introduced in this simulation, defining thus a "temperature" $T_b \equiv k_BT/\epsilon_b$. This sets a characteristic time for the passage of a segment across the barrier $\tau_b = \tau_0 \exp(1/T_b)$. Different adsorption dynamics has then been found, depending on the ratio of τ_b and the Rouse time: $\tau_b/\tau_R \simeq N^{-2\nu-1} \exp(1/T_b)$. The case $\tau_b/\tau_R \ll 1$ (at $T_b \geq 1$) corresponds to *strong physisorption*. On the other hand if the chain is relatively short and the barrier is high enough (T_b is low enough) then $\tau_b/\tau_R \gg 1$, which corresponds to *chemisorption*.

They argue that at $\tau_b/\tau_R \ll 1$ the adsorption follows a *zipping mechanism* whereby the chain adsorbs predominantly by means of sequential, consecutive attachment of monomers, a process that quickly erases existing loops. The process is fast and the

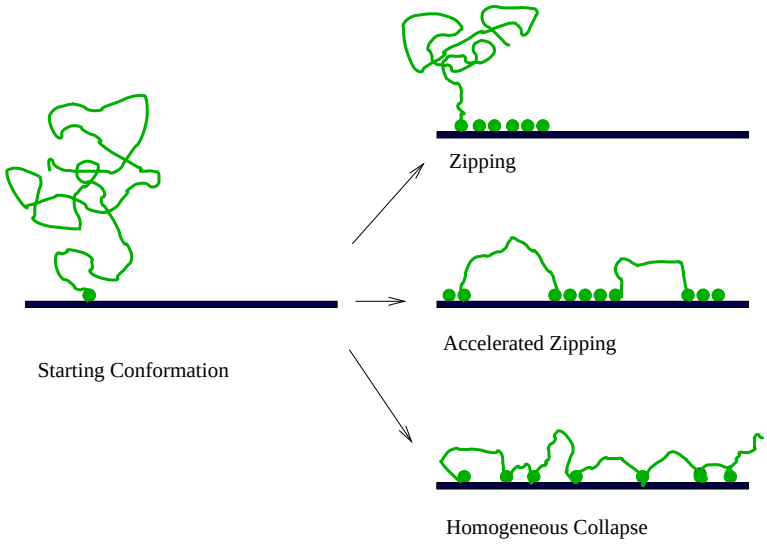

Figure 5.1: Schematic diagram of the different modes of adsorption of a single chain : simple zipping, accelerated zipping and homogeneous collapse.

characteristic adsorption time τ_{ads} is smaller than the relaxation time of the chain. In this case $\tau_{\rm ads} \sim N^{1.57}$ for a SAW chain in agreement with Shaffer's results [77]. In the opposite limit (chemisorption), the presence of a barrier enhances loop formation in the course of adsorption. This is because a large number of monomer-surface collisions are required to overcome the barrier. It was shown that in the presence of even a modest local barrier, zipping is quenched and a new mechanism involving loop formation is favoured. The characterstic adsorption time $\tau_{\rm ads}$ is greater than the relaxation time of the tethered chain. The scaling law now reads $\tau_{\rm ads} \sim N^{\alpha}$, where the exponent $\alpha = 0.8 \pm 0.2$.

The irreversible chemisorption from the dilute polymer solution has been theoretically studied [5, 66] by making use of scaling theory and the master equation (ME) method [89] for the loops distribution function. The authors suggest that there are three modes of chemisorption : zipping , accelerated zipping , and homogeneous collapse. The three modes are depicted in Fig. 5.1 The authors argue that for dilute solutions, the process is dominated by *accelerated zipping* when the sequential adsorption is disrupted by large loops formation.

For strong physisorption the *simple zipping* mechanism, as opposed to the accelerated zipping, has been also recently considered by Descas, Sommer and Blumen [21]. The authors [21] used the BFM and suggested a simple theoretical description of the corresponding adsorption dynamics based on what they call a "stem - corona" model.

This leads to the scaling prediction, $\tau_{\text{ads}} \sim N^{1+\nu}$, which is in reasonably good agreement with the simulation result. In the model proposed by the authors, the polymer chain is described by an adsorbate portion connected to the non-adsorbed monomers (corona) by a stretched part (stem). During the main stage of adsorption, the stem grows at the expense of the corona. This leads to a greater separation of the corona and the surface which supresses further nucleation events *i.e.* formation of large loops. Hence the process is dominated by zipping.

We have investigated the case of strong physisorption by means of an off-lattice dynamic MC method. The simulations make it possible to describe the adsorption dynamics not only in terms of the average fraction of adsorbed segments but also to include train and tail distribution functions which furnish the main constituents of the dynamic adsorption theory. Our observations indicate that the dominant mechanism of adsorption is the zipping process. Based on inputs from the simulations, we have proposed a "stem-flower model describing the dynamics of adsorption, which shares many common features with the one suggested by Descas *et al.* [21]. We have used this model within the ME-formalism to treat the time evolution of the distribution of adsorbed monomers (as well as the distributions of the monomers forming trains and tails). The problem was mapped onto a drift-diffusion process governed by a Fokker-Planck equation. The MC findings are in good agreement with the theoretical predictions. We have also investigated the adsorption of regular multi-block and random copolymers using dynamic MC. However, the theory, in this case is yet to be developed in these cases.

In the following sections we first discuss the MC model and then present a detailed description of the adsorption dynamics model which shares many common features with the one suggested by Descas *et al.* [21]. In Section 5.4 we present the main results obtained from simulations as well as from the ME. We show that our MC-findings are in good agreement with the theoretical predictions. We summarize our results and conclusions in Section 5.5. Some details of the train distribution function calculation are relegated to the Appendix.

5.2 Monte Carlo Simulation Model

The dynamic Monte Carlo method is based on a Markov process that provides a rule whereby a system changes from one state to another. The choice of moves is arbitrary to some extent as it does not represent the real physical evolution of the system.

We have used the classic Metropolis algorithm for the kinetic simulations. A Monte Carlo step consists of attempting a transition to a new configuration choosing from a set of allowed moves. The attempt is accepted with a probability, $\min\left[1, \exp\left(-\Delta U/k_B T\right)\right]$,

where ΔU is the difference between the final and initial energy. The interpretation of Carlo Monte dynamics is that it is equivalent to solving numerically the Master Equation

$$\frac{\partial P_n(t)}{\partial t} = -\sum_{m \neq n} [P_n(t) W_{n \to m} - P_m(t) W_{m \to n}]$$

where $P_n(t)$ is the probability of the system being in state n at time t and $W_{n \to m}$ is the probability of the transition $n \to m$. The Metropolis algorithm is stochastic. What is important is not a single trajectory but the trajectories averaged over the randomness. We have used the off-lattice bead spring model [58] described in Chapter 2 to investigate the adsorption kinetics of a single chain on a solid substrate. The dynamics is realized only by *local moves*. Our system consists of a single chain tethered at one end to a flat structureless surface. The chains length is varied between 32 and 256. The size of the box is $64 \times 64 \times 64$. We use periodic boundary conditions in the $x - y$ directions and impenetrable walls in the z direction. The adsorbing wall is at $z = 0$. While investigating copolymers, we had two kinds of monomers: "A" and "B", of which only the "A" type feels an attraction to the surface. The surface interaction of the "A" type monomers is described by a square well potential $U_w(z) = \epsilon$ for $z < \delta$ and $U_w(z) = 0$ otherwise. Here ϵ/k_BT is varied from 2.5 to 10.0. The effective bonded interaction is described by the FENE (finitely extensible nonlinear elastic) potential described in Chapter 2. The nonbonded interactions are described by the Morse potential.

Apart from homopolymers, we have also studied copolymer chains with block size M between 1 and 16 and random copolymers (with a fraction of attractive monomers, $p = 0.25,\ 0.5,\ 0.75$). The time is given by Monte Carlo Steps (MCS). For a chain length of N, a Monte Carlo Step is elapsed after N attempts of elementary moves in which each monomer has an equal chance of performing a move.

Before the surface adsorption potential is switched on, the polymer chain is equilibrated by the MC method for a period of about 10^6 MCS whereupon one performs 1000 measurement runs, each of length 2×10^6 MCS with the surface adsorption potential switched on. Therefore, at the starting conformation of the physisorption is always a new equilibriated, anchored but non-adsorbed chain configuration. The numbers provided here are for a chain of length 256. For shorter chains, length of the runs are shorter.

In the case of random copolymers, for a given composition, i.e., percentage p of the $A-$monomers, we create a new polymer chain in the beginning of the simulation run by means of a randomly chosen sequence of segments. This chain is then sampled during the course of the run, and replaced by a new sequence in the beginning of the next run.

5.3 Theory : Adsorption dynamics

Consider a single polymer molecule (grafted with one end to a flat structureless surface) in an adsorption experiment which is repeated over and over again. The monomer - surface interaction is considered attractive with a sticking energy ϵ. Starting from a non-adsorbed conformation, two different mechanisms of adsorption are depicted in the sketches. The first figure shows the process of sequential adsorption or zipping. The next one shows the process of accelerated zipping in which the process is mediated by the formation of new nucleation points arising from large loops. The formation of large loops can accelerate the process of adsorption since the loop-ends act as new nucleation centres from which zipping can proceed. The first question, we must ask is - which of the two mechanisms mentioned above is the dominant process of physisorption. Our simulations provide the clue. Figure 5.2 gives snapshots of the chain conformation from our simulations . Here we have plotted the z-component (*i.e.* the height) of the monomers against the index of the monomer along the chain contour. It strongly suggests a zipping process. Indeed, large loops are so infrequent that we may ignore them in the construction of a theory of physisorption.

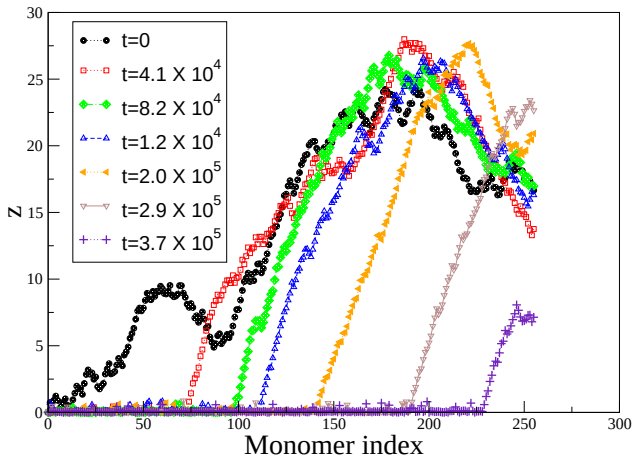

Figure 5.2: Snapshots of an $N = 256$ chain conformation, taken at successive time moments during the adsorption process. The z-coordinate of the i-th monomer is plotted against monomer index i.

5.3.1 Stem-flower scenario: A macroscopic law

Our observation that simple zipping is the preferred mechanism in the strong physisorption regime, is in accordance with earlier MC-simulation results [70, 21]. From

Figure 5.2, we see that the chain conformation can be considered within the framework of a "stem-flower" picture which was discussed first by Brochard-Wyart [10] as characteristic for a polymer chain under strong stationary flow. Recently the "stem-flower" picture was employed in the case of non-stationary pulled polymer chain [74]. This picture shares many common features with the "stem-corona" model, suggested by Descas *et al* [21]. Here we reconsider it in a more systematic way and employ it as a basic model to include fluctuations within the ME - formalism.

Fig. 5.3 presents schematically the stem-flower scenario of the adsorption dynamics. Prior to the adsorption process, the chain is in a mushroom like state with one end tethered to the surface. When the adsorption starts, the monomers closest to the grafting point get adsorbed first. The number of adsorbed monomers at time t is denoted by $n(t)$. Most of the chain does not feel the surface. As the zipping proceeds, the monomers are successively pulled down to the surface. This causes to a tension to build up between the last adsorbed monomer and its immediate non-adsorbed neighbour. However, monomers far from the last adsorbed monomer, still do not feel the tension. Therefore, nonadsorbed portion of the chain is subdivided into two parts: a stretched part ("stem") of length $m(t)$, and a remaining part ("flower") which is yet not perturbed by the tensile force of the substrate. The stem is formed after the first few adsorption events. In this period , the portion of the chain near the grafting point unravels and is stretched by the tensile force . After the first few zipping events, we enter the main stage of adsorption in which there is a distinct stem from which the monomers are sequentially pulled to the surface. Based on this model, we now derive a dynamic equation for the zipping. The tensile force propagation front is at distance $R(t)$ from the surface . The rate of adsorbtion is denoted as $v(t) = a\frac{dn(t)}{dt}$, where a is the chain (Kuhn) segment length.

A single adsorption event occurs with energy gain ϵ and entropy loss $\ln(\mu_3/\mu_2)$, where μ_3 and μ_2 are the connectivity constants in three and two dimensions, respectively [90]. As a result, the driving force for adsorption can be expressed as

$$f_{\text{drive}} = \frac{\epsilon - k_B T \ln(\mu_3/\mu_2)}{a} = \frac{F}{a} \tag{5.2}$$

where $F = \epsilon - k_B T \ln(\mu_3/\mu_2)$ is the change in free energy. The friction force is directly proportional to the size of the stem , $m(t)$ and the speed at which the stem is dragged, $v(t)$, i.e.

$$f_{\text{fric}} = \zeta_0 \, a \, m(t) \, \frac{dn(t)}{dt} \tag{5.3}$$

where ζ_0 is the Stokes friction coefficient of a single bead. All the monomers in the stem are assumed to move together. The equation of motion follows from the balance

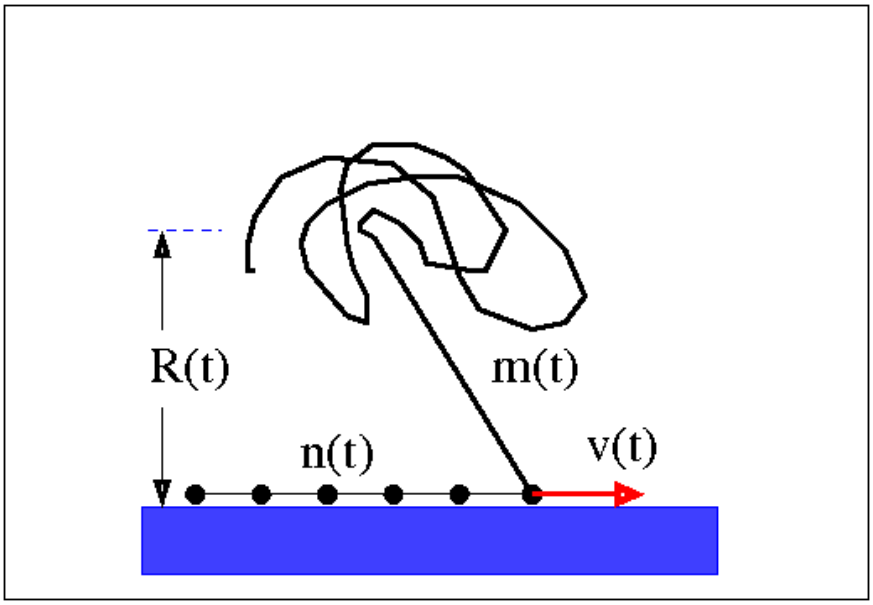

Figure 5.3: Stem-flower picture of the adsorption dynamics. The total number of adsorbed monomers at time t is denoted by $n(t)$. The tail which, contains all non-adsorbed monomers, consists of a stretched part, a "stem", of length $m(t)$, and of a nonperturbed part which is referred to as "flower". The rate of adsorption is $v(t)$. The distance between the surface and the front of the tension propagation is $R(t)$.

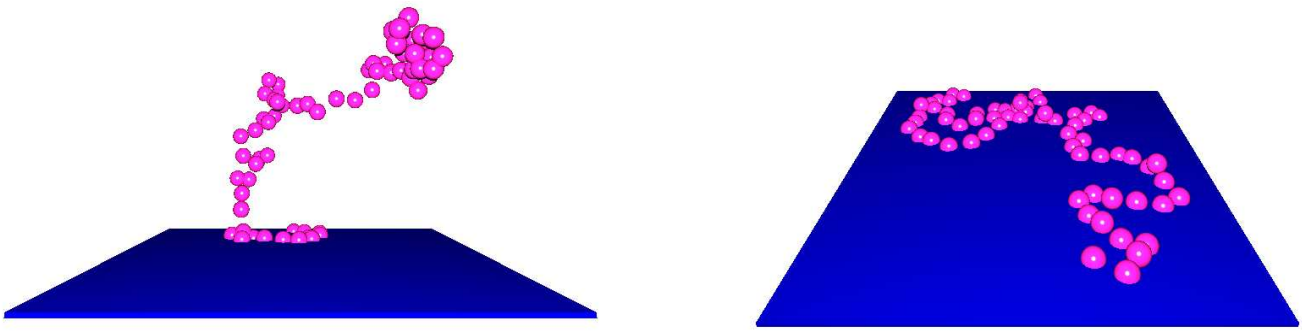

Figure 5.4: Snapshots of a chain of length $n = 128$ on an attractive surface during the early and late stages of adsorption.

of driving, $f_{\rm drive}$, and drag force, $f_{\rm fric}$, which yields

$$\zeta_0 \; m(t) \, \frac{dn(t)}{dt} = \frac{F}{a^2} \tag{5.4}$$

One may express $m(t)$ in terms of $n(t)$, if one assumes that at time t the "flower" (which is placed on average at a distance $R(t)$ from the surface) is not affected by the tensile force. This means that $R(t)$ is the size which the chain portion $n(t) + m(t)$ occupied before the adsorption has started, i.e.,

$$a \, [n(t) + m(t)]^{\nu} = R(t) \tag{5.5}$$

where ν is the Flory exponent (e.g., $\nu = 3/5$ in $d = 3$-dimensions) [90]. We have assumed the usual excluded volume scaling. On the other hand, as shown in Fig. 5.3,

$$a \, m(t) \approx R(t) \tag{5.6}$$

up to a geometrical factor of order unity. Therefore the relation between $m(t)$ and $n(t)$ is given as

$$n(t) \simeq m(t)^{1/\nu} - m(t) \tag{5.7}$$

During most of the adsorption process the stem is sufficiently long, $m(t) \gg 1$, so that $m(t)^{5/3} \gg m(t)$, i.e., $m(t) \simeq n(t)^{\nu}$ and Eq.(5.4) becomes

$$\zeta_0 \, n(t)^{\nu} \, \frac{dn(t)}{dt} = \frac{F}{a^2} \tag{5.8}$$

The solution of Eq. (5.8) reads

$$n(t) \propto \left[\frac{F}{a^2 \zeta_0} \, t \right]^{1/(1+\nu)} \tag{5.9}$$

As result, (for $d = 3$ where $\nu = 3/5$) one obtains a law for the adsorption kinetics, $n(t) \propto t^{0.62}$, which is in a good agreement with MC-findings [77, 70, 21]. In the course of adsorption the "stem" grows and the "flower" moves farther away from the surface. This, as it was mentioned in Ref. [21], makes the nucleation of a new adsorption site on the surface less probable.

In the late stages of adsorption the "flower" has been largely consumed and vanishes so that the non-adsorbed part of the macromolecule exists as a "stem" only. From this moment on the closure relation reads

$$n(t) + m(t) = N \tag{5.10}$$

Comparison of Eq. (5.10) with Eq. (5.7) shows that this pure "stem" regime starts at $n(t) \geq N - N^{\nu} \approx N$, i.e., it could be basically neglected for sufficiently long chains.

The scaling result derived in this section, Eqn.(5.9), can be compared to our simulation results. This is discussed in detail in Sec. 5.4.1.

The stem-flower scenario which we used in this section as well as the macroscopic equation of motion, Eq.(5.8), are employed below as a starting point for the treatment of fluctuations.

5.3.2 Time evolution of the distribution of adsorbed monomers

The Master Equation

Let us consider the distribution function $P(n,t)$ of the instantaneous number of adsorbed monomers (i.e., the total train length). The number of adsorbed segments n and the number monomers in the nonadsorbed chain tail l are mutually complementary, if one neglects the loops. We argue below that in the strong adsorption regime the loop contribution is, indeed, rather small and reduces mainly to loops of size unity. With this assumption, the corresponding tail distribution function, $T(l,t)$, reads

$$T(l,t) = P(N-l,t). \tag{5.11}$$

where N is the length of the polymer chain.

Both $P(n,t)$ and $T(l,t)$ can be obtained either from the simulation or by solving a set of coupled kinetic equations. For the latter we use the method of the Master Equation [89]. We treat the adsorption as a sequence of elementary events, describing the zipping - unzipping dynamics while keeping in mind that within an elementary time interval only one monomer may change its state of sorption. Thus one can treat the (un)zipping dynamics as an *one-step process*, shown schematically in Fig. 5.5a. The figure depicts a chain of length N undergoing a single step process . The chain has two parts : an adsorbed train of length n on the surface and a non adsorbed tail of length $N-n$. In an elementary time interval, the train can gain or lose a segment by an adsorption or desorption event. The rate constants of these two events are denoted by $w^+(n)$ and $w^-(n)$ respectively. The figure depicts the zipping mechanism. Hence we ignore the "touch down" events of distant monomers, *i.e.* the formation of loops. In order to specify the rate constants, we use the detailed balance condition [89] which in our case (cf. Fig. 5.5a) reads

$$\frac{w^+(n-1)}{w^-(n)} = \mathrm{e}^{F/k_BT} \tag{5.12}$$

where again $F = \epsilon - k_BT\ln(\mu_3/\mu_2)$ is the free energy gain upon a monomer adsorption event and the energy gain $\epsilon = E_1 - E_2$.

Detailed balance condition Eq. (5.12) is, of course, an approximation for the non-equilibrium adsorption process in question. This implies that, despite the global non-equilibrium, close to a "touch-down" point the monomers are in local equilibrium with

respect to adsorption-desorption events. This also means that the monomer size is small enough as compared to the "stem" length, so that this approximation is a good one, compatible with the "stem-flower" picture of adsorption dynamics.

The detailed balance requirement fixes only the ratio of the rate constants and does not fully determine their values. Let us choose

$$\begin{aligned} w^-(n) &= q[m(n)]\, \mathrm{e}^{-F/k_BT} \\ w^+(n-1) &= q[m(n)]. \end{aligned} \tag{5.13}$$

In Eq. 5.13 the *transmission* factor $q[m(n)]$ is determined by the friction coefficient ζ which, within our stem-flower model, is defined as $\zeta = \zeta_0 m$. Therefore, one obtains

$$q[m(n)] = \frac{k_BT}{a^2\zeta} = \frac{k_BT}{a^2\zeta_0\, m}. \tag{5.14}$$

The notation $q[m(n)]$ implies that the stem length m depends on the total train length n and, furthermore, the relationship $m(n)$ is given by the closure Eq. (5.7) which also holds for the instantaneous values, i.e.,

$$n \simeq m^{1/\nu} - m \tag{5.15}$$

With the rate constants from Eq. 5.13 at hand, the one-step master equation reads [89]

$$\begin{aligned} \frac{d}{dt}\, P(n,t) &= w^-(n+1)\, P(n+1,t) + w^+(n-1)\, P(n-1,t) \\ &- w^+(n)\, P(n,t) - w^-(n)\, P(n,t) \end{aligned} \tag{5.16}$$

or, in a more compact form

$$\frac{d}{dt}\, P(n,t) = \Delta\left[w^-(n)\, P(n,t)\right] + \Delta^{-1}\left[w^+(n)\, P(n,t)\right] \tag{5.17}$$

where the finite-difference operators $\Delta,\ \Delta^{-1}$ are defined as

$$\begin{aligned} \Delta f(n) &\equiv f(n+1) - f(n) \\ \Delta^{-1} f(n) &\equiv f(n-1) - f(n) \end{aligned} \tag{5.18}$$

The total number of the adsorbed monomers varies between 1 and N, i.e., $1 \le n \le N$. For $n = 1$ the Eq. (5.16) has to be replaced by

$$\frac{d}{dt}P(1,t) = w^-(2)P(2,t) - w^+(1)P(1,t) \tag{5.19}$$

Similarly, for $n = N$ the ME reads

$$\frac{d}{dt}P(N,t) = w^+(N-1)P(N-1,t) - w^-(N)P(N,t) \tag{5.20}$$

Finally, the set of master equations (5.16), (5.19) and (5.20) should be supplemented by the initial condition

$$P(n, t = 0) = \delta(n - 1) \tag{5.21}$$

because the adsorbtion starts from the state of a one chain end grafted at the surface.

The equation of motion for the first statistical moment, $\langle n \rangle = \sum_{n=1}^{\infty} nP(n, t)$, can be obtained from Eq. (5.17) by performing the summation by parts:

$$\sum_{n=0}^{N-1} g(n)\Delta\, f(n) = g(N)f(N) - g(0)f(0) + \sum_{n=1}^{N} f(n)\Delta^{-1}g(n) \tag{5.22}$$

where $f(n)$ and $g(n)$ are arbitrary functions. Taking this into account and keeping in mind that $P(N, t) = P(0, t) = 0$ for simplicity, the equation of motion for $\langle n \rangle$ then yields

$$\frac{d}{dt}\ \langle n \rangle = -\left\langle w^{-}(n) \right\rangle + \left\langle w^{+}(n) \right\rangle \tag{5.23}$$

With the relations for the rate constants, Eqs. (5.13) and 5.14, this equation of motion becomes

$$\zeta_0\, m(t)\, \frac{d}{dt}\, n(t) = \frac{k_B T}{a^2}\ \left[1 - \mathrm{e}^{-F/k_B T}\right] \tag{5.24}$$

where for brevity we use the notations $n(t) = \langle n \rangle$ and $m(t) = \langle m \rangle$. The result, Eq. (5.24), should be compared with Eq. (5.4) derived earlier by means of a simplified physical consideration (see also [21] where this result was obtained before us). Formally, Eq. (5.24) transforms back into Eq. (5.4) when adsorption is very weak, $F/k_B T \ll 1$. Importantly, Eq. (5.24) has the same structure as Eq. (5.4) even when the adsorption is not weak and the quantity $F/k_B T$ is not small; the only difference between these equations is that the effective force in Eq. (5.24) has the form $(k_B T/a)\left[1 - e^{-F/k_B T}\right]$ instead of just F/a. This can be understood by the analogy with the second virial coefficient of interaction between the monomer and the surface. Indeed, we know that the contribution to the free energy of an imperfect gas due to pair collisions is proportional to the second virial coefficient rather than just interaction energy; similarly in the case of adsorption, the effective second virial coefficient is the quantity that describes the effect of monomer attraction to the wall. Thus, the zipping as a strongly non-equilibrium process can not be treated quasi-statically by making use of a simple "force-balance". The inclusion of fluctuations by employing the ME-formalism is important in order to obtain the correct result for the driving force.

Fokker - Planck equation and boundary conditions

We now change from the discrete representation, Eqs. (5.17), (5.19) and (5.20), to a continuous one, namely, to the Fokker-Planck equation for the distribution function $P(n,t)$ with proper boundary conditions. This can be done by the substitution

$$\begin{aligned} \Delta &\simeq \frac{\partial}{\partial n} + \frac{1}{2}\frac{\partial^2}{\partial n^2} \\ \Delta^{-1} &\simeq -\frac{\partial}{\partial n} + \frac{1}{2}\frac{\partial^2}{\partial n^2} \end{aligned} \tag{5.25}$$

After that, Eq.(5.17) takes on the form

$$\frac{\partial}{\partial t}\,P(n,t) = \frac{\partial}{\partial n}\left\{\left[w^-(n) - w^+(n)\right]\;P(n,t)\right\} + \frac{1}{2}\frac{\partial^2}{\partial n^2}\left\{\left[w^-(n) + w^+(n)\right]\;P(n,t)\right\} \tag{5.26}$$

where $[w^+(n) - w^-(n)]$ and $[w^-(n) + w^+(n)]/2$ play the roles of drift velocity and diffusion coefficient, respectively.

It is necessary to derive the proper boundary conditions. We know that at $n = 1$ the ME has a different form, given by Eq.(5.19). It is convenient to require that Eq. (5.16) is still valid with the additional condition

$$\left[w^+(n-1)P(n-1,t) - w^-(n)P(n,t)\right]_{n=1} = 0 \tag{5.27}$$

i.e., the transitions between a fictitious state $n = 0$ and the state $n = 1$ are also balanced.

Similarly, to reconcile the equation at $n = N$, given by Eq. (5.20), with the general ME, Eq. (5.16), one should impose the condition

$$\left[w^-(n+1)P(n+1,t) - w^+(n)P(n,t)\right]_{n=N} = 0 \tag{5.28}$$

which again expresses the balance between an artificial state $n = N + 1$ and the state $n = N$. In order to gain a deeper insight into the boundary conditions given by Eqs.(5.27) and (5.28) let us represent Eq. (5.16) in the form

$$\frac{d}{dt}P(n,t) = \Delta\left[w^-(n)P(n,t) - w^+(n-1)P(n-1,t)\right] \tag{5.29}$$

This representation looks like a discrete version of the continuity equation, stating that the value in the square brackets is the probability current (with a negative sign), i.e.,

$$J(n) = w^+(n-1)P(n-1,t) - w^-(n)P(n,t) \tag{5.30}$$

A comparison of Eq. (5.30) with Eqs. (5.27) and (5.28) allows one to conclude that

$$J(n=1) = 0 \qquad \text{and} \qquad J(n=N+1) = 0 \tag{5.31}$$

i.e., one should impose *reflecting* boundary conditions on both ends of the interval.

Within the Fokker-Planck formalism the probability current has the form

$$J(n) = \left[w^+(n) - w^-(n)\right] P(n,t) - \frac{1}{2}\frac{\partial}{\partial n}\left\{\left[w^+(n) + w^-(n)\right] P(n,t)\right\} \qquad (5.32)$$

Thus the Fokker-Planck formalism makes it possible to map the strong adsorption case onto a one-dimensional random walk problem with drift and diffusion coefficients given in terms of rate constants, Eq. (5.26). While such a description provides physical insight into the problem, from the viewpoint of numerics it is much easier to deal with the ME discrete set Eqs. (5.16), (5.19) and (5.20). We will discuss the results of this solution in Sec. 5.3.4.

5.3.3 Train distribution

Our MC-simulation results show that the distribution of loops in case of strong physisorption is mainly dominated by the shortest loops of length unity. These loops can be considered as defects during the process of zipping. Moreover, this distribution sets on much faster than the time for complete adsorption. Thus one may consider the total number of the adsorbed monomers $n(t)$ as a slow variable in comparison to the number of defects (or loops of length unity). The adsorbed monomers can be seen as an array of trains, separated by an equilibrium number of defects (see Fig. 5.5b). The partition function of this one-dimensional array can be determined rigorously (see Appendix A). Using the partition function, one can derive an expression for the train distribution function

$$D(h,t) = \frac{1}{h_{\rm av}(t)} \exp\left[-\frac{h}{h_{\rm av}(t)}\right] \qquad (5.33)$$

where $h_{\rm av}(t)$ is the average train length. Eq.(5.33) is the Flory-Schulz distribution which usually governs the molecular weight distribution in equilibrium polymerization of a broad class of systems, referred to as *living* polymers [38].

5.3.4 The Numerical Solution of the Master Equation

The set of ordinary differential equations (5.16), (5.19) and (5.20) with the initial condition, Eq.(5.21), has been solved numerically in this investigation. Typically, we use a chain length $N = 32$, the total time interval takes 300 units of the the elementary time $\tau_0 = a^2\zeta_0/k_BT$, the sticking energy was chosen (in units of k_BT) as $\epsilon = 4.0$, whereas the entropy loss $\ln(\mu_3/\mu_2) = \ln 2$. Figure 5.6 demonstrates the result of this solution.

As it can be seen from Fig.5.6, the adsorbtion kinetics follows indeed the drift - diffusion picture. The initial distribution is very narrow: the adsorption starts with

$n(0) = 1$ as a grafted chain configuration. As time goes by, the distribution maximum moves to larger adsorbed monomer numbers and the distribution itself broadens. Eventually, the random process hits the boundary $n = N$ and stays there due to drift and the reflecting boundary conditions. As a result, the final distribution is a very narrow again, and is concentrated around the boundary $n = N$. It is interesting that in the double logarithmic coordinates the distribution maximum follows a straight line (cf. Fig. 5.6 right panel) which reveals a clear scaling law. Based on the numerical results for $P(n, t)$ and making use the relation, Eq. (5.11), one can calculate the tail distribution function $T(l, t)$ as well. We will discuss this in Sec. 5.4.3 where we present our MC-results. There it will be seen that our MC-findings are in a good agreement with these theoretical predictions.

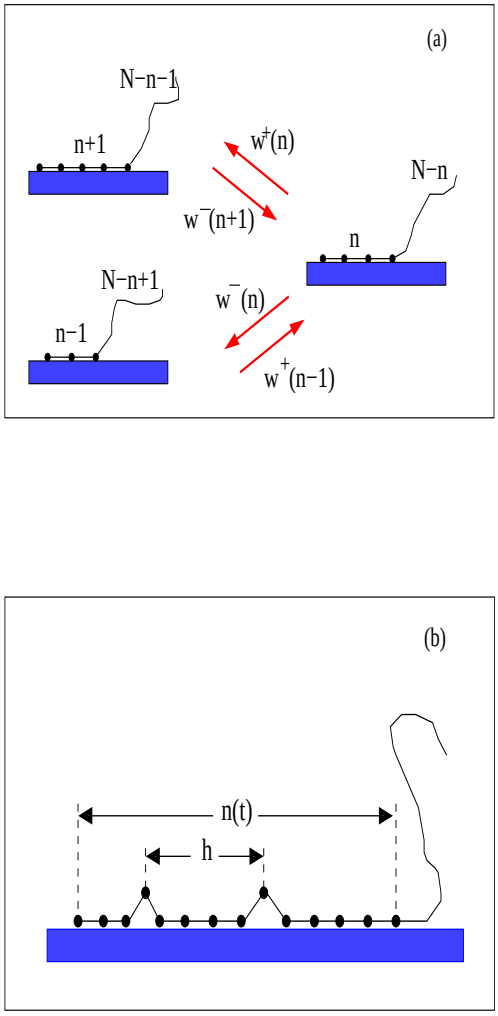

Figure 5.5: (a) Creation - annihilation of an adsorption state with n-monomers due to a single-step process. The arrows indicate possible single-step transitions with $w^+(n)$ and $w^-(n)$ being the rate constants of adsorption and desorption events, respectively. (b) The adsorbed monomers form trains, divided by defects (loops of length unity). The total number of adsorbed monomers at time t is denoted by $n(t)$. The train length, h, itself is a random number, subject to an exponential distribution $D(h,t)$ - Eq.(5.33).

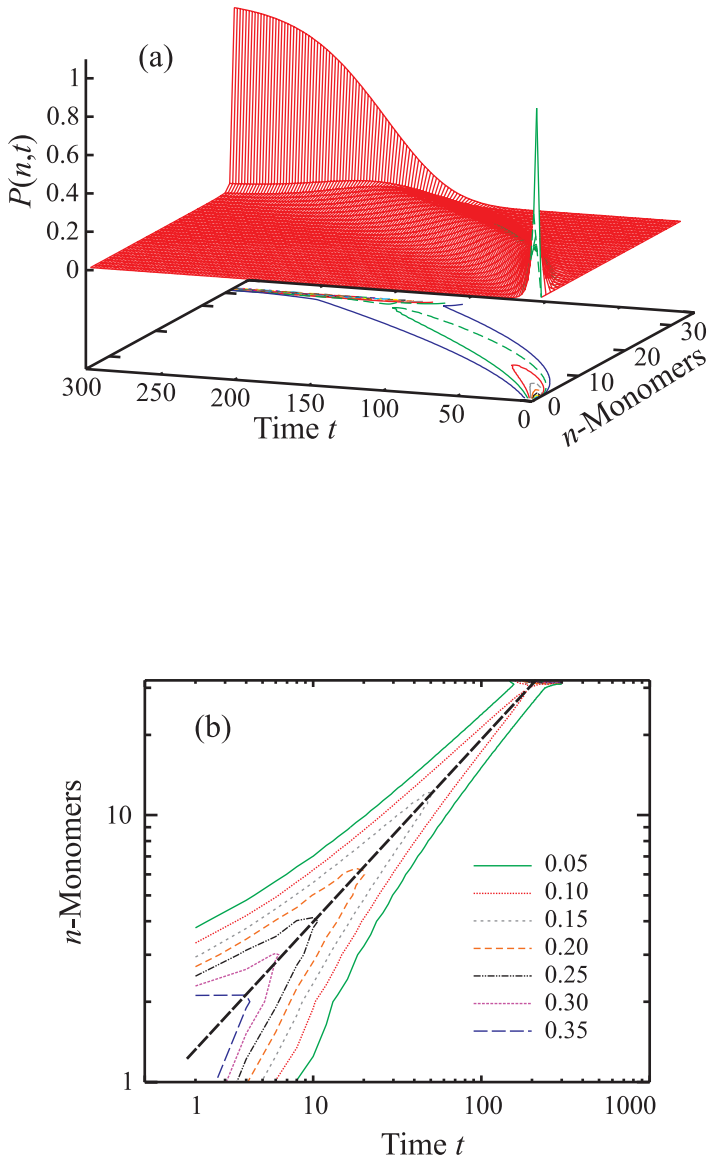

Figure 5.6: Adsorbed monomer number distribution function $P(n,t)$ (a) and its isolines as a 2-dimensional log-log plot (b). The variation of the distribution maximum, $n_{max}(t)$, is a straight (dashed) line with slope 0.63.

5.4 Results and Analysis

We present here the main results from the computer simulation of the adsorption kinetics and compare them to those from the solution of the Master Equation, Eqs. (5.16), (5.19) and (5.20), validating thus the theoretical picture of Section 5.3.

5.4.1 Order Parameter Kinetics - homopolymers

The first step in the analysis of the process of physisorption is to determine the characteristic time scales involved. We use the order parameter, *i.e.* the fraction of adsorbed segments, to obtain the time of adsorption.

In Fig. 5.7 we show the adsorption time transients from our MC simulations which describe the time variation of the order parameter $n(t)/N$ for homopolymer chains of different length N and strong adhesion $\epsilon/k_BT = 4.0$. This surface potential is much higher than the critical adsorption potential, $\epsilon^{cr} \simeq 1.72$ determined from earlier equilibrium simulations (see Chapter 4 Sec. 4.6). In double logarithmic coordinates these transients appear as straight lines , suggesting that the time evolution of the adsorption process is governed by a power law. As the chain length N is increased, the slope of the curves grows steadily, and for length $N = 256$ it is equal to ≈ 0.56. This value is close to the theoretically expected slope of $(1+\nu)^{-1} \approx 0.62$ - cf. Eq. 5.9, and for even longer lengths of the polymers, the slope would probably approach the predicted value. In long time scales, the curves reach a plateaux due to the finite size of the chains.

The total time τ it takes a polymer chain to be fully adsorbed can be determined from the intersection of the respective late time plateau of each transient with the straight line tangent to this transient. This method is shown in Fig. 5.9, where the order parameter is plotted against the time for a homopolymer chain of length 256. The point where the tangent to the curve during the main stage of adsorption intersects the tangent to the plateaux (in the late stages) gives us the adsorption time of the polymer.

Thus one may check the scaling of τ with polymer length N. In the inset to Fig. 5.7 we show the observed scaling of the adsorption time with chain length, $\tau \propto N^{\alpha}$. The straight line represents a fit through the points which lead to the dynamical exponent $\alpha \approx 1.51$ which is again somewhat smaller than the expected one $1+\nu \approx 1.59$. This small discrepancy is most probably due to finite-size effects too.

We can compare these with results obtained from the numerical solution of the Master Equation. The first moment $n(t)$ of the distribution function $P(n,t)$ also exhibits well expressed scaling behavior, $n(t) \sim t^{0.66}$, as shown in Fig. 5.8. In the inset we also show the resulting relationship for the time of adsorption, $\tau \propto N^{1.6}$, as expected from

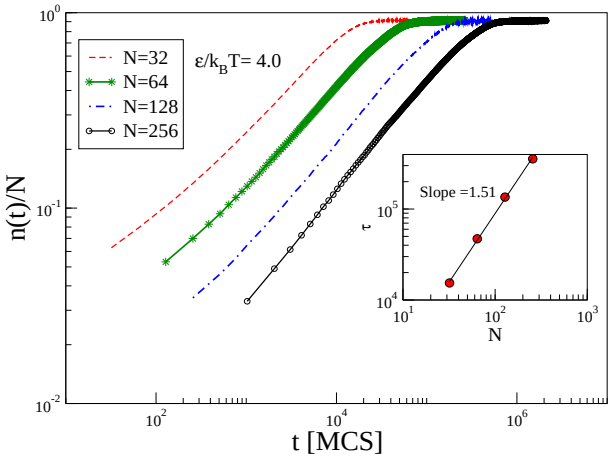

Figure 5.7: Time evolution of the order parameter (fraction of adsorbed segments) from the MC simulations for four different chain lengths $N = 32,\ 64,\ 128,$ and 256 at surface potential $\epsilon/k_BT = 4.0$. The slope of the $N = 256$-curve is 0.56. The inset shows the scaling of the adsorption time with chain length,$\tau \propto N^{1.51}$. T.

Eq. 5.9.

It is known that the characteristic time of chain fluctuations in equilibrium is given by the Rouse time. This has the form $\tau \propto N^a$ where $a = 1 + 2\nu = 2.176$ [26]. Comparing the exponents α and a, it is clear that the time scale of physisorption is much smaller than the Rouse relaxation time. This means that the chain has no time to relax and that non-equilibrium effects are dominant.

Fig. 5.10 presents the adsorption transients for a chain of constant length, $N = 256$, for different strength of the surface potential. Evidently, as the surface potential gets stronger, the final (equilibrium) values of the transients at late times $t \to \infty$ grow while the curves are horizontally shifted to shorter times. Notwithstanding, the slope of the $n(t)$ curves remains *unchanged* when ϵ/k_BT is varied, suggesting that the kinetics of the process is well described by the assumed zipping mechanism.

The changing plateau height may readily be understood as reflecting the correction in the equilibrium fraction of adsorbed monomers due to the presence of defects (vacancies) for any given value of ϵ/k_BT. This is demonstrated in the upper left inset in Fig. 5.10 where the observed plateau values are shown to be perfectly described by the expression $n_{t\to\infty} = 1 - 5\exp(-\epsilon/k_BT)$ under the assumption that the probability of a monomer to desorb from the surface (and create a vacancy in the train) is determined by the Boltzmann factor $\exp(-\epsilon/k_BT)$. Evidently, the factor of 5 in front of the

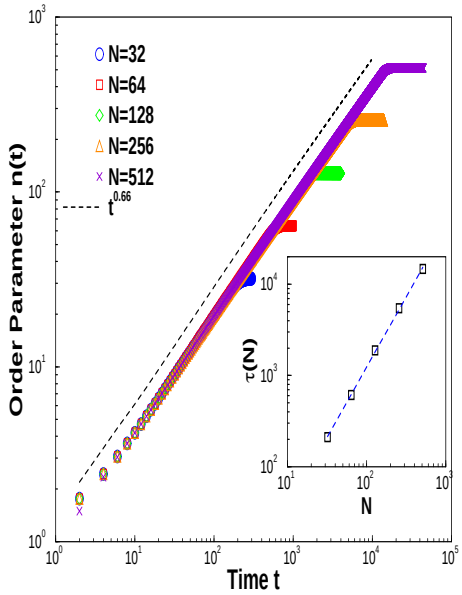

Figure 5.8: The average adsorbed number of monomer vs. time for different chain lengths N obtained from the numerical solution of the ME. Dashed line denotes the slope, $t^{0.66}$, following from Eq. 5.9. In the inset we show the resulting scaling of the adsorption time with chain length, $\tau \propto N^{1.6}$.

exponent yields the entropic gain in free energy when an adsorbed monomer detaches from the surface while its nearest neighbors still stick to it.

The second inset in Fig. 5.10 shows that the adsorption time transients collapse on a master curve, if one rescales the time axis appropriately. Note that for a very strong potential, $\epsilon/K_BT = 10.0$, the corresponding transient deviates somewhat from the master curve since the establishment of local equilibrium (which we assumed in the theory to happen much faster than the adsorption process itself) is hampered. Also the transient for $\epsilon/k_BT = 2.5$ (not shown in this inset) was found not to fit into the master curve since this strength is close to that of the critical threshold for adsorption, the attraction to the surface is comparatively weak and zipping is not the adequate mechanism. For the transients which do collapse on a master curve, however, one may view the rescaling of the time axis in Fig. 5.10 by the expression $t \to t[1-13.7\exp(-\epsilon/k_BT)]$ as a direct confirmation of Eq. 5.24 where the time variable t may be rescaled with the driving force of the process (i.e., with the expression in square brackets). The factor ≈ 13.7 gives then the ratio μ_3/μ_2 of the effective coordination numbers in 3- and 2-dimensions of a polymer chain with excluded volume interactions. μ_3 and μ_2 are model-dependent and characterize, therefore, our off-lattice model.

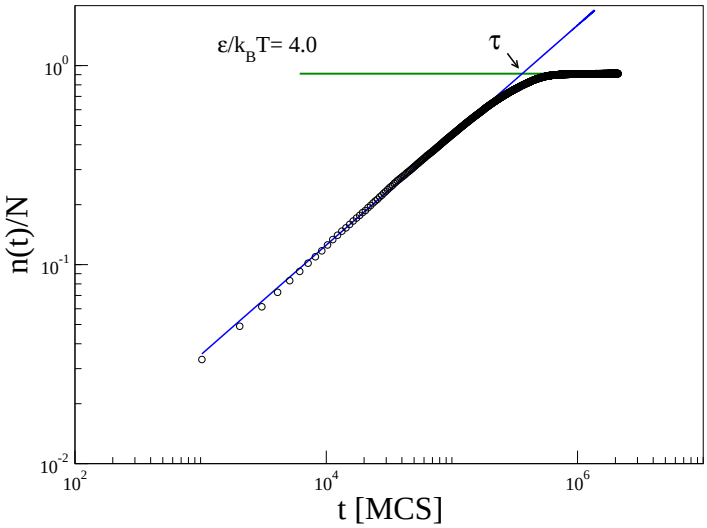

Figure 5.9: Plot of the order parameter vs. the time for a homopolymer chain of length 256. The time τ is determined from the intersection point of the late time plateau with the tangent $t^{0.56}$ to the $n(t)/N$ vs. t curve .

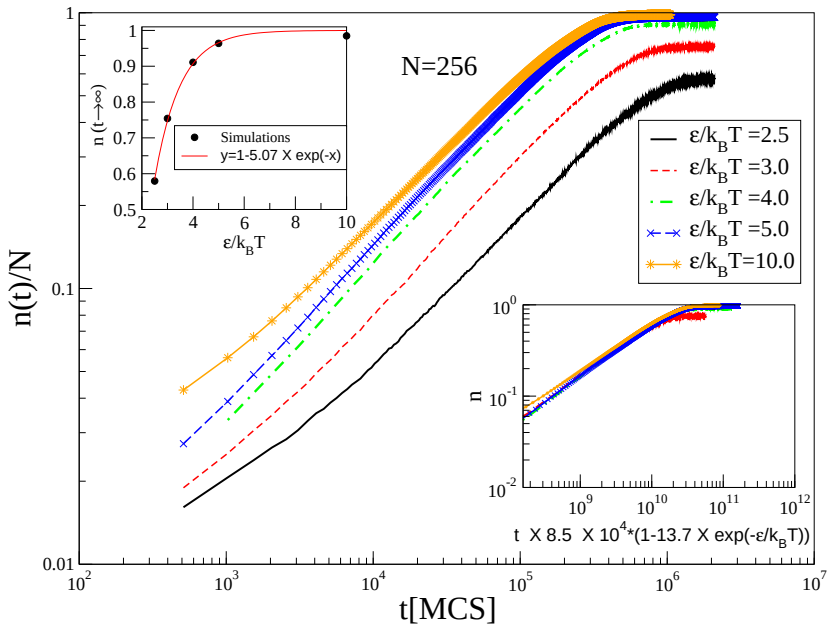

Figure 5.10: Adsorption kinetics for different strengths ϵ of the surface potential. The variation of the plateau height (i.e., the fraction of adsorbed monomers at equilibrium) with ϵ is depicted in the upper inset where the solid line $n_{t\to\infty} = 1 - 5\exp\left(-\epsilon/k_BT\right)$ describes the equilibrium number of defects (vacancies). The lower inset shows a collapse of the adsorption transients on a single 'master curve', if the time axis is rescaled appropriately.

5.4.2 Order Parameter Kinetics - random and regular block-copolymers

In Fig. 5.11 we examine the adsorption kinetics for the case of regular block copolymers with block size M - Fig. 5.11a, and for random copolymers - Fig. 5.11b, bearing in mind that the zipping mechanism, assumed in our theoretical treatment, is by no means self-evident when the file of sticking A-monomers is interrupted by neutral B segments. It becomes evident from Fig. 5.11a, however, that, except for a characteristic 'shoulder' in the adsorption transients, the power-law character of the order parameter variation with time remains unchanged. Evidently, only the first shoulder in the adsorption transient is well expressed while the subsequent ones are against the background of much larger time scales in the log-log representation of Fig. 5.11a. If, however, one monitors the adsorption of only a *single* adsorption event with time then one observes in normal coordinates a series of such shoulders like a 'staircase' in $N_{ads}(t)$ as seen in Figure 5.12 .

The variation of the power exponent, α, with block length M, where α describes the scaling of the total adsorption time with polymer size N, $\tau \propto N^{\alpha}$, is displayed in the inset on the right. Evidently, α *declines* as the block size is increased. This finding appears surprising at first sight, since it goes against the general trend of regular multiblock copolymers resembling more and more homopolymers (with $\alpha = 1 + \nu$ for the latter), as the block size $M \to \infty$. Moreover, it would imply shorter adsorption times for smaller block size, $M \to 1$, although the shoulder length visibly grows with growing M - see Fig. 5.11a. In fact, however, as one may readily verify from Fig. 5.11a, the transients are systematically shifted to longer times (i.e., the total adsorption takes longer) due to a growing prefactor for $M \to 1$ which does not alter the scaling relationship $\tau \propto N^{\alpha}$. One may thus conclude that the frequent disruption of the zipping process for smaller blocks M slows down the overall adsorption process (a transient 'staircase' with numerous short steps) in comparison to chains with larger M where the zipping mechanism is fast (a 'staircase' with few longer steps). Fig. 5.12 displays the time evolution order parameter of a homopolymer and a regular block copolymer with block size 16. Both have a chain length of 256. The order parameter plotted here, is obtained for a single run and is not the statistical average of many runs. It is evident that the order parameter of the homopolymer increases smoothly with time whereas in the case of the block copolymer, it increases in short bursts that look like a "staircase". The presence of non-adsorbing blocks in the chain lead to the intervals in the graph where the order parameter remains constant (with some fluctuations).

A characteristic "shoulder" in the adsorption transients of regular multiblock co-

polymers manifests itself in the early stage of adsorption and lasts progressively longer when M grows. We interpret the temporal length of this shoulder with the time it takes for a segment from the *second* adsorptive A-block in the polymer chain to be eventually captured by the attractive surface, once the first A-block has been entirely adsorbed. For sufficiently large blocks one would therefore expect that this time interval, τ_s, associated with the capture event, will scale as the Rouse time, $M^{1+2\nu}$, of a non-adsorbing tethered chain of length M. The observed τ_s versus M relationship has been shown in the upper left inset in Fig. 5.11a. The slope of ≈ 1.49 is less that the Rouse time scaling exponent, 2.18, which one may attribute to the rather small values of the block length M that were accessible in our simulation. One should also allow for scatter in the end time of the shoulder due to the mismatch in the capture times of all the successive A-blocks in the course of our statistical everaging over many chains during the computer experiment. In the case of random copolymers, Fig. 5.11b, the observed adsorption transients resemble largely those of a homopolymer chain with the same number of beads again, apart from the expected difference in the plateau height which is determined by the equilibrium number of adsorbed monomers. One should note, however, that a rescaling of the vertical axis with the fraction of sticking monomers, p, does not lead to coinciding plateau height - evidently the loops whose size also depends on p also affect the equilibrium number of adsorbed monomers. The variation of the observed scaling exponent α with composition p is shown in the inset to Fig. 5.11b wherefrom one gets $\alpha \approx 1.6$. Note that this value is considerably lower than the power of 2.24 which has been observed earlier [77], however, for very short chains with only 10 sticking beads. One may conclude that even for random copolymer adsorption the typical time of the process scales as $\tau \propto N^{\alpha}$, as observed for homo - and regular block copolymers. It is conceivable, therefore, that an *effective* zipping mechanism in terms of renormalized segments, that is, segments consisting of an A and B diblock unit of length $2M$ for regular multiblock copolymers provides an adequate notion of the way the adsorption kinetics may be treated even in such more complicated cases. For random copolymers the role of the block length M would then be played by the typical correlation length.

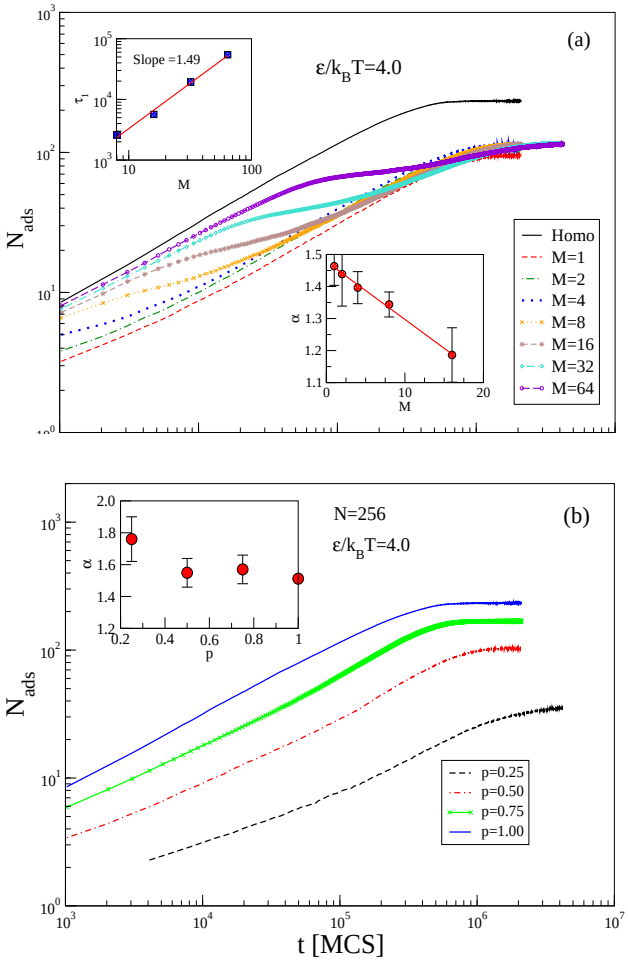

Figure 5.11: (a) Number of adsorbed segments, $N_{ads}(t)$), versus time t for regular AB-copolymers with block size $M = 1 \div 64$ and length $N = 256$. For comparison, the transient of a homopolymer is shown by a solid line too. The time interval, taken by the initial "shoulder", is shown in the upper left inset. The lower inset displays the variation of the scaling exponent, α, for the time of adsorption $\tau \propto N^{\alpha}$ versus block length relationship. (b) The same as in (a) but for random copolymers of length $N = 256$ and different composition $p = 0.25,\ 0.5,\ 0.75$. For $p = 1$ one has the case of a homopolymer. The inset shows the variation of α with p.

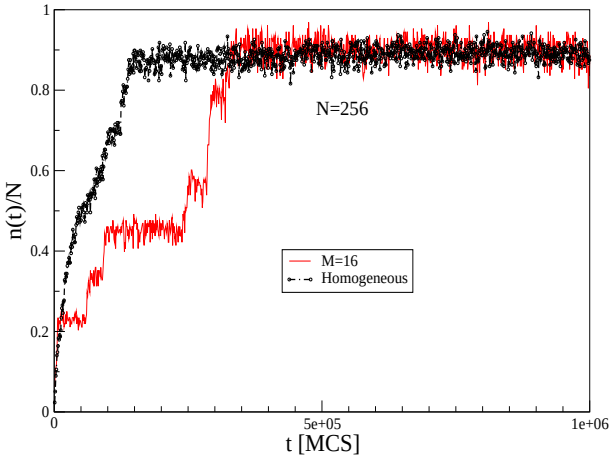

Figure 5.12: Order parameter $n(t)/N$, versus time t for a homopolymer and regular AB-copolymers with block size $M = 64$ both with length $N = 256$. The order parameter is measured for a single run.

5.4.3 Probability Distribution Functions

The time evolution in the corresponding Probability Distribution Functions (PDF) of all the trains, loops and tails of adsorbed polymers provides a lot of information and insight in the kinetics of the adsorption process. In the Appendix we have derived theoretically the expected train distribution under the assumption that local equilibrium of loops of unit length is established much faster than the characteristic time of adsorption itself. The resulting distribution of possible train lengths is shown to be exponential, in close analogy to that of living polymers [38]. In Fig. 5.13a we plot the observed PDF of train lengths for a chain with $N = 256$ at two strengths ϵ/k_BT of the adsorption potential. When scaled with the mean train length $h_{av}(t) = \langle h(t) \rangle$, at time t, in both cases for $\epsilon/k_BT = 3.0$ and 5.0 one finds an almost perfect straight line

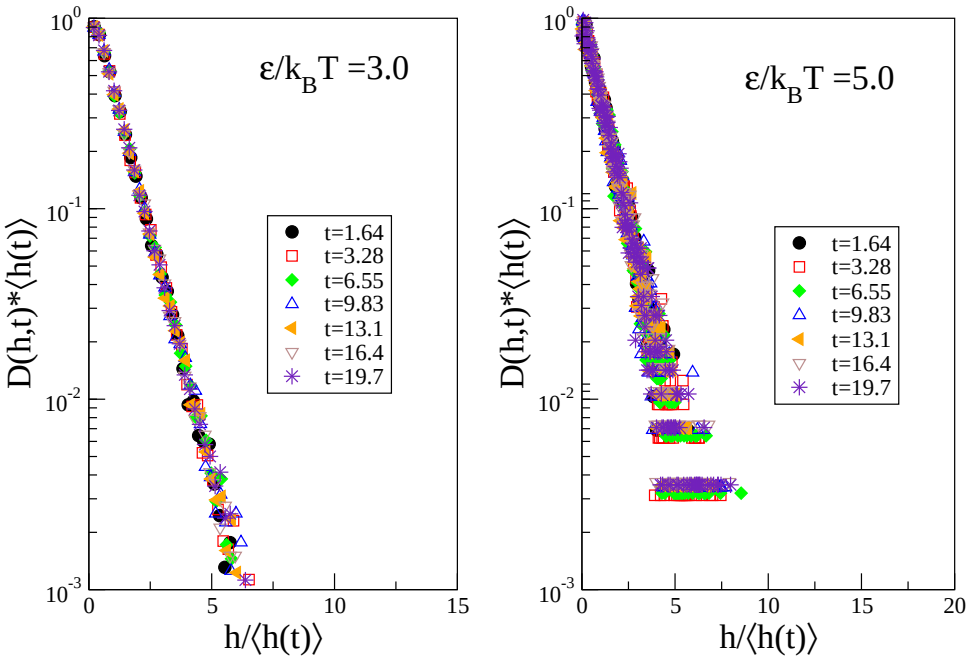

Figure 5.13: Distribution of train lengths during the adsorption process of a homopolymer chain with $N = 256$ at two strengths of the adsorption potential ϵ, shown in semi-log coordinates. PDFs for different times (in units of 10^5 MCS) collapse on master curves when rescaled by the mean train length $h_{\rm av}(t)$.

One may thus conclude that the PDF for train lengths preserves its exponential form during the course of the adsorption process, validating thus the conjecture of rapid local equilibrium. The latter, however, is somewhat violated for the case of rather strong adsorption - $\epsilon/k_BT = 5.0$ - shown in Fig. 5.13 which is manifested by the increased scatter of data at *late* times when the adsorption process overtakes to some

extent the relaxation kinetics on the surface. The PDF of loops $W(k,t)$ at different times after the onset of adsorption is shown in Fig. 5.14. Evidently, the distribution is sharply peaked at size one whereas less than the remaining 20% of the loops are of size two. Thus the loops can be viewed as single thermally activated defects (vacancies) consisting of a desorbed single bead with both of its nearest neighbors still attached to the adsorption plane. As the inset in Fig. 5.14 indicates, the PDF of loops is also described by an exponential function. Large loops which are directly related to the nucleation of new adsorption spots, have a very low probability. This confirms that zipping is the dominant mechanism.

Eventually, in Fig. 5.15a we present the observed PDF of tails for different times t after the start of adsorption, and compare the simulation results with those from the numeric solution for $T(l,t)$ according to Eq. 5.11. One may readily verify from Fig. 5.15 that the similarity between simulational and theoretic results is really strong. In both cases one starts at $t = 1$ with a strongly peaked PDF at the full tail length $l(t = 1) = N$. As time goes by, the distribution becomes broader and its maximum shifts to smaller values. At late times the moving peak shrinks again and the tail either vanishes, or reduces to a size of single segment which is expressed by the sharp peak at the origin of the abscissa.

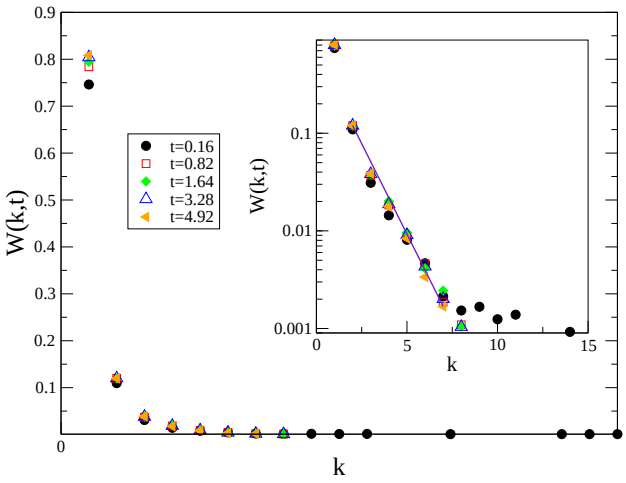

Figure 5.14: Distribution of loop lengths $W(k,t)$ for $N = 256$ and $\epsilon/k_BT = 4.0$ during ongoing polymer adsorption. The time is given in units of 10^5 MCS. In the inset the PDF plotted in semi-log coordinates appears to be a straight line.

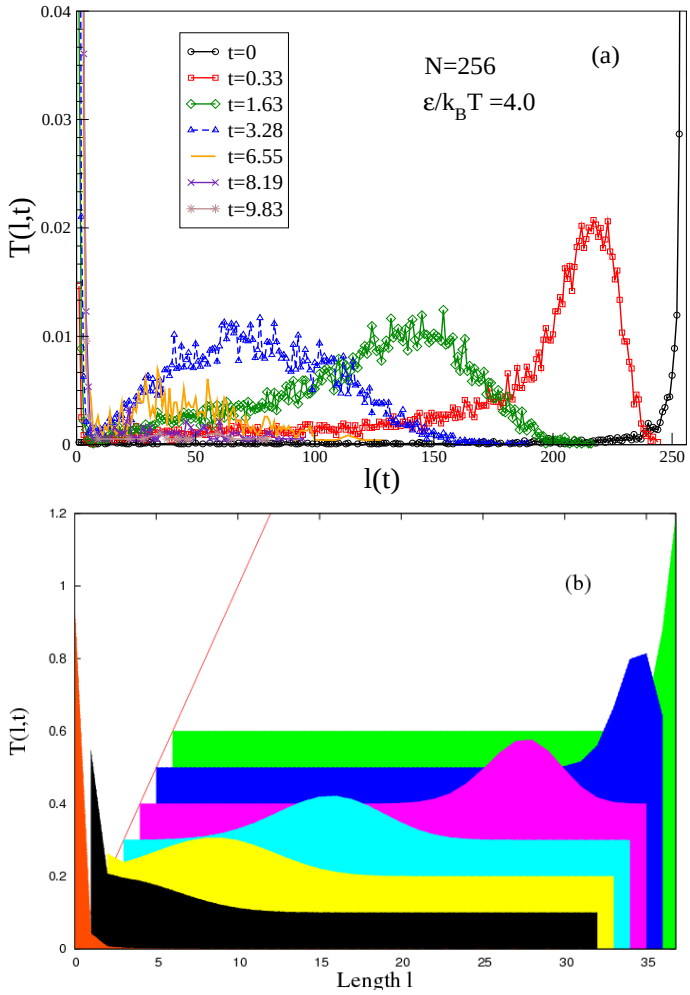

Figure 5.15: (a) Distribution of tail size for different times (in units of 10^5 MCS) during the polymer chain adsorption for a chain with $N = 256$ at $\epsilon/k_BT = 4.0$. (b) The same as in (a) as derived from the solution of the ME for chain length $N = 32$. For better visibility the time slices for $t = 1,\ 5,\ 30\ 100,\ 150,\ 200,$ and 300 are shifted along the time axis and arranged such that the initial distribution for $t = 1$ is represented by the most distant slice.

5.5 Discussion

In this chapter, we have presented the results of our investigations of the adsorption kinetics of a single polymer chain on a flat structureless plane in the strong physisorption regime. We have studied the system analytically as well as by means of dynamic Monte Carlo simulations with a bead-spring model. Adopting the stem-flower model for a chain conformation during adsorption, and assuming the segment attachment process to follow a "zipping" mechanism, we have developed a scaling theory which describes the time evolution of the fraction of adsorbed monomers for polymer chains of arbitrary length N at adsorption strength of the surface ϵ/k_BT. In this model, the non-adsorbed part of the chain consists of a stretched 'stem' that connects the adsorbate to the 'flower' which does not feel the tension during the main stage of adsorption.

We have derived a Master Equation as well as the corresponding Fokker-Planck equation for the time-dependent PDF of the number of adsorbed monomers and for the complementary PDF of tails, and defined the appropriate reflecting boundary conditions.

Inherent in this derivation is the assumed condition of detailed balance which makes it possible to relate the elementary steps of adsorption/desorption.

From the numeric solution of the equivalent discrete set of coupled first-order differential equations we have found that the growth of the adsorbed fraction of monomers with time is governed by a power law,

$$n(t) \propto t^{\frac{1}{1+\nu}}$$

while the typical time of adsorption τ scales with the length of the polymer N as

$$\tau \propto N^{\alpha}$$

with $\alpha = 1 + \nu$.

The adsorption transients, found in the Monte Carlo simulation are in good agreement with these predictions, if one takes into account the finite-size effects due to the finite length of the studied polymer chains.

We demonstrate also that the height of the long time plateau in the adsorption transients is determined by the equilibrium number of vacancies (defects) in the trains of adsorbed monomers. The transients themselves are found to collapse on a single master curve, if time is measured in reduced units which scale with the corresponding driving force for adsorption as determined by the surface potential ϵ/k_BT.

A deeper insight into the adsorption kinetics is provided by our detailed study of the relevant probability distributions of trains, loops and tails during the adsorption. The predicted exponential expression for the PDF of trains is in a very good agreement with our simulational findings. The loops in the strong physisorption regime

are observed to reduce to occasional desorbed segments (vacancies) which play little role in the dominating picture of trains and tails. The PDFs of the latter are found from the simulation data to present a shape which is fully consistent with that of the theoretic treatment. It should be noted also that for chemisorption, a monomer adsorption event involves a significant local activation barrier [5, 66]. In this so-called "accelerated zipping" regime, the loops formation disrupts the adsorption process and the corresponding dynamics differs significantly from the one investigated in this study.

Finally, in the case of regular multiblock and random copolymers we find that the adsorption kinetics strongly resembles that of homopolymers. The observed deviations from the latter suggest plausible interpretations in terms of polymer dynamics, however, it is clear that additional investigations will be warranted before a complete picture of the adsorption kinetics in this case is established too.

Having discussed the statics and kinetics of the adsorption of single polymer chain on a flat surface, we now turn our attention to a variation of the problem : adsorption of a polymer in the presence of a pulling force.

Chapter 6

Pulling an adsorbed polymer from a surface I: the f-ensemble

6.1 Introduction

In the previous chapters we have explored the statics and kinetics of polymer adsorption on planar surfaces. We now consider the adsorption and desorption of a polymer under the influence of a pulling force. This study is motivated by recent advances in the field of single macromolecule experiments which have made it possible to manipulate individual polymer chains and biological macromolecules such as proteins and DNA. The upsurge of interest into the statics and dynamics of single macromolecules at surfaces has been spurred by the use of Atomic Force Microscopy (AFM) [41, 45, 71, 47] and optical/magnetic tweezers [82, 88, 4]. It is now possible to pull or push individual molecules and even study a single molecule undergo a force-driven phase transition. Manipulation of single macromolecules has become an important method for understanding their mechanical properties and characterizing the intermolecular interactions [84, 12]. Measurements of the force, needed to detach a chain from an adsorbing surface, and most notably, of the force versus extension relationship which exhibits sharp discontinuities have been interpreted as indication for the presence of unadsorbed loops on the surface. In turn, this has initiated a number of theoretical studies [42, 32, 2] which have helped to get better insight into the thermodynamic behavior and the mechanism of polymer detachment from adhesive surface under a pulling external force. A comprehensive treatment of the problem for the case of a phantom polymer chain can be found in the paper of Skvortsov et al. [81]. There is a close analogy between the forced detachment of an adsorbed polymer chain like polyvinilamine and polyacrylic acid, adhering to a solid surface such as mica or a self-assembled monolayer, when the chain is pulled by the end monomer, and the unzipping of homogeneous double-stranded DNA. In the context of DNA denaturation and the

simple single chain adsorption, this analogy has been discussed already in the middle 60s [44]. Recently, the DNA denaturation and its unzipping have been reconsidered by Kafri, Mukamel and Peliti [94]. The consideration was based on the Poland and Sheraga' s Grand Canonical Ensemble (GCE) approach [68] as well as on Duplantier's analysis of the number of configurations in polymer networks of arbitrary topology [27]. Duplantier's analysis makes it possible to calculate the values of universal exponents which undergo renormalization due to excluded volume effects. In particular, it has been shown by Kafri et al. [94] that this renormalization procedure changes even the order of the melting (or denaturation) transition in DNA from second to first order.

In this chapter, we use the approach of Kafri et al.[94] in order to treat the detachment of a single chain from a sticky substrate when the chain end is pulled by external force. It has been pointed out earlier[81] that the problem may be considered within the framework of two different statistical ensembles, i.e., by keeping the pulling force *fixed* while measuring the (fluctuating) position of the polymer chain end, or, by measuring the (fluctuating) force necessary to keep the chain end at *fixed* distance above the adsorbing plane. Our study is presented in two parts. In this chapter, we are primarily concerned with the fixed force ensemble. In the next chapter, we discuss the fixed distance ensemble which is more common in experiments. We start with a brief review of the properties of the simulation model in Section 6.2. Then, in Sec. 6.3 , we begin with the consideration of the conventional adsorption (i.e. force-free) problem where we derive a basic expression for the *crossover exponent* describing polymer adsorption. There we also consider theoretically some basic features of adsorbed polymer chains as the variation of the average length of loops and tails in the chain with changing strength of the adsorption potential. In Section 6.4 we extend our theoretical analysis to the case of polymer adsorption in the presence of external force, and obtain results for the main conformal properties of such chains as well as the relevant phase diagram of the system. Then in Section 6.5 we report on our most important results, gained in the course of the computer experiment, and compare them to theoretical predictions. We end this chapter in Section 6.6 with a brief summary and discussion of the most salient results of the present investigation.

6.2 Monte Carlo Simulation Model

We have investigated the force induced desorption of a polymer by means of extensive Monte Carlo simulations. We use a coarse grained off-lattice bead-spring model [9] which has proved rather efficient in a number of polymers studies so far. The system consists of a single polymer chain tethered at one end to a flat impenetrable

structureless surface. The surface interaction is described by a square well potential,

$$U_w(z) = \begin{cases} \epsilon, & z < \delta \\ 0, & z \geq \delta \end{cases} \tag{6.1}$$

The strength ϵ is varied from 2.0 to 7.0 and $k_BT = 1$. The effective bonded interaction is described by the FENE (finitely extensible nonlinear elastic) potential:

$$U_{FENE} = -K(1 - l_0)^2 ln \left[1 - \left(\frac{l - l_0}{l_{max} - l_0}\right)^2\right] \tag{6.2}$$

with $K = 20, l_{max} = 1, l_0 = 0.7, l_{min} = 0.4$. The nonbonded interactions between monomers are described by the Morse potential.

$$\frac{U_M(r)}{\epsilon_M} = \exp(-2\alpha(r - r_{min})) - 2\exp(-\alpha(r - r_{min})) \tag{6.3}$$

with $\alpha = 24,\ r_{min} = 0.8,\ \epsilon_M/k_BT = 1$.

We employ periodic boundary conditions in the $x - y$ directions and impenetrable walls in the z direction. The lengths of the studied polymer chains are typically 32, 64, and 128. The size of the simulation box was chosen appropriately to the chain length, so for example, for a chain length of 128, the box size was $256 \times 256 \times 256$. The box size used here is larger than the size used in the previous studies. This is because we are dealing with a stretched chain . All simulations were carried out for constant force. A force f was applied to the last monomer in the z-direction, i.e., perpendicular to the adsorbing surface.

As in previous studies, the standard Metropolis algorithm was employed to govern the moves with self avoidance automatically incorporated in the potentials. In each Monte Carlo update, a monomer was chosen at random and a random displacement attempted with $\Delta x,\ \Delta y,\ \Delta z$ chosen uniformly from the interval $-0.5 \leq \Delta x, \Delta y, \Delta z \leq 0.5$. If the last monomer was displaced in z direction, there was an energy cost of $-f\Delta z$ due to the pulling force. The transition probability for the attempted move was calculated from the change ΔU of the potential energies before and after the move was performed as $W = \exp(-\Delta U/k_BT)$. As in a standard Metropolis algorithm, the attempted move was accepted, if W exceeds a random number uniformly distributed in the interval $[0, 1]$.

As a rule, the longest polymer chains, *i.e.* those with $N = 128$, have been originally equilibrated in the MC method for a period of about 5×10^5 MCS after which typically 500 measurement runs were performed, each of length 2×10^6 MCS. The equilibration period and the length of the run were chosen according to the chain length and the values provided here are for the longest chain length.

In the next section, we consider theoretically the basic features of adsorbed polymer chains.

6.3 Single chain adsorption: loop-, train-, and tail statistics

A single chain, adsorbed on a solid plane, is built up from loops, trains and a free tail. In order to derive expressions for the mean values of these basic structural units, one may treat the problem within the Grand Canonical Ensemble (GCE). In the GCE approach the lengths of these building blocks are not fixed and are allowed to fluctuate. The GC-partition function is given as

$$\Xi(z) = \sum_{N=0}^{\infty} \Xi_N \, z^N = \frac{V_0(z)\, Q(z)}{1 - V(z)U(z)} \tag{6.4}$$

where Ξ_N is the canonical partition function of a chain of length N and z is the fugacity. $U(z)$, $V(z)$ and $Q(z)$ denote the GC partition functions of loops, trains and a tail respectively. The building block adjacent to the tethered chain end is allowed for by $V_0(z) = 1 + V(z)$.

The series given by Eq. (6.4) is a geometric progression with respect to $U(z)V(z)$. Figure 6.1 gives a pictorial representation of this series.

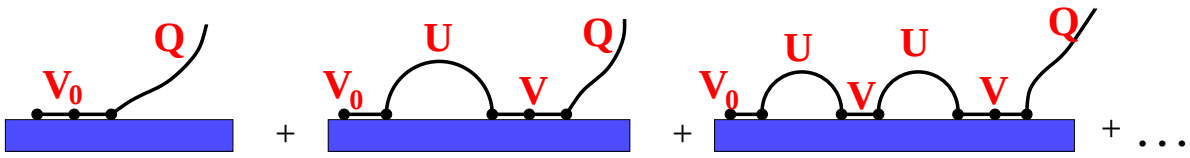

Figure 6.1: Schematic representation of the series expansion given by Eq. (6.4)

The GC-partition function of the loops is defined by

$$U(z) = \sum_{n=1}^{\infty} \Omega_n \, z^n = \sum_{n=1}^{\infty} \frac{(\mu_3 z)^n}{n^{1-\gamma_{11}}} \tag{6.5}$$

where Ω_n is the number of surface n-loops (i.e., self-avoiding walks of length n which start and terminate on the surface) configurations. For an isolated n-loop this number of configurations is given by $\Omega_n = \mu_3^n n^{\gamma_{11}-1}$ where μ_3 is the $3d$ connective constant (in three dimensions, $d = 3$, one has $\mu_3 = 4.68$, and the exponent $\gamma_{11} = -0.390$)[90]. Below we will demonstrate that the exponent γ_{11} changes due to the excluded volume interactions between different loops.

The train GC-partition function reads

$$V(z) = \sum_{n=1}^{\infty} \Psi_n \, z^n = \sum_{n=1}^{\infty} \frac{(\mu_2 w z)^n}{n^{1-\gamma_{d=2}}} \tag{6.6}$$

where the number of train configurations of length n (which are located in the $d = 2$ surface plane) is given by $\Psi_n = w^n \, \mu_2^n \, n^{\gamma_{d=2}-1}$. Here $\mu_2 = 2.6$ and $\gamma_{d=2} = 1.343$ [90]. In Eq. (6.6) we have taken into account that each adsorbed segment of the chain gains an additional statistical weight $w = \exp(\varepsilon/k_B T) \equiv \exp(\epsilon)$, where T is the temperature and the Boltzmann constant k_B is set to unity. In what follows the notation ϵ stands for the dimensionless adsorption energy of a single monomer. In fact, ϵ denotes the potential well depth of the short-ranged surface potential, defined in the description of our simulation model in Section 6.2.

The GC-partition function for the chain tail is given by

$$Q(z) = 1 + \sum_{n=1}^{\infty} \Lambda_n \, z^n = 1 + \sum_{n=1}^{\infty} \frac{(\mu_3 z)^n}{n^{1-\gamma_1}} \tag{6.7}$$

where the n-tail number of configuration equals $\Lambda_n = \mu_3^n \, n^{\gamma_1 - 1}$, and in $d = 3$ the exponent $\gamma_1 = 0.680$ [90].

With the knowledge of the GC partition function, given by Eq.(6.4), it is possible to calculate the number of weighted configurations of a polymer chain, containing N segments (i.e., its canonical partition function), Ξ_N. From the generating function method (see, e.g., Sec. 2.4 in the book by Rudnick and Gaspari [73]) it is well known that at $N \to \infty$ the coefficient at z^N *i.e.* Ξ_N (the canonical partition function) is defined by a singular point (a pole or a branch point) of $\Xi(z)$ which lies closest to the origin. Thus,

$$\Xi_N = \frac{1}{2\pi i} \oint \frac{\Xi(z)}{z^{N+1}} dz \tag{6.8}$$

or,

$$\Xi_N \simeq (z^*)^{-N} Res \quad \Xi(z^*) \tag{6.9}$$

In our case this is a simple pole, z^*, which is determined from the condition

$$V(z^*) \, U(z^*) = 1 \tag{6.10}$$

The principal contribution to this coefficient at z^N is $(z^*)^{-(N+1)}$, i.e., $\Xi_N \approx (z^*)^{-N}$, and so the corresponding free energy

$$F = -T \ln \Xi_N = TN \ln z^* \tag{6.11}$$

In Section 6.4, devoted to the adsorption of a pulled polymer chain, we shall see that an important singularity arises also from the tail generating function. The average fraction of adsorbed monomers, $n = N_s/N$ (where N_s is the number of adsorbed monomers) which we use as an order parameter for the degree of adsorption, can be calculated then as follows

$$n \equiv \frac{N_s}{N} = \frac{1}{N} \, \frac{\partial \, \ln \Xi_N}{\partial \ln w} = -\frac{\partial \ln z^*}{\partial \ln w} \tag{6.12}$$

The generating functions, given by Eqs. (6.5), (6.6), and (6.7), can be conveniently expressed in terms of the *polylog function* [30]. In Appendix B we sketch the properties of the polylog function and its behavior in the vicinity of the singular point. Here, we briefly mention the main properties : The polylog function $\Phi(\alpha, z)$ is defined by the series

$$\Phi(\alpha, z) = \sum_{n=1}^{\infty} \frac{1}{n^{\alpha}}\, z^n \tag{6.13}$$

which converges at $|z| < 1$. The polylog function at $z \to 1$ may be expressed as

$$\Phi(\alpha, z) \approx \begin{cases} \frac{\Gamma(1-\alpha)}{(1-z)^{1-\alpha}}, & \text{at} \quad \alpha < 1 \\ \ln\left(\frac{1}{1-z}\right), & \text{at} \quad \alpha = 1 \\ \zeta(\alpha) - a_\alpha (1-z)^{\alpha-1} - b_\alpha (1-z) + \ldots, & \text{at} \quad 1 < \alpha < 2 \end{cases} \tag{6.14}$$

where the coefficients $a_\alpha = \pi/\Gamma(\alpha)|\sin(\pi\alpha)|$ and $b_\alpha = \zeta(\alpha - 1)$.

Hence

$$U(z) = \Phi(1 - \gamma_{11}, \mu_3 z) = \Phi(1.39, \mu_3 z) \tag{6.15}$$

$$V(z) = \Phi(1 - \gamma_{d=2}, \mu_2 w z) = \Phi(-0.343, \mu_2 w z) \tag{6.16}$$

$$Q(z) = 1 + \Phi(1 - \gamma_1, \mu_3 z) = \Phi(0.32, \mu_3 z) \tag{6.17}$$

In terms of the polylog function (see Appendix B) the basic Eq.(6.10) is then given by

$$\Phi(\alpha, \mu_3 z^*) = \Phi^{-1}(\lambda, \mu_2 w z^*) \tag{6.18}$$

where the exponents $\alpha = 1 - \gamma_{11} \approx 1.39 > 1$ and $\lambda = 1 - \gamma_{d=2} \approx -0.343 < 1$. One should note that the exponent $\alpha = 1 - \gamma_{11}$ corresponds to a loop treated as an *isolated* one *i.e.* the interactions of the loop with the rest of the chain are neglected. This is an important feature of the method which handles the main building blocks (loops, trains and tails) as independent objects (see, e.g., Eq.(6.4)). Nevertheless, in Sec. 6.3.2, following Kafri et al. [94], we shall show that by taking into account the excluded volume interaction between a loop and the rest of the chain one ends up with a renormalized value of the exponent α (it increases). This is important because the value of α determines itself the value of the well known surface (or, *crossover*) exponent ϕ in all the basic scaling laws pertaining to polymer adsorption (see below).

Close to the critical point, $z_c = z^*$ which is defined by $\mu_3 z_c = 1$, the l.h.s. of Eq.(6.18) can be expanded (cf. Eq.(B.11)) as follows

$$\zeta(\alpha) - a_\alpha (1 - \mu_3 z^*)^{\alpha-1} - b_\alpha (1 - \mu_3 z^*) = \Phi^{-1}(1 - \gamma_{d=2}, \mu_2 w z^*) \tag{6.19}$$

with $\zeta(x)$ denoting the Riemann zeta-function. At the critical adsorption point (CAP), ϵ_c and $w_c = \exp(\epsilon_c)$, the solution of Eq. (6.18) is $z^* = z_c = 1/\mu_3$ so that w_c is given by the expression

$$\zeta(\alpha) = \Phi^{-1}(1 - \gamma_{d=2}, \mu_2 w_c/\mu_3). \tag{6.20}$$

The expansion of Eq.(6.19) around the critical point, $z^* = z_c$ and $w = w_c$, could be effected by the substitution of $w = w_c + \delta$ and $z^* = z_c - \Delta$ in Eq. (6.19). Here δ and Δ are corresponding infinitesimal increments and we took into account that z^* decreases with increasing w. Substituting this in Eq. (6.19) gives

$$\begin{aligned} \zeta(\alpha) - a_\alpha(\mu_3\Delta)^{\alpha-1} &\approx \Phi^{-1}(1 - \gamma_{d=2}, \mu_2 w_c z_c) \\ &\quad -\Phi^{-2}(1 - \gamma_{d=2}, \mu_2 w_c z_c) \left[\frac{d}{dx}\,\Phi(1 - \gamma_{d=2}, x)\right]_{x=\mu_2 w_c z_c} \delta \end{aligned} \tag{6.21}$$

Taking into account the condition for the critical point, Eq. (6.20), as well as the identity Eq. (B.2), the solution for z^* can be recast in the form

$$z^*(w) \approx \frac{1}{\mu_3}\left[1 - \left(\frac{A}{a_\alpha}\right)^{1/(\alpha-1)} (w - w_c)^{1/(\alpha-1)}\right] \tag{6.22}$$

where the constants

$$\begin{aligned} A &= \frac{\mu_2 \Phi(-\gamma_{d=2}, \mu_2 w_c/\mu_3)}{\Phi^2(1 - \gamma_{d=2}, \mu_2 w_c/\mu_3)} \\ a_\alpha &= \frac{\pi}{\Gamma(\alpha)|\sin(\pi\alpha)|}, \end{aligned} \tag{6.23}$$

and w_c is defined by Eq. (6.20). The full numerical solution for the order parameter as well as for the pole $z^*(w)$ is displayed in Fig. 6.2.

Having the solution Eq.(6.22) at hand, one can use the expression Eq.(6.12) for the average fraction of adsorbed monomers.

$$n \equiv \frac{\partial \ln z^*}{\partial \ln w} \tag{6.24}$$

and

$$\ln z^* \simeq \left(\frac{A}{a_\alpha}\right)^{\frac{1}{\alpha-1}} (w - wc)^{\frac{1}{\alpha-1}} \tag{6.25}$$

After some straightforward calculations we arrive at

$$n(\epsilon) \propto (\epsilon - \epsilon_c)^{\frac{1}{\alpha-1}-1} \tag{6.26}$$

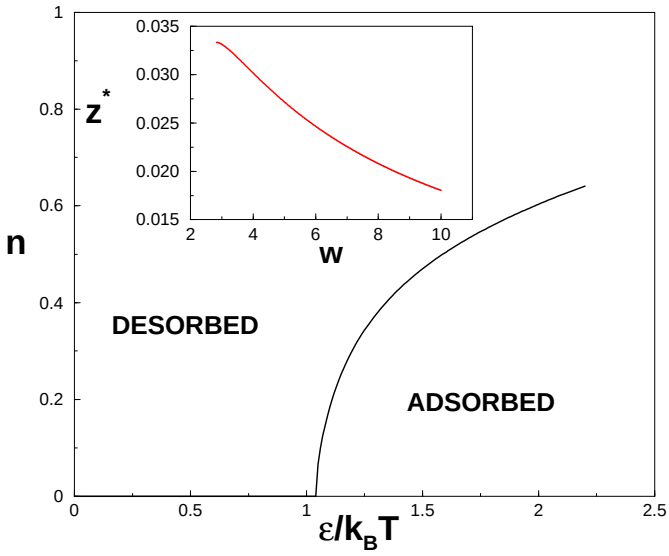

Figure 6.2: The 'order parameter' (i.e., the fraction of adsorbed chain segments), n, against the surface potential, ϵ, in the absence of detachment force, $f = 0$. The inset shows the variation of the fugacity z^* with $w = \exp(\epsilon)$, Eq. (6.18).

where we have used $w - w_c \approx \exp(\epsilon_c)\,(\epsilon - \epsilon_c)$. On the other hand, it is well known [90] that the scaling behavior in the vicinity of the critical adsorption energy is described by the crossover exponent ϕ (see Chapter 4). The corresponding scaling relationship (see Chapter 4 eq. 4.5) is given by

$$n(\epsilon) \propto \begin{cases} N^{\phi-1}, & \text{at} \quad \epsilon = \epsilon_c \\ (\epsilon - \epsilon_c)^{\frac{1}{\phi}-1} & \text{at} \quad \epsilon > \epsilon_c \end{cases} \tag{6.27}$$

If the result, given by Eq.(6.26), is compared to that of Eq. (6.27), it becomes apparent that

$$\phi = \alpha - 1 \tag{6.28}$$

which is one of the central results in the present investigation. As stated above, if the loops are treated as independent non-interacting objects, the exponent $\alpha = 1 - \gamma_{11}$, so that

$$\phi = -\gamma_{11} \approx 0.39 \tag{6.29}$$

In Sec. 6.3.2 we shall demonstrate that by taking into account the excluded volume interactions between a loop and the rest of the chain one finds an increase of the values of α, and ϕ, respectively.

6.3.1 Loops and tails distributions

Here we examine how the size distribution of polymer loops and tails looks like close to the critical point of adsorption. The GC-partition function for loops, given by Eq.(6.5), yields immediately

$$P_{\rm loop}(l) \approx \left.\frac{(\mu_3 z)^l}{l^\alpha}\right|_{z=z^*} = \frac{(\mu_3 z^*)^l}{l^{1+\phi}} \tag{6.30}$$

where we have used the essential relation between the loop exponent α and the crossover exponent ϕ, Eq.(6.28). Close to the critical point, $\mu_3 z^* \leq 1$ (see Eq.(6.22)) and the l-dependence is mainly described by inverse power-law

$$P_{\rm loop}(l) \approx \frac{1}{l^{1+\phi}} \tag{6.31}$$

Deeper in the region of adsorption, however, the exponential part in Eq. (6.30) dominates. Taking into account Eq.(6.22), one obtains

$$P_{\rm loop}(l) \approx \frac{1}{l^{1+\phi}} \exp\left[-c_1(\epsilon-\epsilon_c)^{1/\phi}\, l\right], \tag{6.32}$$

i.e., with increasing adsorption energy ϵ the size distribution becomes narrower.

The distribution of tails (at the CAP, i.e., at $\mu_3 z^* \leq 1$) is even broader, namely

$$P_{\rm tail}(l) \approx \frac{(\mu_3 z^*)^l}{l^\beta} \tag{6.33}$$

where for an isolated tail $\beta = 1-\gamma_1 \approx 0.32$. We will show below (see Eq.(6.57)) that if the interaction of a tail with the rest of the chain is taken into account this leads to a larger value of $\beta = 0.51$. One should be aware, however, that this result, Eq. (6.33), is only valid for $\epsilon \geq \epsilon_c$ since a solution for Eq. (6.18) does not exist for subcritical values of the adsorption potential. It is clear, however, that even in the subcritical region, $\epsilon < \epsilon_c$ there are still monomers which occasionally touch the substrate, creating thus single loops at the expense of the tail length. This affects and modifies therefore the distribution $P_{\rm tail}$ in the vicinity of ϵ_c. One can take into account this additional contribution by considering a single loop - tail configuration. Pictorially the latter can be inferred from Fig. 6.4b where instead of two loops and a tail one should imagine a single loop adjacent to the tail. The partition function of such configuration is given by

$$Z_{l-t} = \frac{\mu_3^{N-l}}{(N-l)^{1+\phi}}\,\frac{\mu_3^l}{l^\beta}$$

(from eq. 6.30 and 6.33). On the other side, the partition function of a tethered chain is $Z_t = \mu_3^N\, N^{\gamma_1-1}$. Thus the probability $P^<_{\rm tail}(l)$ to find a tail of length l next to a single loop of length $N-l$ can be estimated as

$$P^<_{\rm tail}(l) = \frac{Z_{l-t}}{Z_t} \propto \frac{N^{1-\gamma_1}}{l^\beta (N-l)^{1+\phi}}. \tag{6.34}$$

Evidently, Eq. (6.34) predicts a singularity (that is, a steep maximum) in the distribution of tails when $l \cong N$. One may expect that in the vicinity of the critical point, $\epsilon \approx \epsilon_c$, the observed distribution of tails will be given by an interpolation between the expressions shown in Eq. (6.33) and Eq. (6.34). As in the case of loop, distributions, deeper in the region of adsorption, we use Eq. (6.30) to obtain

$$P_{\text{tail}}(l) = \frac{1}{l^\beta} \exp\left[-c_1(\epsilon - \epsilon_c)^{1/\phi}\, l\right]$$

Hence, the overall tail distribution can be represented as

$$P_{\text{tail}}(l) = \begin{cases} \frac{1}{l^\beta} \exp\left[-c_1(\epsilon - \epsilon_c)^{1/\phi}\, l\right], & \epsilon > \epsilon_c \\ \frac{A_1}{l^\beta} + \frac{A_2 N^{1-\gamma_1}}{l^\beta (N-l)^{1+\phi}}, & \epsilon = \epsilon_c \\ \frac{N^{1-\gamma_1}}{l^\beta (N-l)^{1+\phi}}. & \epsilon < \epsilon_c \end{cases} \tag{6.35}$$

Evidently, close to the CAP this distribution is expected to attain a U-shaped form with maxima at $l \approx 1$ and $l \cong N$. This shape of $P_{\text{tail}}(l)$ has been predicted earlier for a Gaussian chain by Gorbunov et al.[36]. In close analogy with Eq. (6.35), the distribution of loops reads

$$P_{\text{loop}}(l) = \begin{cases} \frac{1}{l^\beta} \exp\left[-c_1(\epsilon - \epsilon_c)^{1/\phi}\, l\right], & \epsilon > \epsilon_c \\ \frac{B_1}{l^{1+\phi}} + \frac{B_2 N^{1-\gamma_1}}{l^{1+\phi}(N-l)^\beta}, & \epsilon = \epsilon_c \\ \frac{N^{1-\gamma_1}}{l^{1+\phi}(N-l)^\beta}. & \epsilon < \epsilon_c \end{cases} \tag{6.36}$$

In Eqs. (6.35)-(6.36) A_1, A_2, B_1, B_2 are some constants. As we shall see in Section 6.5, the simulation results for $P_{\text{tail}}(l), P_{\text{loop}}(l)$ are in good agreement with the predictions, Eqs. (6.35)-(6.36).

Divergence of the average loop and tail lengths at criticality

The average loop length is defined by the loop GC-partition function, Eq.(6.5), as

$$L = z\, \frac{\partial \ln U(z)}{\partial z}\bigg|_{z=z^*} = \frac{\Phi(\alpha - 1, \mu_3 z^*)}{\Phi(\alpha, \mu_3 z^*)} \tag{6.37}$$

where we have used Eq.(B.2). Taking into account the polylog function behavior given by Eq.(B.11) with the requirement that $1 < \alpha < 2$ as well as the solution for z^*, Eq.(6.22), one gets

$$L \approx \frac{\Gamma(2-\alpha)}{\zeta(\alpha)} \left(\frac{a_\alpha}{A}\right)^{\frac{2-\alpha}{\alpha-1}} \frac{1}{(w - w_c)^{\frac{2-\alpha}{\alpha-1}}} \propto \frac{1}{(\epsilon - \epsilon_c)^{\frac{1}{\phi}-1}} \tag{6.38}$$

where the result Eq.(6.28) has been used. This result is compatible with the scaling prediction based on Eq. (6.27). Indeed, close to criticality, $L \approx N/N_s$. From Eq.(6.27) one obtains then the same result, $L \propto (\epsilon - \epsilon_c)^{1-1/\phi}$. The free energy goes as $F = TN \ln z^* \propto -N(\epsilon - \epsilon_c)^{1/\phi}$ where one has used Eq.(6.22). On the other hand, the free energy is proportional to the number of adsorption blobs, i.e., $F \propto N/g$, where g is the length (number of segments) of the blob. The adsorption blobs are defined to contain as many monomers g as necessary to be on the verge of adsorption and therefore carry an adsorption energy of the order of k_BT each. In result the blob length scales as $g \propto (\epsilon - \epsilon_c)^{-1/\phi}$. The size of the adsorbed chain perpendicular to the surface, $R_\perp$, is nothing but the blob size, that is, $R_\perp \approx g^\nu$. Thus one obtains

$$R_\perp \propto \frac{1}{(\epsilon - \epsilon_c)^{\nu/\phi}}. \tag{6.39}$$

Consider now the average tail length S. In terms of the GC-partition function for blobs, Eq. (6.7), it reads

$$S = z \left.\frac{\partial \ln Q(z)}{\partial z}\right|_{z=z^*} = \frac{\Phi(\beta - 1, \mu_3 z^*)}{1 + \Phi(\beta, \mu_3 z^*)} \tag{6.40}$$

with the exponent $\beta = 1 - \gamma_1 = 0.32 < 1$. This value of the exponent β does not allow for the interaction of the tail with other building blocks of the adsorbed chain and will be corrected in Sec.6.3.2. Using the results, Eqs. (B.11) and (6.22), the expression for the average tail length Eq.(6.40) can be recast in the form

$$S \approx (1 - \beta) \left(\frac{a_\alpha}{A}\right)^{\frac{1}{\alpha - 1}} \frac{1}{(w - w_c)^{\frac{1}{\alpha - 1}}} \propto \frac{1}{(\epsilon - \epsilon_c)^{\frac{1}{\phi}}} \tag{6.41}$$

Notably, the exponent β drops out of this expression. The corresponding tail size $R_\mathrm{S} \sim S^\nu$ scales as

$$R_\mathrm{S} \propto \frac{1}{(\epsilon - \epsilon_c)^{\nu/\phi}} \tag{6.42}$$

Note that the tail size, Eq.(6.42), scales exactly like the *blob* (and not the loop!) size, Eq. (6.39).

6.3.2 Role of *interacting* loops and tails

As mentioned above, the exponent α, which governs the numbers of loops in the configuration of adsorbed polymer, determines also the crossover exponent ϕ so that it is of prime importance to know the exact value of α. If the surface loops are treated as isolated objects (i.e., loop-loop or loop-tail interactions are ignored), the exponent $\alpha = 1 - \gamma_{11} = 1.39$. Recently Kafri *et al.* [94] have shown in the context of DNA

melting that the interaction of a loop with the rest of the chain increases the loop exponent α. In their work the authors of ref. [94] essentially used some results of the renormalization theory of arbitrary polymer graphs, developed earlier by Duplantier [27]. This approach makes it possible to treat also polymer chains which are grafted onto a solid surface. Here we give a short sketch of Duplantier's results for a polymer graph located close to the surface and then demonstrate how the loop-loop and loop-tail interactions lead to the enhancement of the effective surface loop exponent.

For an arbitrary self-avoiding polymer graph $\mathcal{G}$, which is grafted on the surface, it has been shown by Duplantier [27] by renormalization methods that the total number of configurations is given by the standard asymptotic expression:

$$Z(\mathcal{G}) = \mu_3^N \; N^{\gamma^s - 1} \tag{6.43}$$

where $N = \sum_{j=1}^{\mathcal{N}} M_j$ is the total length of the graph made of $\mathcal{N}$ chains (or edges) of length M_j. The surface exponent γ^s is given by the following general relationship

$$\gamma^s = 1 - \nu(d\mathcal{L} + \mathcal{L}_s + \mathcal{V}_s - 1) + \sum_{k\geq 1} (n_L \sigma_k + n_k^s \sigma_L^s) \tag{6.44}$$

where ν is the Flory exponent and d stands for the space dimensionality. In Eq. (6.44) $\mathcal{L}$ is the total number of independent constitutive polymer loops in the graph $\mathcal{G}$ (i.e., the surface loops are not included in $\mathcal{L}$). $\mathcal{L}_s$ is the total number of extremities of polymer lines upon contact to the surface. n_k and n_k^s are the numbers of bulk and surface vertices of order k respectively, thus $\mathcal{L}_s = \sum_{k\geq 1} k\, n_k^s$. $\mathcal{V}_s$ gives the number of surface vertices, i.e., $\mathcal{V}_s = \sum_{k\geq 1} n_k^s$. Finally, σ_k and σ_k^s are critical bulk and surface exponents which correspond to the k-arm vertices. In $d < 4$ these exponents can be calculated analytically via the ε-expansion but some of them could be also expressed in terms of the conventional exponents ν, γ, γ_1 and γ_{11} [27]. Figure 6.3 gives an example of a polymer graph with the specification of its topological elements.

The number of configurations given by Eq.(6.43) holds when the lengths of all components M_a are large and comparable to the total length N. As long as at least one of them becomes small, i.e. $M_a \ll N$, then one gets

$$Z(\mathcal{G}) = \mu_3^N \; N^{\gamma^s - 1} \, G\left(\frac{M_1}{N}, \frac{M_2}{N}, \ldots, \frac{M_{\mathcal{N}}}{N}\right) \tag{6.45}$$

where the scaling function $G(x_1, x_2, \ldots, x_{\mathcal{N}})$ has a singularity, provided any of the arguments x_a goes to zero. In fact, in this limit the polymer graph changes its topology and, therefore, the surface exponent γ^s changes too. In the next subsection we show how these results could be used to calculate the effective exponent α which takes into account the interaction of a surface loop with the rest of the chain.

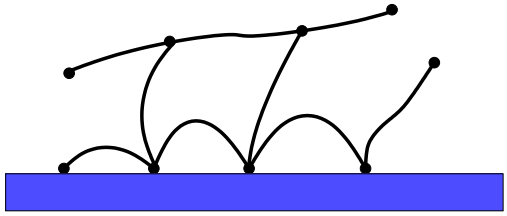

Figure 6.3: A polymer graph located close to the surface has the following topological characteristics: $\mathcal{L} = 1$, $\mathcal{L}_s = 9$, $\mathcal{V}_s = 4$, $n_1 = 3$, $n_3 = 2$, $n_1^s = 1$, $n_2^s = 1$, $n_3^s = 2$. One surface vertex is fixed whereas the other vertices may move freely.

Surface loop embedded in an adsorbed chain

Consider the configurations of a chain (tethered with one end on the surface) in the vicinity of the adsorption critical point (see Fig. 6.4). Let M be the length of a surface loop while K measures the length of the rest of the chain, i.e., $M + K = N$. The number of configurations of the polymer graph, depicted in Fig.6.4a, is

$$Z = \mu_3^{M+K}\,(M+K)^{\gamma_a^s-1}\,G\left(\frac{M}{M+K}\right) \tag{6.46}$$

where γ_a^s is the exponent which could be calculated using Eq.(6.44) (see below) and the scaling function $G(x) \approx 1$ for large M and K. In the case when $M/K \to 0$ one has a crossover to the polymer graph shown in Fig 6.4b where the number of configurations $Z \sim \mu_3^K\,(K)^{\gamma_a^s-1}\,(1/K)^{\gamma_a^s-\gamma_b^s}$ (with γ_b^s being the surface exponent of the corresponding graph). These arguments fix the form of the scaling function which can be written as

$$G(x) \approx \begin{cases} x^{\gamma_a^s-\gamma_b^s}, & \text{at} \quad x \ll 1 \\ 1, & \text{at} \quad x \approx 1 \end{cases} \tag{6.47}$$

In the case of a small surface loop, embedded in an adsorbed polymer, with $M \gg 1$ and $K \gg 1$ (but with $M/K \ll 1$) one obtains for the total number of configurations

$$Z \sim \mu_3^{M+K}\,K^{\gamma_a^s-1}\left(\frac{M}{K}\right)^{\gamma_a^s-\gamma_b^s} \sim \mu_3^M\,M^{\gamma_a^s-\gamma_b^s}\;\mu_3^K\,K^{\gamma_b^s-1}. \tag{6.48}$$

The last result indicates that the total partition function may be factorized to $Z \sim Z_{\rm loop}\,Z_{\rm rest}$ where $Z_{\rm loop}$ and $Z_{\rm rest}$ are the partition functions of the small loop and the rest of the chain, respectively. Thus, using the notations of Eq.(6.5), one obtains $\Omega_n = \mu_3^n/n^{\gamma_b^s-\gamma_a^s}$, i.e., the effective exponent α becomes

$$\alpha = \gamma_b^s - \gamma_a^s. \tag{6.49}$$

Now we are in a position to determine the exponents γ_a^s and γ_b^s. Let us assume that the polymer graph in Fig. 6.4a is made of $\mathcal{N}$ subchains ($\mathcal{N} - 1$ being loops and 1 - a

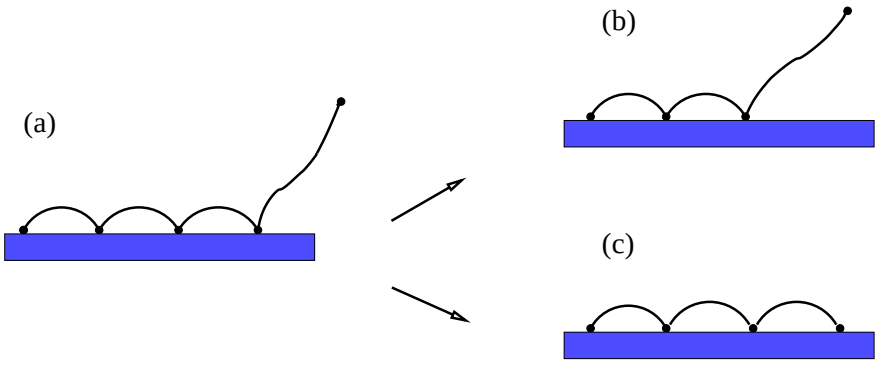

Figure 6.4: An array of surface loops close to criticality. One of the surface loops of length M in the limit $M/N \ll 1$ is contracted, changing the topology of the polymer graph from (a) to (b). This contraction procedure makes it possible to derive the scaling function $G(x)$. By similar contraction of a tail the graph goes over from (a) to (c).

tail). The topological characteristics can be specified as follows: $\mathcal{L} = 0$, $\mathcal{L}_s = 2\mathcal{N} + 1$, $\mathcal{V}_s = \mathcal{N}$, $n_1 = 1$, $n_1^s = 1$, $n_2^s = \mathcal{N} - 1$. Earlier it has been shown [27] that the critical exponent $\sigma_2^s = 2\nu + 1$. With these values Eq.(6.44) yields

$$\gamma_a^s = 2 - \mathcal{N}(\nu + 1) + \sigma_1 + \sigma_1^s \tag{6.50}$$

The corresponding expression for γ_b^s can be obtained from Eq. (6.50) by the substitution $\mathcal{N} \to \mathcal{N} - 1$. This yields

$$\gamma_b^s = 3 + \nu - \mathcal{N}(\nu + 1) + \sigma_1 + \sigma_1^s \tag{6.51}$$

The final expression for the exponent α, given by Eq. (6.49), then reads

$$\alpha = \gamma_b^s - \gamma_a^s = \nu + 1. \tag{6.52}$$

With this theoretical prediction the value of the crossover exponent, given by Eq. (6.28), is determined as:

$$\phi = \alpha - 1 = \nu = 0.588 \tag{6.53}$$

where we have taken the best numerical estimate for the Flory exponent ν at $d = 3$ [90]. A comparison of Eq.(6.53) with Eq. (6.29) leads to the important conclusion that, depending on the range of the excluded volume interaction, the value of ϕ may vary significantly. Indeed, if the interactions affect beads from the same surface loop only then ϕ is given by Eq.(6.29), otherwise (i.e., when the beads from all loops interact) the value of ϕ will be enhanced markedly (see Eq. (6.53)).

One should emphasize, however, that Eq. (6.52) does not give an *exact* value for the exponent α, but rather an upper limit only. Indeed, the total number of configurations, given by Eq. (6.48), is estimated by a *factorized* expression for the partition function which takes into account the contribution of a loop and the rest of the chain. As a matter of fact this is a Mean Field approach which overestimates interactions at the expense of correlations, reducing thus the total number of configurations of a loop. The latter is reflected by an increase of α. The precise value of α therefore satisfies the inequality $1 - \gamma_{11} < \alpha < 1 + \nu$. In the special case of a Gauissian chain both the lower and upper limits for α merge while for a phantom chain one has $\gamma_{11} = -0.5$ (cf. Section 6.2 in [27]) and $\nu = 0.5$. Thus, for Gaussian chains one obtains the well known value $\phi = 0.5$.

Following the same way of reasoning, one may expect that the exponent for the tail, β (see Eq. (6.40)), is also renormalized due to interaction with the rest of the adsorbed chain. Tail contraction when going from (a) to (c) in Fig. 6.4 enables one to obtain for the renormalized β-exponent the following relationship

$$\beta = \gamma_c^s - \gamma_a^s \tag{6.54}$$

where γ_c^s is the surface exponent of the polymer graph given in Fig. 6.4c. Again, if the polymer graph given in Fig. 6.4a is made of $\mathcal{N}$ chains then the exponent γ_c^s for the graph Fig. 6.4c becomes

$$\gamma_c^s = 3 - \nu - \mathcal{N}(\nu + 1) + 2\sigma_1^s \tag{6.55}$$

Taking into account Eq. (6.50), one obtains $\beta = 1 - \nu + \sigma_1^s - \sigma_1$, whereby the critical exponents (see [27]) are given by

$$\begin{aligned} \sigma_1 &= \frac{\gamma - 1}{2} \\ \sigma_1^s &= \nu + \gamma_1 - \frac{\gamma + 1}{2} \end{aligned} \tag{6.56}$$

The calculation gives finally

$$\beta = \gamma_1 - \gamma + 1 \tag{6.57}$$

with $\gamma_1 \approx 0.68$ and $\gamma \approx 1.17$ so that $\beta \approx 0.51$. As expected, the value of the β-exponent *increases* as compared to the "isolated tail" case, $\beta = 1 - \gamma_{11} \approx 0.32$.

Comparison with other results

The result, given by Eq. (6.53), deserves a more detailed discussion. One should point out that, generally, the value of ϕ for the good solvent case in three dimension

has been so far fairly controversial. For example, Monte-Carlo (MC) data (albeit for relatively short chains $N \leq 100$) on a diamond lattice yield $\phi = 0.588 \pm 0.03$ [29] which is in complete agreement with Eq.(6.53). A recent MC-investigation [20] has suggested that the uncertainty in the value of ϕ might be related to the limited accuracy in the determination of the critical adsorption energy ϵ_c. Namely, for the bond fluctuation model (BFM), which has been used by Descas, Sommer and Blumen [20], ϵ_c ranges between 0.98 and 1.01, i.e., within $\pm 2.5\%$. This relatively small change leads to significant variation of ϕ between 0.5 and 0.59. The same authors have shown that the set of parameters, $\epsilon_c = 1.01$ and $\phi = 0.59$, leads to a more accurate scaling prediction. The adsorption of the tethered SAW chain on a simple cubic lattice for chain lengths of up to $N = 1000$ (by means of the so-called "scanning method") gives: $\phi = 0.53 \pm 0.007$ [56]. In yet another MC-study, based on the pruned-enriched Rosenbluth method (PERM) [43], it was found that ϕ is pretty close to 0.5. However, in a more recent study of the same author [37] one determined for ϕ an even smaller value: $\phi = 0.484 \pm 0.002$. The value $\phi = 0.5$ was also been supported by the MC-simulation results based on the off-lattice model [57].

The analytical methods for calculation of ϕ are based on the field-theoretical renormalization group (RG) study of the semi-infinite n-vector model in the $n \to 0$ limit. In earlier investigations [23, 22, 28] the ε-expansion (where $\varepsilon = 4 - d$) up to order ε^2 lead to the prediction $\phi = 0.67$ which deviates widely from all MC-findings. In a more recent investigation the so-called massive field-theory approach at fixed d (i.e., the ε-expansion has been avoided) was extended to systems with surfaces [24, 25]. The result for the crossover exponent reads $\phi \approx 0.52$. Thus we believe that the present study elucidates the origin for the diversity of results concerning the precise value of ϕ and provides a physical background of it.

6.4 Adsorption under external detaching force

The adsorption of a Gaussian chain on a solid plane under detaching force acting on the chain end has been studied first by Skvortsov, Gorbunov and Klushin [35, 80] in the early 90s. For a Gaussian chain the problem can be solved rigorously even for a finite chain length N. The adsorption-desorption transition is of the first order, however, phase coexistence and metastable states are absent.

Below we apply the GC - ensemble approach to the case of self-avoiding polymer chain adsorption under the presence of detaching force. Again, the problem has much in common with the unzipping transition of double-stranded DNA [94]. When a force f is applied to the free end of the tethered chain, the tail GC partition function in

Eq.(6.4) changes. The total GC-partition function is then given by

$$\Xi(z) = \frac{V_0(z)\, R(z)}{1 - V(z)U(z)} \tag{6.58}$$

where the tail GC - partition function now takes on the form

$$R(z) = 1 + \sum_{n=1}^{\infty} \Xi_{\text{tail}}(n)\, z^n \tag{6.59}$$

In Eq.(6.59) $\Xi_{\text{tail}}(n)$ is the canonical partition function of the tail under applied force:

$$\Xi_{\text{tail}}(n) = \frac{\mu_3^n}{n^\beta} \int d^3r\, P_n(\mathbf{r})\, \exp\left(fz/T\right). \tag{6.60}$$

Here we take into account that the pulling force is directed perpendicular to the plane (in z-direction). In Eq. (6.60) $P_n(\mathbf{r})$ is the end-to-end distance probability distribution function (PDF). To estimate this function on large distances from the solid plane, i.e., at $z \gg R_n \approx an^\nu$, we assume, following Kreer et al. [51], that under this condition the PDF is given by the des Cloizeaux expression [19] for the bulk:

$$P_n(\mathbf{r}) = \frac{1}{R_n^3}\, F\left(\frac{\mathbf{r}}{R_n}\right) \tag{6.61}$$

where the scaling function $F(x)$ is

$$F(x) = Bx^t\, \exp\left(-Dx^\delta\right). \tag{6.62}$$

In Eq. (6.62) B and D are constants while the exponents δ and t are given by

$$\delta = \frac{1}{1-\nu} \tag{6.63}$$

and

$$t = \frac{\beta - d/2 + d\nu}{1-\nu}. \tag{6.64}$$

Here $\beta = 1 - \gamma_1$ is the tail surface exponent and $d = 3$. Note that in the limit $z \gg R_n$ the only difference between the PDFs in the bulk and in the semi-infinite case lies in the fact that instead of the exponent γ in Eq. (6.64) one has γ_1. The integration over x and y coordinates in Eq.(6.60) is readily carried out and one obtains

$$\begin{aligned} \Xi_{\text{tail}}(n) &= \frac{\mu_3^n}{n^\beta}\, \frac{C}{R_n} \int_0^\infty dz\, \left(\frac{z}{R_n}\right)^{2+t-\delta} \exp\left[-D\left(\frac{z}{R_n}\right)^\delta + \frac{fz}{T}\right] \\ &= C\, \frac{\mu_3^n}{n^\beta} \int_0^\infty dx\, x^{2+t-\delta} \exp\left(-Dx^\delta + \tilde{f}_n x\right) \end{aligned} \tag{6.65}$$

where the normalization constant $C = \delta D^{(3+t)/\delta-1}/\Gamma[(3+t)/\delta-1]$. The integral in Eq. (6.65) can be tackled by the saddle point method (since $\tilde{f}_n \equiv fR_n/T \gg 1$). The saddle point itself is defined by the value $x_{\rm sp} = (\tilde{f}_n/(\delta D))^{1/(\delta-1)} \sim \tilde{f}_n^{1/\nu-1}$, or, in terms of the z-variable,

$$z_{\rm sp} \approx R_n \left(\tilde{f}_n\right)^{1/\nu-1} \approx an \left(\frac{fa}{T}\right)^{1/\nu-1} \tag{6.66}$$

which is nothing but the well-known Pincus deformation law [14]. Finally, Eq. (6.65) becomes

$$\Xi_{\rm tail}(n) = a_1 \, (\tilde{f})^\theta \, \frac{\mu_3^n}{n^{\beta-\theta\nu}} \, \exp\left(a_2 \tilde{f}^{1/\nu} n\right) \tag{6.67}$$

with a_1 and a_2 being constants, the dimensionless force $\tilde{f} \equiv fa/T$, and the exponent $\theta = (2+t-3\delta/2)/(\delta-1)$. Thus the GC-partition function , Eq. (6.59), can be written as

$$\begin{aligned} R(z) &= 1 + a_1 \, (\tilde{f})^\theta \sum_{n=1}^{\infty} \frac{1}{n^\psi} \left[z\mu_3 \exp(a_2 (\tilde{f})^{1/\nu}\right]^n \\ &= 1 + a_1 \, (\tilde{f})^\theta \, \Phi(\psi, z\mu_3 \exp(a_2 (\tilde{f})^{1/\nu}) \end{aligned} \tag{6.68}$$

where we have defined the new exponent

$$\psi = \beta - \nu\theta = \frac{d-1}{2} - (d-2)\nu. \tag{6.69}$$

One should point out that the exponent β drops out from the final expression for ψ which for $d = 3$ is defined as $\psi = 1 - \nu$.

It is evident from Eq. (6.68) that (cf. Eq.(B.11)) at $z \to \mu_3^{-1} \exp(-a_2 \tilde{f}^{1/\nu})$ the tail GC-partition function has a branch point at $z = z^\#$, i.e.

$$R(z) \sim a_1 \, (\tilde{f})^\theta \, \frac{\Gamma(1-\psi)(z^\#)^{1-\psi}}{[z^\# - z]^{1-\psi}} \tag{6.70}$$

where $1 - \psi < 1$ and

$$z^\# = \mu_3^{-1} \, \exp(-a_2 \tilde{f}^{1/\nu}). \tag{6.71}$$

Turning back to the total GC-partition function, Eq.(6.58), one may conclude that $\Xi(z)$ has two singularities on the real axis Rez: the pole z^* which is defined by Eq.(6.10), and the branch point $z^\#$ given by Eq. (6.71). It is well known (see, e.g., Sec. 2.4.3 in [73]) that in the thermodynamic limit, $N \to \infty$, the contribution to the coefficient of z^N (i.e., to Ξ_N) consists of contributions by the pole and by the branch singular points, i.e.

$$\Xi_N \sim C_1 \, (z^*)^{-(N+1)} + \frac{C_2}{\Gamma(1-\psi)} \, N^{-\psi} \, (z^\#)^{-(N+1-\psi)} \tag{6.72}$$

The singular points, z^* and $z^\#$, are involved in Eq.(6.72) with large negative exponents. Hence, for large N only the smallest of these points matters. On the other hand, z^* depends on the dimensionless adsorption energy ϵ only (or, on $w = \exp(\epsilon)$) whereas $z^\#$ is controlled by the dimensionless external force $\tilde{f}$ (cf., Eq.(6.71)). Therefore, in terms of the two *control parameters*, ϵ and $\tilde{f}$, the equation

$$z^*(\epsilon) = z^\#(\tilde{f}) \tag{6.73}$$

determines the critical line of transition between the adsorbed phase and the force-induced desorbed phase. In the following this line will be referred to as the *detachment line*. The controll parameters, ϵ_D and $\tilde{f}_D$, which satisfy Eq. (6.73), will be named detachment energy and detachment force, respectively. On the detachment line the system undergoes a first-order phase transition. The detachment line at $\tilde{f}_D \to 0$ terminates in the critical adsorption point, ϵ_c, where the transition becomes of second order. In the vicinity of the critical adsorption point the detachment force $\tilde{f}_D$ behaves as

$$\tilde{f}_D \sim (\epsilon - \epsilon_c)^{\nu/\phi} \tag{6.74}$$

where we have used Eq.(6.73) as well as Eqs. (6.22) and (6.71).

6.4.1 Order parameter

Let us study first how the fraction of adsorbed monomers $n = N_s/N$, which we use as an order parameter, depends on the pulling force at fixed value of the contact energy $\epsilon_1 > \epsilon_c$. For $\tilde{f} < \tilde{f}_D$ it is clear that $z^* < z^\#$ and the first term in Eq. (6.72) dominates over the second one. In this case the order parameter

$$n = -\left.\frac{\partial \ln z^*(w)}{\partial \ln w}\right|_{w=\exp(\epsilon_1)} \tag{6.75}$$

is constant independent of the force. At $\tilde{f} > \tilde{f}_D$ (i.e., after crossing the detachment line) $z^* > z^\#$ and the second term in Eq. (6.72) prevails. Since $z^\#$ is w-independent, it is evident that $n = 0$, i.e., the polymer is totally detached. In result, the n vs. $\tilde{f}$ dependence resembles a step - function with a jump at $\tilde{f} = \tilde{f}_D$.

Now let us fix the force $\tilde{f} = \tilde{f}_1$ and investigate how the order parameter n depends on the adsorption energy ϵ or on the fugacity w. Again, Eq.(6.73) at $\tilde{f} = \tilde{f}_1$ defines a detachment energy ϵ_D. At $\epsilon < \epsilon_D$ one has still $z^\# < z^*$ and the second term in Eq. (6.72) dominates so that the chain is completely desorbed (i.e., $n = 0$). At $\epsilon > \epsilon_D$ only the first term in Eq.(6.72) survives so that the relationship n vs. ϵ follows the conventional adsorption dependence without any force-influence. The transition at $\epsilon = \epsilon_D$ is of first order whereby the order parameter jump grows as the force $\tilde{f}_1$ increases.

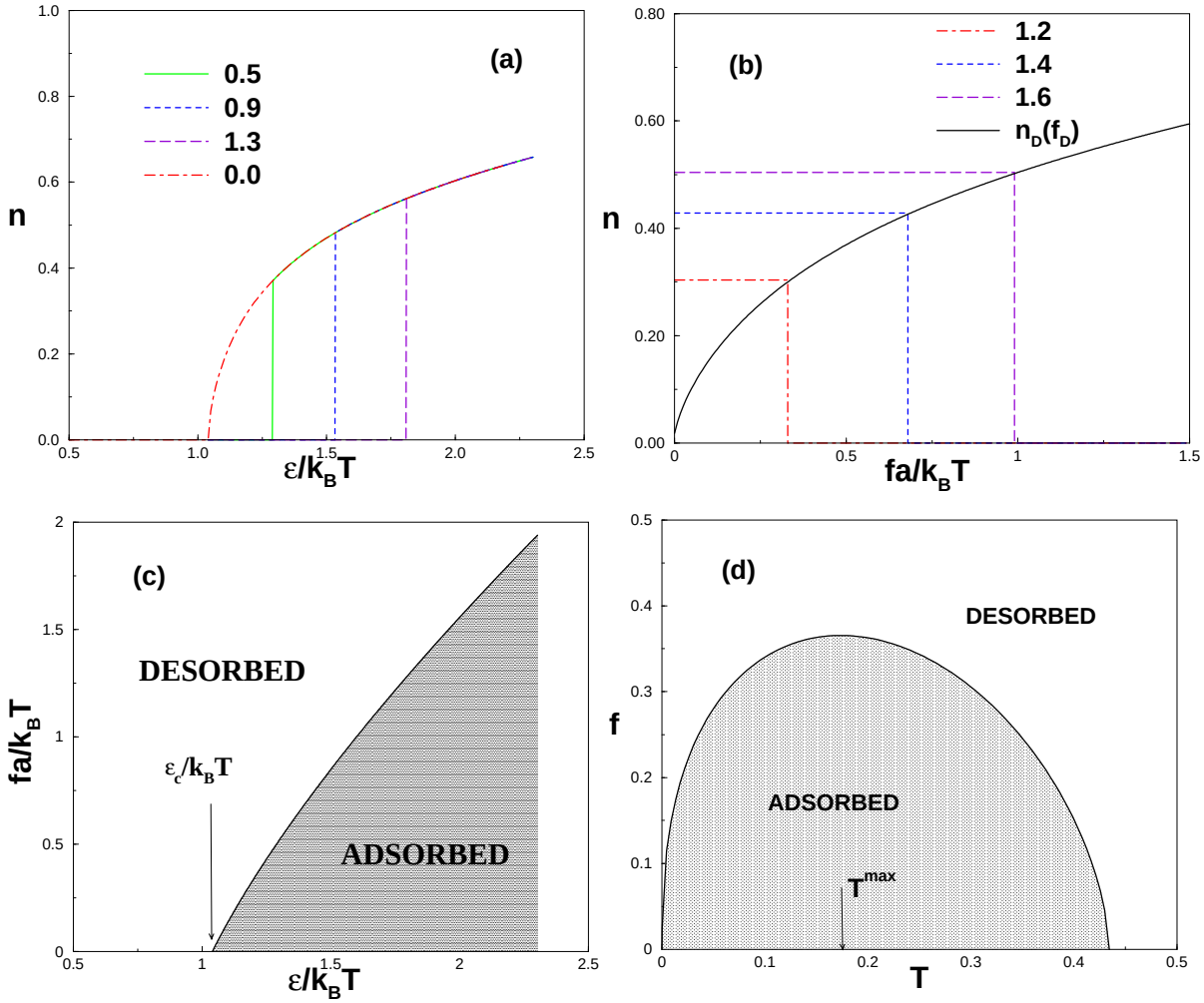

Figure 6.5: The 'order parameter' , n, against the: (a) energy of adsorption ϵ (f is given as a parameter); (b) - against the pulling force f, with ϵ a parameter. Vertical lines denote the discontinuous jumps of n, indicating a $1^{st}-$ order transition. The $n_D(f_D)$ (full line) in (b) denotes the order parameter value at the detachment line. (c) The phase diagram of the adsorption-desorption transition under puling force f in dimensionless units. An arrow at ϵ_c denotes the point of critical adsorption for $f = 0$. (d) The *reentrant* phase diagram - the same as in (c) but with force against temperature in dimensional units at fixed value of $\epsilon > \epsilon_c$. The largest force f for which chain adsorption may still take place occurs at temperature $T^{\max}$, as indicated by an arrow.

In Figure 6.5a,b we show the predicted variation of the order parameter for an infinitely long chain, following from the present consideration. The boundary of the region of adsorbtion, shown in the phase diagram in Figure 6.5c, denotes the line of critical values of detachment force for any given attraction of the substrate as described by Eq. (6.73).

The adsorption-desorption first order phase transition under pulling force has a clear dichotomic nature (i.e., it follows an "either - or" scenario): in the thermodynamic limit $N \to \infty$ there is *no* phase coexistence! The configurations are divided into adsorbed and detached (or stretched) dichotomic classes. The metastable states are completely absent. Basically, this is in line with the general thermodynamic principles which argue that in thermal equilibrium the thermodynamic potentials are convex functions of their order parameters. This excludes multiple minima and metastable states [8].

6.4.2 Reentrant behavior of the phase diagram

The results given in Section 6.4.1 demonstrate that the detachment line on the phase diagram is a monotonous function in terms of the dimensionless quantities $\tilde{f}_D$ vs. ϵ_D. Recently, it has been revealed that the detachment line, when represented in terms of *dimensional* variables, force f_D versus temperature T, goes (at the relatively low temperature) through a maximum, that is, the desorption transition shows a reentrant behavior! Below we demonstrate that this result follows directly from our theory.

First, one should note that the low temperature limit implies large values of the ratio $\epsilon = \varepsilon/k_BT$. On the other hand, the solution $z^*(w)$, which results from Eq.(6.18), goes to zero, i.e., $z^* \to 0$, when $\varepsilon \to \infty$. One may assume that under these conditions $z^*\mu_2 \mathrm{e}^{\epsilon} \to 1^-$ (this will be proven *a posteriori*). Then the polylog function in the l.h.s. of Eq.(6.18) reads $\Phi(\alpha, \mu_3 z^*) \approx \mu_3 z^*$ but $\Phi^{-1}(\lambda, \mu_2 w z^*) \approx c_1(1 - \mu_2 w z^*)^{1-\lambda}$ (where we have used Eq. (B.11) and the fact that $\lambda < 1$). Taking into account Eq.(6.18), one arrives at the following result

$$\mu_3 z^* \approx c_1(1 - \mu_2 w z^*)^{1-\lambda} \tag{6.76}$$

This equation determines the function $z^*(w)$ at large w. To zero-order approximation the solution reads $z^*_{(0)} \approx (\mu_2 w)^{-1}$. Within the first order approximation $z^*_{(1)} \approx (\mu_2 w)^{-1} - \delta$ where the decrement δ is found as $\delta = (1/\mu_2 w)(\mu_3/\mu_2 w)^{1/(1-\lambda)}$. This result is consistent with the assumption $z^*\mu_2 \mathrm{e}^{\epsilon} \to 1^-$ so that the solution of Eq. (6.76) in the main approximation can be written as

$$z^* \approx \frac{1}{\mu_2}\, \mathrm{e}^{-\epsilon} \tag{6.77}$$

By making use of this solution as well as of the result given by Eq.(6.71) in the Eq.(6.73), the detachment line at large dimensionless detachment energy $\epsilon_D \equiv \varepsilon/k_BT$ and force

$\tilde{f}_D \equiv a f_D / k_B T$ can be written as

$$\tilde{f}_D = \frac{1}{a_2^\nu} \left[\epsilon_D - \ln\left(\frac{\mu_3}{\mu_2}\right) \right]^\nu . \tag{6.78}$$

Thus, in terms of the dimensionless controll parameters $\tilde{f}_D$ increases as the energy ϵ_D increases. Notably, however, if the same detachment line is represented in terms of the dimensional control parameters, detachment force f_D vs. detachment temperature T_D (with the dimensional adsorption energy ε_0 being fixed), one encounters a nonmonotonic behavior

$$f_D = \frac{k_B T_D}{a} \left[\frac{\varepsilon_0}{k_B T_D} - \ln\left(\frac{\mu_3}{\mu_2}\right) \right]^\nu \tag{6.79}$$

which is shown in Fig. 6.5d. The curve given by Eq.(6.79) goes through a maximum at a temperature given by

$$T_D^{\max} = \frac{(1-\nu)\varepsilon_0}{k_B \ln\left(\frac{\mu_3}{\mu_2}\right)}. \tag{6.80}$$

For simplicity we assume $k_B = 1$. Such nonmonotonic behavior is termed *reentrant* and can be observed in the DNA unzipping process [55, 65, 62] as well as in the case of stretched polymer adsorption on solid surfaces [67, 50]. At very low T, however, the expression eq. 6.61 for $P_m(\mathbf{r})$ [65] predicts divergent chain deformation [9] , i.e., becomes unphysical. One can readily show that in this case the correct behavior is given by $fa = \varepsilon_0 + k_B T \ln(\mu_3/\mu_2)$.

6.4.3 Average loop and tail lengths close to the detachment line

As long as the adsorption energy $\epsilon > \epsilon_c$ (or $w > w_c$), the average loop length L remains finite upon the detachment line crossing. At $\tilde{f} < \tilde{f}_D$ the fugacity $z = z^*(w)$ and the average loop length are given by

$$L = z \left. \frac{\partial \ln U(z)}{\partial z} \right|_{z=z^*(w)} = \frac{\Phi\left(\alpha - 1, \mu_3 z^*(w)\right)}{\Phi\left(\alpha, \mu_3 z^*(w)\right)}. \tag{6.81}$$

Thus, at $\tilde{f} < \tilde{f}_D$ the force does not effects the loop length. At $\tilde{f} > \tilde{f}_D$ the fugacity is given by $z = z^{\#}(\tilde{f})$ where $z^{\#}$ is determined from Eq. (6.71). In this case the average loop length reads

$$L = z \left. \frac{\partial \ln U(z)}{\partial z} \right|_{z=z^{\#}(\tilde{f})} = \frac{\Phi\left(\alpha - 1, \mu_3 z^{\#}(\tilde{f})\right)}{\Phi\left(\alpha, \mu_3 z^{\#}(\tilde{f})\right)} \tag{6.82}$$

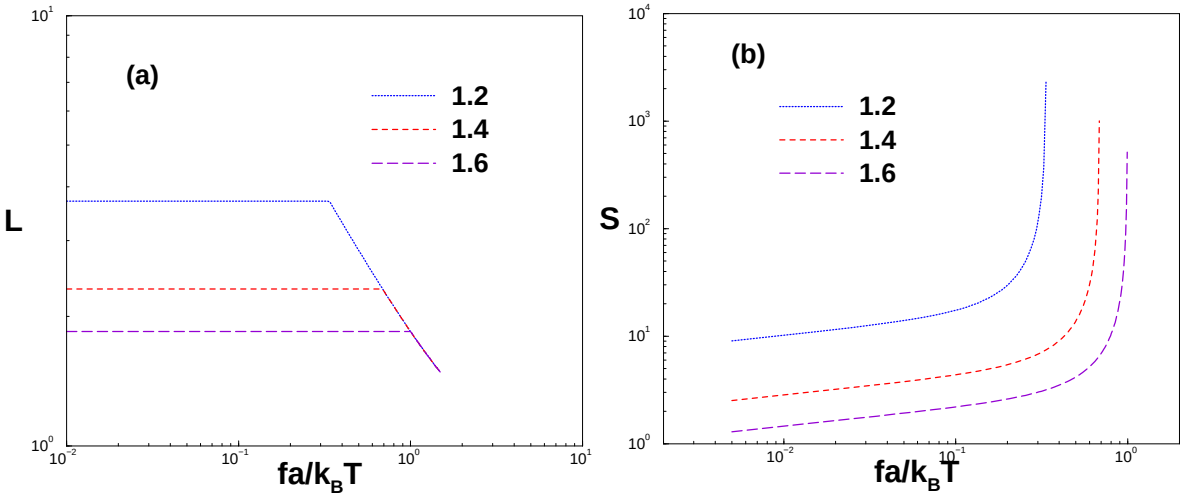

Figure 6.6: Variation of the average loop size, L, with detachment force strength f for several values of the adsorption energy ϵ (given as a parameter). (b) Mean tail size S against f at different substrate attraction ϵ.

Since at $\epsilon > \epsilon_c$ and $\tilde{f} > \tilde{f}_D$ we have $\mu_3 z^{\#} < \mu_3 z^* < 1$. In this case the function given by Eq. (6.82) declines when the force grows - see Figure 6.6a.

In contrast, the average tail length S diverges in the vicinity of the detachment line. Indeed, at $\tilde{f} < \tilde{f}_D$ the average tail length is given by

$$S = z\,\frac{\partial \ln R(z)}{\partial z}\bigg|_{z=z^*(w)} = \frac{a_1 \tilde{f}^{\theta}\Phi\left(\psi - 1, \mu_3 z^*(w)\exp(a_2\tilde{f}^{1/\mu})\right)}{1 + a_1 \tilde{f}^{\theta}\Phi\left(\psi, \mu_3 z^*(w)\exp(a_2\tilde{f}^{1/\mu})\right)} \approx \frac{1}{\left[1 - \mu_3 z^* \exp(a_2\tilde{f}^{1/\mu})\right]} \tag{6.83}$$

because $\psi < 1$ and $\mu_3 z^* \exp(a_2\tilde{f}^{1/\mu}) \leq 1$ (cf. Eq. (B.11)). In the vicinity of the detachment line $1 - \mu_3 z^*(w)\exp(a_2\tilde{f}^{1/\nu}) \approx (\tilde{f}_D - \tilde{f})/(\nu\tilde{f}_D)$ and, therefore,

$$S \propto \frac{\tilde{f}_D}{\tilde{f}_D - \tilde{f}}. \tag{6.84}$$

At $\tilde{f} \geq \tilde{f}_D$ the fugacity $z = z^{\#}(\tilde{f})$ and hence,

$$S = z\,\frac{\partial \ln R(z)}{\partial z}\bigg|_{z=z^{\#}(\tilde{f})} \to \infty. \tag{6.85}$$

The divergence in Eq.(6.85) follows immediately from Eq.(6.70) which holds in the thermodynamical limit. In practice, however, for a large but finite chain length $S \to N$ at $\tilde{f} \geq \tilde{f}_D$. Thus, despite the abrupt first order phase transition, as far as the order parameter n is concerned, the detachment in terms of the tail length S starts diverging already at $\tilde{f} \leq \tilde{f}_D$ as one comes close to the critical detachment force $\tilde{f}_D$.

6.4.4 Latent heat variation upon detachment

Finally we study the change in the internal energy of the system while crossing the line of detachment. At $\tilde{f} > \tilde{f}_D$ the stretching energy E follows the Pincus law, so that

$$E(\tilde{f} = \tilde{f}_D + 0) = N k_B T \tilde{f}_D^{1/\nu} \tag{6.86}$$

In the adsorbed phase

$$E(\tilde{f} = \tilde{f}_D - 0) = -N k_B T \, \epsilon_D \, n(w_D) \tag{6.87}$$

As a result, the latent heat q, consumed upon detachment (or, due to force-induced desorption,) reads

$$q \equiv E(\tilde{f} = \tilde{f}_D + 0) - E(\tilde{f} = \tilde{f}_D - 0) = N k_B T \left[\tilde{f}_D^{1/\nu} + \epsilon_D \, n(w_D) \right] > 0 \tag{6.88}$$

i.e., the heat is absorbed by the system during the force -induced desorption. In the vicinity of the critical point $\tilde{f}_D \sim (\epsilon - \epsilon_c)^{\nu/\phi}$ and $n \sim (\epsilon - \epsilon_c)^{1/\phi - 1}$, thus to a leading order

$$q \approx N k_B T \epsilon_c \, (\epsilon - \epsilon_c)^{1/\phi - 1}. \tag{6.89}$$

6.5 Monte Carlo Simulation Results

In the previous sections, we have discussed the simulation methods as well as developed a detailed analytical theory to explain the force induced desorption of polymer chains from a surface. In this section we discuss the results of the computer experiment and how they compare with the theoretical predictions.

6.5.1 Determination of the detachment point

In the absence of external pulling force, the transition of a polymer from desorbed to adsorbed state is known to be of second order, and the fraction of adsorbed monomers, n, can be identified as an order parameter. Therefore, in our computer experiment we use n to determine the point of polymer detachment from the adsorbing surface. At constant surface potential, ϵ, one finds that n steeply decreases upon a small increase of the pulling force whereby the polymer chain undergoes a transition from an adsorbed phase to a grafted-detached state. In order to locate the point of chain detachment, we draw a tangent at the inflexion point of the curve n vs. f. The detachment force, f_D, is then identified as the point where the tangent intersects the abscissa (f-axis) - see Fig. 6.7(a). This is the same as the method described in Chapter 4 Figure 4.6(a). Thus one can determine the detachment force as a function of the adsorption potential

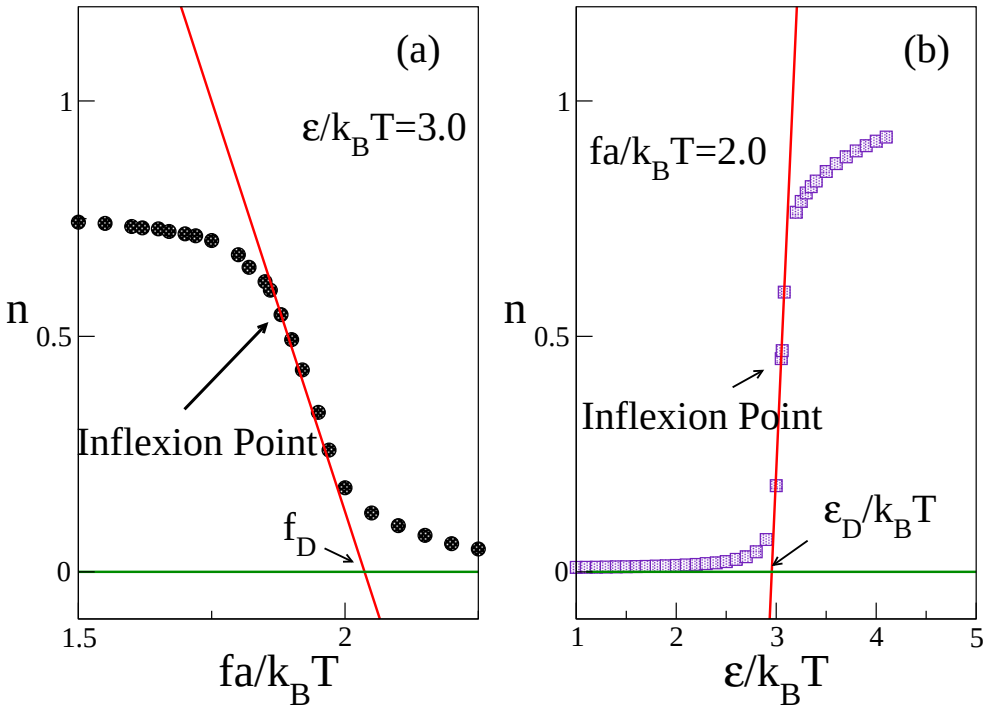

Figure 6.7: (a) Plot of the 'order parameter', n, against pulling force f, for an adsorption strength $\varepsilon/k_BT = 3.0$. The polymer chain length is N=128. The tangent at the inflexion point of the curve meets the abscissa at f_D which we define as the detachment force. (b) The 'order parameter', n, against the adsorption potential ϵ for fixed pulling force $f = 2.0$. The tangent at the inflexion point of the curve meets the abscissa at ε_D/k_BT where the polymer adsorbs at the surface plane.

ϵ. Alternately, from the plot of n against the adsorption potential ϵ, with the pulling force f held constant, one can observe that as sharp growth of n as the potential is slightly increased. The critical potential for chain attachment at the transition point can be found similarly as indicated in Fig. 6.7(b).

Fig. 6.8(a) shows the variation of the order parameter with changing surface potential for several values of the pulling force. Evidently, the larger the pulling force, the stronger the surface potential, needed to keep the polymer adsorbed on the plane. In the absence of a force, the order paramenter changes smoothly. For larger forces, however, the transition becomes rapidly abrupt. This abrupt behavior of the order parameter is in close agreement with our theoretical predictions, depicted in Fig. 6.5. In Fig. 6.8(b) we show the variation of the order parameter n with changing force f for various adsorption potentials ϵ. The threshold values for polymer desorption, $\epsilon_D(f)$ and $f_D(\epsilon)$, as obtained for chains of different length, are then extrapolated to obtain the corresponding values in the thermodynamic limit $N \to \infty$ as described earlier in

Chapter 4 Sec. 4.

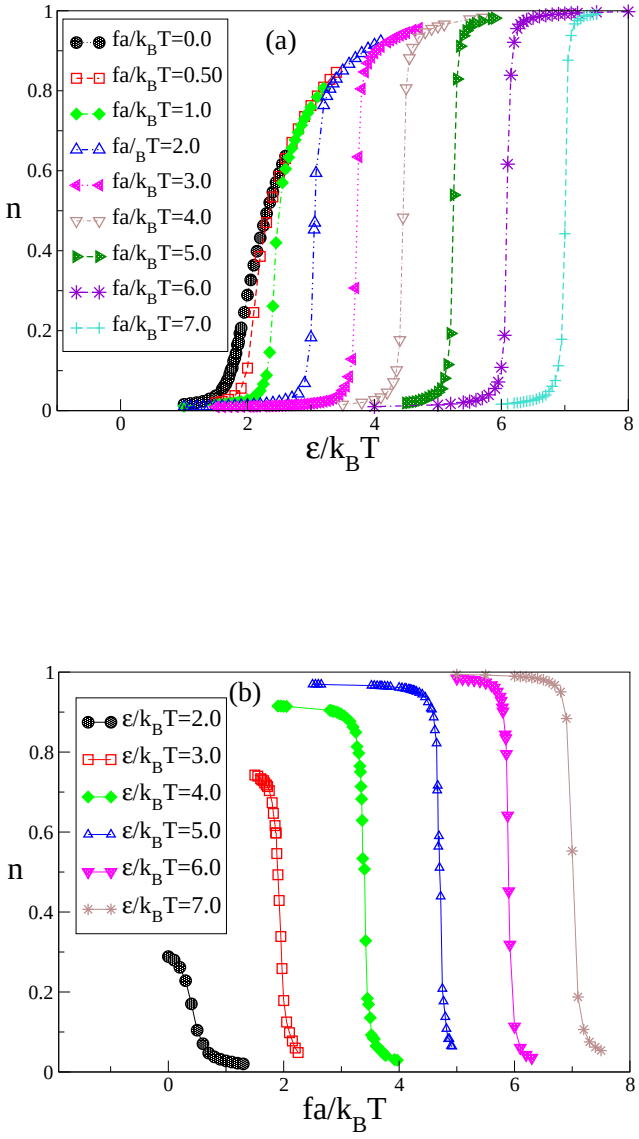

Figure 6.8: (a) The 'order parameter', n, against the surface potential, ϵ, for various pulling forces. The chain has length N=128. (b) Variation of n with the pulling force, f, for several surface potentials.

Our observations show that ϵ_D increases slightly (i.e., the finite-size effects are rather small) with growing chain length N. By extrapolating the data to $1/N \to 0$ one obtains then ϵ_D for infinite length of the polymer chain. Similarly, the detachment force at fixed surface potential ϵ may be determined in the thermodynamic limit.

6.5.2 Adsorption-desorption phase diagram under pulling

Using the threshold values of f_D and ϵ_D for critical adsorption/detachment in the thermodynamic limit, one can construct the adsorption-desorption phase diagram for a polymer chain. The phase diagram may be obtained by any of the two methods, i.e., (i) by fixing of the force and locating ϵ_D, and/or (ii), by fixing of the surface potential and locating the detachment force f_D. The resulting phase diagram is displayed in Figure 6.9. The inset in Fig 6.9 shows that $f_D \propto (\epsilon - \epsilon_c)^{0.97}$ which may be compared to the theoretical prediction $f_D \sim (\epsilon - \epsilon_c)^{\nu/\phi}$. Hence, this method gives us an estimate for the crossover exponent ϕ. For $\epsilon_c = 1.67$, we find $\phi \sim 0.59 \pm 0.02$.

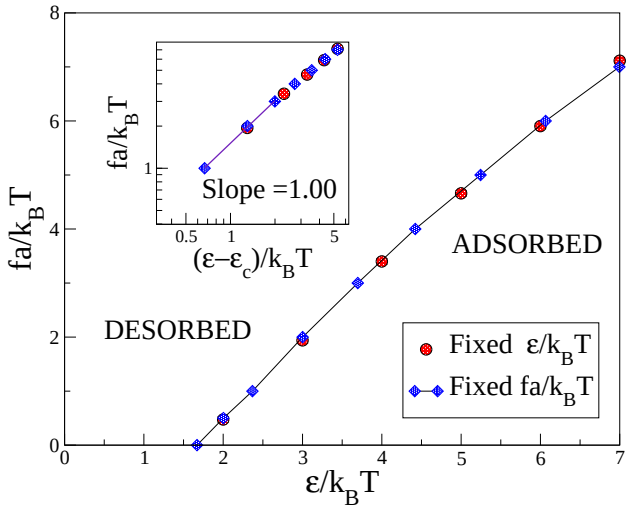

Figure 6.9: Plot of the critical detachment force f_D against the surface potential ϵ. In the inset in a double logarithmic plot f_D is plotted against $(\epsilon - \epsilon_c)/k_BT$. The critical adsorption potential for zero force has been found earlier [6] to be $\epsilon_c = 1.67$.

6.5.3 Average lengths of loops and tails

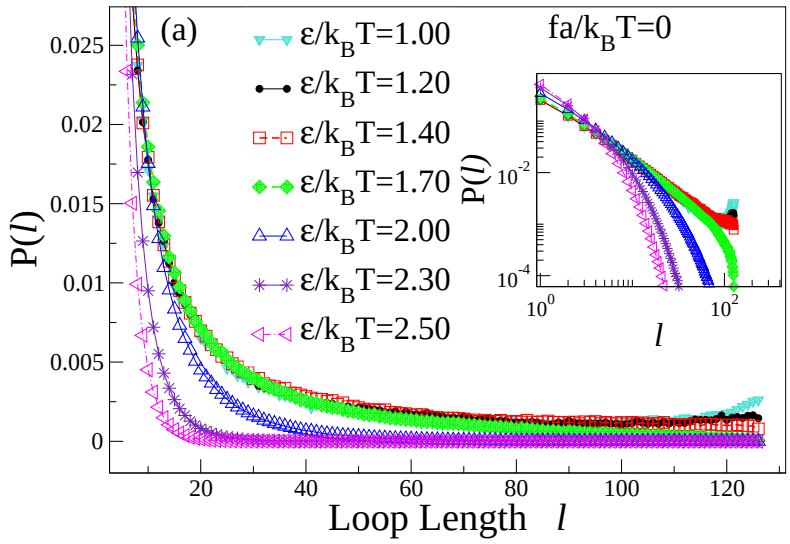

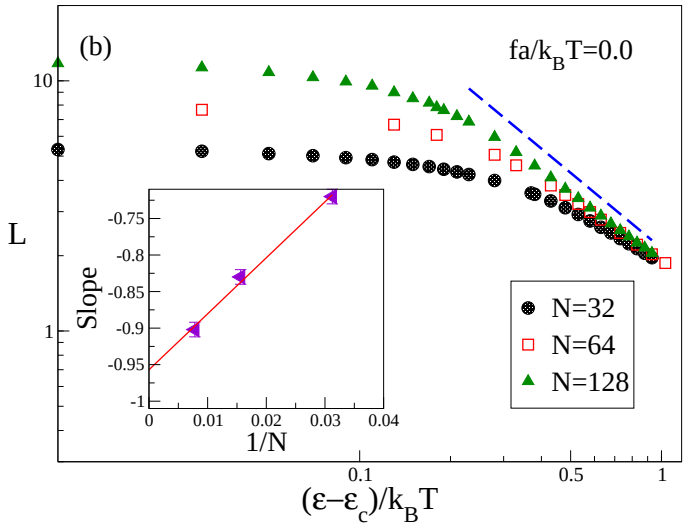

Figure 6.10: (a) Distribution of loop sizes for chain length $N = 128$ at different strength of the surface potential and no pulling force. The inset shows the same in double logarithmic coordinates. The measured slope at $\epsilon_c/k_BT = 1.67$ (full line) is -1.38 ± 0.02 which practically coincides with the prediction Eq.(6.30). (b) The average loop length plotted against $(\epsilon - \epsilon_c)/k_BT$ where $\epsilon_c/k_BT = 1.67$, for various chain lengths in double logarithmic coordinates. The slopes x, indicated by a dashed line, are obtained from the L vs. $(\epsilon - \epsilon_c)/k_BT$ curves, and plotted against $1/N$ in the inset. Extrapolation to $1/N \to 0$ yields $x \approx 0.95$.

In Fig 6.10a we plot the PDF of the loop sizes for a chain with $N = 128$ at several strengths of the adsorption potential ϵ in the absence of pulling. One may readily verify that the PDF has a peak for loops of size unity which suggests that most frequently single-segment defects (that is, vacancies in the monomer trains) occur in the conformation of adsorbed chain. However, for $\epsilon < \epsilon_c$ one may detect clearly in Fig 6.10a slight increase in the distribution for loops of size $l \approx N$ which becomes more pronounced at smaller $\epsilon \approx 1.0 - 1.2$ in full agreement with the double-peaked shape, predicted by Eq. (6.36).

The average loop size L is plotted against the surface potential (with regard to its critical value at the adsorption point), $(\epsilon - \epsilon_c)/k_BT$ in Fig 6.10b. We find that, well inside the region of adsorption, L scales as a power law, $L \propto (\epsilon - \epsilon)^x$. The exponent x, plotted as a function of N in the inset, is negative, therefore, stronger attraction makes the loops smaller while the mean loop size evidently increases with growing chain length N which is a finite size effect. The exponent x approaches -0.96 in the limit $1/N \to 0$ - see inset in Fig 6.10b. This provides another estimate of the crossover exponent ϕ since $x = 1 - 1/\phi$, according to Eq.(6.38). Thus we find $\phi \approx 0.51 \pm 0.02$. From Fig 6.10b it is evident that the slope of the L vs. $(\epsilon - \epsilon)/k_BT$ curves visibly changes as one comes closer to the CAP. In the immediate vicinity of ϵ_c the slope is small and the corresponding estimate for the crossover exponent in this region is $\phi \approx 0.63$. One should bear in mind, however, that this is due to the finite length of the chains used in the simulation which limits the possibility for the loop size to grow indefinitely, especially at ϵ_c. Therefore, we use and depict measurements of the slope sufficiently far from the CAP where it tends to a constant value, indicated by the dashed line in Fig 6.10b.

In Fig. 6.11(a) we plot the PDF of the tail size for a chain with $N = 128$ at several strengths of the adsorption potential in the absence of pulling. An interesting feature of the tail distribution function for $\epsilon = 1.70$ immediately at the CAP, $\epsilon_c = 1.67$, is the observed *bimodal* character. It means that there are two dominating chain populations, one with few loops and a long tail, and the other with many loops and a very short tail. Our simulation result thus confirms the shape of the tail distribution at criticality, Eq. (6.35), and appears in excellent agreement with the analytic result, derived earlier by Gorbunov et al. [36], indicating that in the vicinity of the critical adsorption point (CAP) chain conformations are either loop- or tail-dominated.

In Fig 6.11(b) the average tail length, S, is plotted against $(\epsilon - \epsilon_c)/k_BT$. Again, S is found to scale as a power law with the adhesion strength, $S \propto (\epsilon - \epsilon_c)^y$ where y is negative, decreases with N, and approaches eventually -1.67 for $1/N \to 0$. This result can be compared to Eq.(6.41). The corresponding estimate of ϕ is thus 0.60.

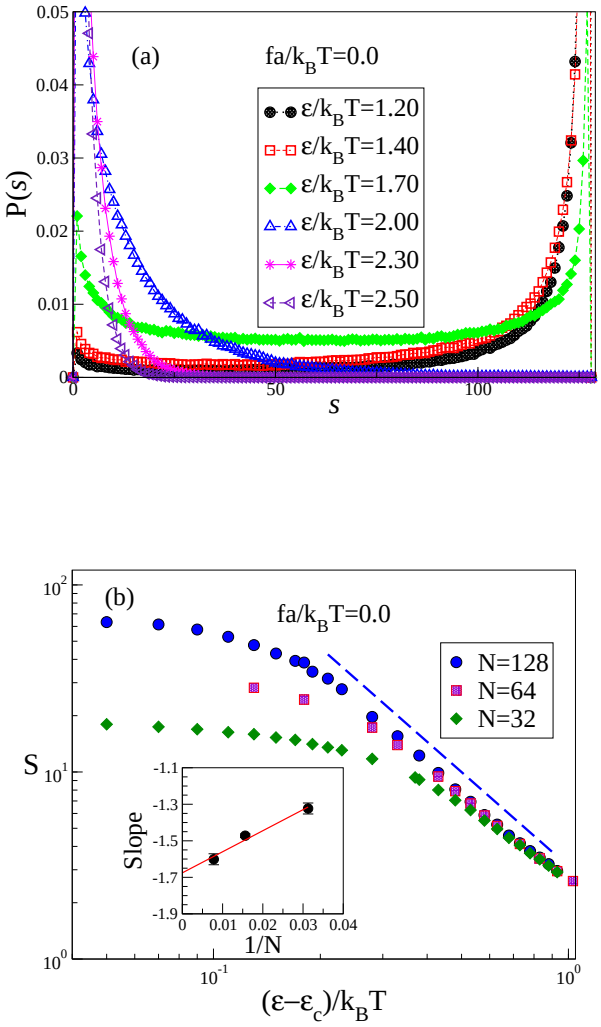

Figure 6.11: (a) Distribution of the tail size for different surface potentials in a polymer of length $N = 128$ with no pulling force. (b) The average tail length S against $(\epsilon - \epsilon_c)/k_BT$ plotted for various chain lengths in double logarithmic coordinates. The slopes obtained from these curves are plotted against $1/N$ in the inset and extrapolated to get the thermodynamic limit $N \to \infty$.

We turn now to the properties of adsorbed chains in the presence of pulling force. A remarkable feature of the probability distribution of the order parameter is the

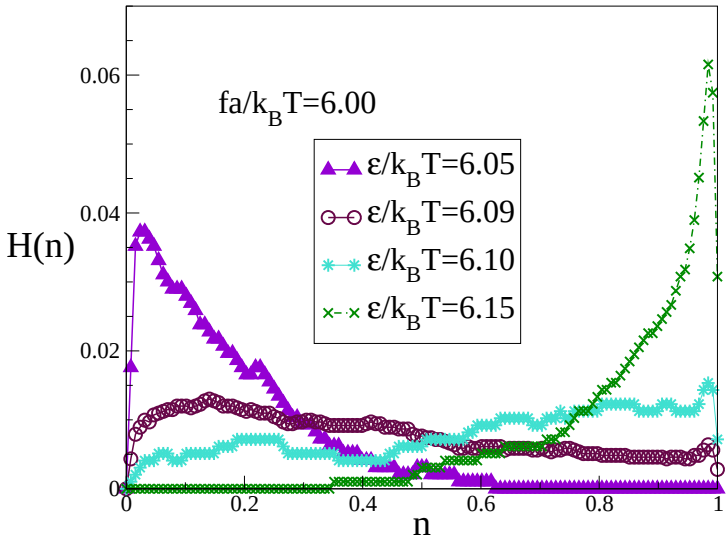

Figure 6.12: Distribution of the order parameter n for a pulling force $fa/k_BT = 6.0$ and different strength of adhesion ϵ/k_BT. The chain length is $N = 128$ and the threshold value of the surface potential for this force is $\epsilon_D \approx 6.095 \pm 0.03$. The values $\epsilon/k_BT = 6.09$ and $\epsilon/k_BT = 6.10$ are on both sides of the detachment line, cf. Fig. 6.9.

absence of a second peak in the vicinity of the critical strength of adsorption, $\epsilon_D \approx 6.095 \pm 0.03$, which still keeps the polymer adsorbed at pulling force $fa/k_BT = 6.0$. Somewhat further away from ϵ_D, one observes a clear maximum in the distribution $H(n)$, indicating a desorbed chain with $n \approx 0.01$ for $\epsilon = 6.05$, or an almost entirely adsorbed chain with $n \approx 0.99$ for $\epsilon = 6.15$. This lack of bimodality in the $H(n)$ confirms the dichotomic nature of the desorption transition which rules out phase coexistence.

In Fig 6.13a, the average loop length, L is plotted against the external pulling force f for $\epsilon/k_BT = 4.0$. For f below the detachment threshold, f_D, the average loop size appears to be constant independent of the force. As the force f exceeds f_D, the average loop size decreases in close agreement with the theoretical prediction, shown in Fig. 6.5a. In Fig 6.13b, the average tail length, S, is plotted against the difference $f_D - f$ for several chain lengths at surface adhesion $\epsilon/k_BT = 4.0$ in double logarithmic coordinates. As the applied pulling force f gradually approaches the threshold force for detachment, f_D, the tail gets systematically longer and comes close to the length of the chain N. Evidently, if one takes into account the finite-size effects which lead to the observed bending of $S \approx N$ at stronger pulling, the tail S scales as $(f_D - f)^{-w}$. The exponent w approaches 1.01 (see inset in Fig 6.13b) at $\epsilon/k_BT = 4.0$. This may be

compared to the theoretical prediction of Eq. (6.84) which predicts indeed $w = 1$.

Eventually, in Fig 6.14(a) the PDF of the tail size s is plotted at different strengths of the surface potential ϵ while the force, applied to the chain end, is held constant, $f = 2.0$. In contrast, in Fig 6.14(b), we display the distribution of tail size s for the case when the adhesion strength is fixed, $\epsilon/k_BT = 4.0$, whereas the pulling force f is varied. Both graphs are remarkable in that they reflect the transition from fully adsorbed polymer, characterized by a sharp peak in the PDF at vanishing tail sizes, to detached chain when the pulling force exceeds the threshold f_D and the corresponding PDF is peaked at $s/N \approx 1$. We emphasize again that although this phase transition of chain detachment is clearly of first order, no trace of a bimodal distribution in the vicinity of the transition line can be detected! Thus, the states on both sides of the phase boundary $f_D(\epsilon)$ *cannot coexist simultaneously* which underlines the peculiar nature of this phase transformation. At this point we should like to point out, however, that this exotic feature of the detachment transitions has meanwhile been established also in the case of the so called *escape* transition of a polymer coil, deformed under the tip of an Atomic Force Microscope [86, 85, 1, 59]. It has been shown rigorously recently [48], that despite its first order nature, the escape transition takes place without phase coexistence. Most probably, this unusual feature is due to the topological connectivity of polymer chain as quasi one-dimensional system.

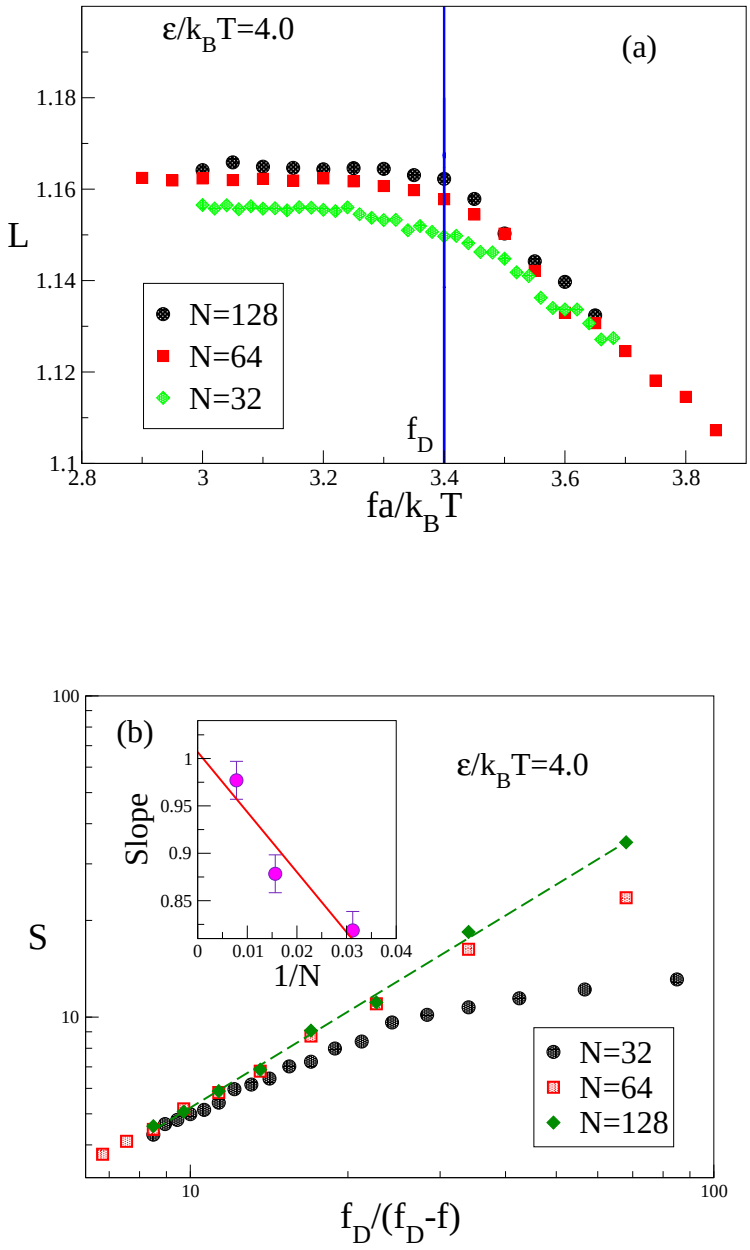

Figure 6.13: (a) The average loop length plotted against the pulling force f for fixed $\epsilon/k_BT = 4.0$. (b) The average tail length S is plotted against the $(f - f_D)^{-1}$ for various chain lengths for $\epsilon/k_BT = 4.0$ in double logarithmic coordinates. The inset shows the extrapolated slope for $N \to \infty$ go to unity, as predicted by Eq. (6.84)

.

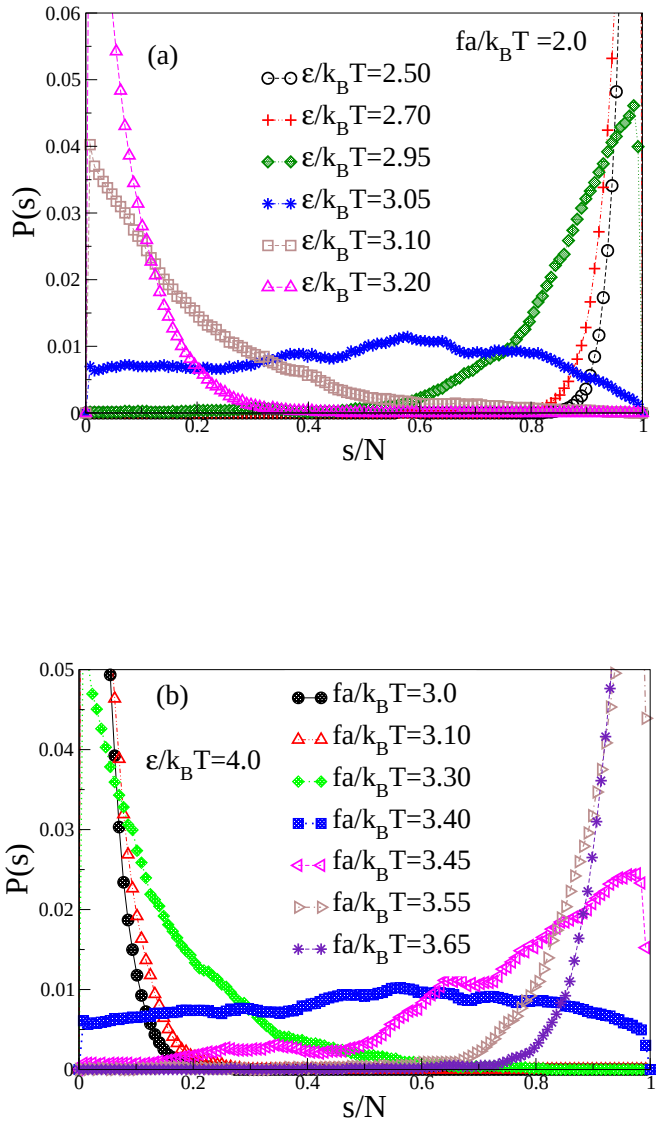

Figure 6.14: (a) Distribution of the tail size for a pulling force $fa/k_BT = 2.0$ and different strength of adhesion ϵ/k_BT. The chain length is $N = 128$. (b) Distribution of the tail size for different force f at $\epsilon/k_BT = 4.0$.

6.6 Discussion

In this chapter, we have studied the force-induced desorption transition of a polymer chain in contact with an adhesive surface. We treat the problem within the framework of the Grand Canonical Ensemble approach and derive analytic expressions for the various conformational building blocks, characterizing the structure of an adsorbed linear polymer chain, subject to pulling force of fixed strength. Closed analytic expressions for the fraction of adsorbed segments (i.e., the order parameter of the desorption transition) and for probability distributions of trains, loops and tails have been derived along with expressions for the corresponding first moments in terms of the surface potential intensity both with and without external force. As expected, all these conformational properties and their variation with the proximity to the CAP are governed by a crossover exponent ϕ.

A central result in the present work is the calculation of ϕ using the approach of Kafri et al. [94] which provides insight into the background of the existing controversial reports about its numeric value. We demonstrate that the value of ϕ may vary within the interval $0.39 \leq \phi \leq 0.6$, depending on the possibility of a single loop to interact with the neighboring loops in the adsorbed polymer. Since this range is model-dependent, one should not be surprised that different models produce different estimates of ϕ in this interval.

A comparison with the results from extensive Monte Carlo simulations demonstrates the good agreement between theoretic predictions and simulation data.

In particular, we verify the gradual transition of the PDF of loops from power-law to exponential decay as one moves away from the critical adsorption point to stronger adsorption. We demonstrate that for vanishing pulling force, $f \to 0$, the mean loop size, $L \propto (\epsilon - \epsilon_c)^{1-\frac{1}{\phi}}$, and the mean tail size, $S \propto (\epsilon - \epsilon_c)^{\frac{1}{\phi}}$, diverge when one comes close to the CAP. In contrast, for a non-zero pulling force, $f \neq 0$, we show that the loops on the average get smaller with growing force while close to the detachment threshold, $f \approx f_D$, the tail length diverges as $S \propto (1 - \frac{f}{f_D})^{-1}$.

Eventually, we derive the overall phase diagram of the force-induced desorption transition for a linear self-avoiding polymer chain and demonstrate its *reentrant* character when plotted in terms of detachment force f_D against system temperature T. We find that despite being of first order, the force-induced phase transition of polymer desorption is dichotomic in its nature, that is, no phase coexistence and no metastable states exist. This unusual feature of the phase transformation is unambiguously supported by our simulation data, e.g., through the comparison of the order parameter probability distributions on both sides in the immediate vicinity of the detachment line whereby no double-peaked structure is detected.

In this work, the simulations have been carried out within the framework of a

constant force ensemble. The next chapter deals with the *constant height* ensemble where one uses the end-monomer z-position as an independent parameter and measures the force, exerted by the chain on the end monomer.

Chapter 7

Pulling an adsorbed polymer from a surface II : the h-ensemble

7.1 Introduction

In the previous Chapter, we discussed the properties of a polymer chain under the influence of an external force that pulls it from an attractive substrate. As we mentioned before, this study was motivated by recent advances in the field of single molecule manipulation techniques such as atomic force microscopy (AFM) and optical/magnetic tweezers.

In these experimments it is customary to anchor a polymer molecule with one end to the substrate whereas the other end is fixed on the cantilever. The polymer molecule can be adsorbed on the substrate while the cantilever recedes from the substrate. In doing so one can prescribe the acting force in AFM experiment whereas the distance between the tip and the surface is measured. Conversely, it is also possible to prescribe the distance and measure the corresponding force. In fact the latter is actually more typical in AFM-experiments. From the standpoint of statistical mechanics these two cases could be qualified as f-ensemble (force is fixed while chain end height is measured) and as h-ensemble (the height, h is fixed while one measures f). Recently these two ways of descriptions as well as their interrelation were discussed for the case of a phantom polymer chain by Skvortsov et al. [81]. Previously, we have discussed the adsorption of a single tethered self-avoiding polymer on a solid substrate with an external force applied to a free chain's end *i.e.* in the f-ensemble.

Now we consider the detachment process of a single self-avoiding polymer chain, keeping the distance h between the free chain's end and the substrate as the control parameter. We demonstrate below that a number of properties behave differently in the vicinity of the phase transition, depending on which of the two equivalent ensembles is used as a basis for the study of systems's behavior.

7.2 Monte Carlo Simulation Model

We have used the coarse grained off-lattice bead-spring model [9] (see Chapter 3) which was employed in our previous studies. The system consists of a single polymer chain tethered at one end to a flat impenetrable structureless surface. The surface interaction is described by a square well potential,

$$U_w(z) = \begin{cases} \epsilon, & z < r_c \\ 0, & z \geq r_c \end{cases} \tag{7.1}$$

The strength ϵ is varied from 0 to 7.0 while the interaction range $r_c = 0.125$. The effective bonded interaction is described by the FENE (finitely extensible nonlinear elastic) potential:

$$U_{FENE} = -K(1 - l_0)^2 ln \left[1 - \left(\frac{l - l_0}{l_{max} - l_0} \right)^2 \right] \tag{7.2}$$

with $K = 20, l_{max} = 1, l_0 = 0.7, l_{min} = 0.4$. The nonbonded interactions between monomers are described by the Morse potential:

$$\frac{U_M(r)}{\epsilon_M} = \exp(-2\alpha(r - r_{min})) - 2\exp(-\alpha(r - r_{min})) \tag{7.3}$$

with $\alpha = 24,\ r_{min} = 0.8,\ \epsilon_M/k_BT = 1$. In few cases, needed to clarify the nature of the polymer chain resistence to stretching, we have taken the nonbonded interactions between monomers as purely repulsive by shifting the Morse potential upward by ϵ_M and removing its attractive branch, $V_M(r) = 0$ for $r \geq r_{min}$.

We employ periodic boundary conditions in the $x - y$ directions and impenetrable walls in the z direction. The lengths of the studied polymer chains are 64, and 128. The size of the simulation box was chosen appropriately to the chain length, so for example, for a chain length of 128, the box size was $256 \times 256 \times 256$ and for chain length $N = 64$, the box size was $128 \times 128 \times 128$. All simulations were carried out for constant position of the last monomer z-coordinate, that is, in the fixed height ensemble.

The standard Metropolis algorithm was employed to govern the moves with self avoidance automatically incorporated in the potentials. In each Monte Carlo update, a monomer was chosen at random and a random displacement attempted with $\Delta x,\ \Delta y,\ \Delta z$ chosen uniformly from the interval $-0.5 \leq \Delta x, \Delta y, \Delta z \leq 0.5$. The last monomer was held at constant height but was free to move in the xy plane.

The transition probability for the attempted move was calculated from the change ΔU of the potential energies before and after the move was performed as $W = exp(-\Delta U/k_BT)$. As in a standard Metropolis algorithm, the attempted move was

accepted, if W exceeds a random number uniformly distributed in the interval $[0, 1]$. In order to get the chain end to the desired height, we used the algorithm described in the previous chapter *i.e.* for the fixed force ensemble. Using a starting configuration in which the chain end is less than (but close to) the desired height, we apply a constant force to the chain and pull it up until it reaches the desired height (withing a small error margin). Once the required height is reached, the force is switched off and the chain is equilibrated in the MC method for a period of about 5×10^5 MCS after which typically 500 measurement runs are performed, each of length 2×10^6 MCS. The equilibration period and the length of the run were chosen according to the chain length and the values provided here are for the longest chain length. An additional consideration in this study was the measurement of the force on the last monomer. The force has two components : the contribution of the bonded interaction with its neighbour and the contribution of the rest of the monomers. The two contributions were measured separately and the total force required to keep the monomer at a constant height was obtained by adding both components.

7.3 Theory : Single chain adsorption with distance as a control parameter

7.3.1 Deformation of a tethered chain

We first examine how a chain tethered to a solid surface responds to stretching. This problem amounts to finding the chain free end probability distribution function (PDF) $P_N(h)$ where N is the chain length, i.e., the number of beads. As described in Chapter 6, the partition function of such chain a with fixed distance h of the chain end from the anchoring plane is given as

$$\Xi_{\text{tail}}(N, h) = \frac{\mu_3^N}{N^\beta}\, l_0 P_N(h) \tag{7.4}$$

where $\beta = 1 - \gamma_1$ and the exponent $\gamma_1 = 0.680$ (see Chapter 4 Section 4.4.1). This may be compared to eq. 6.60 in Chapter 6 which gave the canonical partition function of the tail of a polymer chain under an applied force. Here μ_3 is the model dependent connective constant (see e.g. ref.[90]). In Eq. (7.4) l_0 denotes a short-range characteristic length which depends on the chain model. We discuss the chain deformation within two models: bead-spring (BS) model and freely jointed bond vectors (FJBV) model.In the first case, the bonds are elastic while in the second case the bonds are considered rigid.

Bead-spring model

The form of $P_N(x)$ has been discussed earlier [29, 28] and used later in studies of the monomer density in polymer brushes [51]. A derivation of the form of $P_N(x)$ is sketched in Appendix C. Here we outline this in a way which is appropriate for our purposes. The average end-to-end chain distance reads $R_N = l_0 N^\nu$, where l_0 is the mean distance between two successive beads on a chain and ν is the Flory exponent . The short distance behavior, $h \ll R_N$, is given by

$$P_N(h) \propto \left(\frac{h}{R_N}\right)^\zeta \tag{7.5}$$

where the exponent $\zeta \approx 0.8$ [29]. As described in the previous chapter, for the long distance behavior, $h/R_N \gg 1$, we assume, following Ref.[51], that the PDF of the end-to-end vector $\mathbf{r}$ is given by des Cloizeaux's expression [19] for the bulk : $P_N(\mathbf{r}) = (1/R_N)\, F(\mathbf{r}/R_N)$ where the scaling function $F(x) \propto x^t \exp[-Dx^\delta]$, and the exponents $t = (\beta - d/2 + \nu d)/(1-\nu)$, $\delta = 1/(1-\nu)$ and $\beta = 1 - \gamma_1$. This has been discussed earlier in Chapter 6 Section 6.4 and in the Appendix C. Here and below d denotes the space dimensionality. One should emphasize that the presence of a surface is manifested only through the replacement of γ by γ_1 (as compared to the pure bulk case!). By integration of $P_N(\mathbf{r})$ over the x and y coordinates one obtains $P_N(h) \propto (h/R_N)^{2+t-\delta} \exp[-D(h/R_N)^\delta]$. As the long distance behavior is dominated mainly by the exponential function while the short distance regime is described by Eq. (7.5), we can approximate the overall behavior as

$$P_N(h) = \frac{A}{R_N}\, \left(\frac{h}{R_N}\right)^\zeta \exp\left[-D\left(\frac{h}{R_N}\right)^\delta\right] \tag{7.6}$$

A comparison of the distrbution, Eq. (7.6), with our simulation data is shown in Fig. 7.1. The constants A and D in Eq. (7.6) can be found from the conditions: $\int P_N(h)dh = 1$ and $\int h^2 P_N(h)dh = R_N^2$. This leads to:

$$A = \delta \left[\Gamma\left(\frac{1+\zeta}{\delta}\right)\right]^{-(1+\zeta)/2} \left[\Gamma\left(\frac{3+\zeta}{\delta}\right)\right]^{-(1-\zeta)/2} \tag{7.7}$$

and

$$D = \left[\Gamma\left(\frac{3+\zeta}{\delta}\right)\right]^{\delta/2} \left[\Gamma\left(\frac{1+\zeta}{\delta}\right)\right]^{-\delta/2} \tag{7.8}$$

where $\delta \approx 2.43$ and $\zeta \approx 0.8$. One gets the estimates $A \approx 2.029$ and $D \approx 0.670$.

The free energy of the tethered chain with a fixed distance h takes on the form $F_{\rm tail}(N,h) = -k_BT \ln \Xi_{\rm tail}(N,h)$. By making use of Eqs. (7.4) and (7.6) the expression for the force f_N, acting on the end-monomer when kept at distance h is given by

$$f_N = \frac{\partial}{\partial h} F_{\rm tail}(N,h) = \frac{k_BT}{R_N} \left[\delta D \left(\frac{h}{R_N} \right)^{\delta-1} - \zeta \left(\frac{R_N}{h} \right) \right] \tag{7.9}$$

One should note that at $h/R_N \gg 1$ we have $h \propto R_N(R_N f_N/k_BT)^{1/(\delta-1)}$ which, after taking into account that $\delta^{-1} = 1-\nu$, leads to the well known Pincus deformation law: $h \propto l_0 N(l_0 f_N/k_BT)^{1/\nu-1}$ [14] (see Chapter 2, Section 2.5). In this approximation the (dimensionless) elastic energy reads $U_{\rm el}/k_BT = -N(l_0 f_N/k_BT)^{1/\nu}$. As a result the corresponding tail free energy is given by

$$\frac{F_{\rm tail}}{k_BT} = -N \left(\frac{l_0 f_N}{k_BT} \right)^{1/\nu} - N \ln \mu_3 \tag{7.10}$$

Eq. (7.9) indicates that there exists a height $h_0 = (\zeta/\delta D)^{1/\delta} R_N$ over the surface where the force f_N changes sign and becomes negative (that is, the surface repulsion dominates). According to Eq. (7.9) the force diverges as $f_N \propto -k_BT/h$ upon further decrease of the distance h.

Freely jointed chain

It is well known [39] that the Pincus law, Eq. (7.9), describes the deformation behavior at intermediate force strength, $1/N^\nu \ll l_0 f_N/k_BT \leq 1$. Direct Monte Carlo simulation results indicate that, depending on the model, deviations from Pincus law emerge at $h/R_N \geq 3$ (bead-spring off-lattice model) [78], or $h/R_N \geq 6$ (Bond Fluctuation Model) [93]. In such "overstretched" regime (when the chain is stretched close to its contour length) one should take into account that the chain bonds cannot expand indefinitely. This case could be treated within the simple freely jointed bond vectors (FJBV) model [78, 76] where the bond length l_0 is fixed. In this model the force - deformation relationship is given by

$$f_N = \frac{k_BT}{l_0} \mathcal{L}^{-1} \left(\frac{h}{l_0 N} \right) \tag{7.11}$$

where $\mathcal{L}^{-1}$ denotes the inverse Langevin function $\mathcal{L}(x) = \coth(x) - 1/x$ and l_0 is the bond vector length. We discuss the main results pertaining to FJBV model in Appendix A. The elastic deformation energy reads $U_{\rm el}/k_BT = -(l_0 f_N/k_BT) \sum_{i=1}^{N} < \cos\theta_i >= -N(l_0 f_N/k_BT)\mathcal{L}(l_0 f_N/k_BT)$, where θ_i is the average polar angle of the i-th bond vector (see Appendix A). Thus the corresponding free energy of the tail for the FJBV model reads

$$\frac{F_{\rm tail}}{k_BT} = -N\mathcal{G} \left(\frac{l_0 f_N}{k_BT} \right) - N \ln \mu_3 \tag{7.12}$$

where we have used the notation $\mathcal{G}(x) = x\mathcal{L}(x) = x\coth(x) - 1$. Now we are in a position to discuss the pulling of the adsorbed chain controlled by the chain height h.

7.3.2 Pulling controlled by the chain end position

Consider now an adsorbed chain when the adsorption energy per monomer is sufficiently large, $\varepsilon \geq \varepsilon_c$, where ε_c denotes a corresponding *critical* energy of adsorption. Below we will also use the notation $\epsilon = \varepsilon/k_BT$ for the dimensionless adsorption energy. The problem of force-induced polymer desorption could be posed as follows: how is the process of polymer detachment governed by the chain end position h? Figure 7.2a gives a schematic representation of such a system, and the situation in a computer experiment, as shown in the snapshot Fig. 7.2b, is very similar.

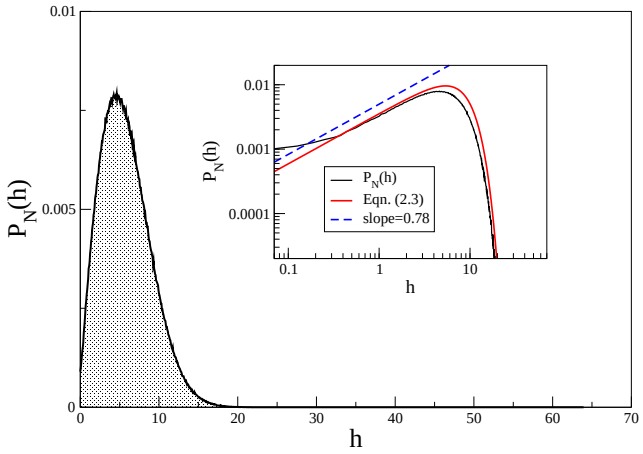

Figure 7.1: Probability distribution $P_N(h))$ of chain end positions h above the grafting plane for a polymer with $N = 128$ monomers at zero strength of the adsorption potential $\epsilon = 0.0$. In the inset the MC data for $P_N(h))$ (solid black line) is compared to the theoretical result, Eq. (7.6). Dashed line denotes the expected slope of $\zeta \approx 0.78$ of the probability distribution for small heights.

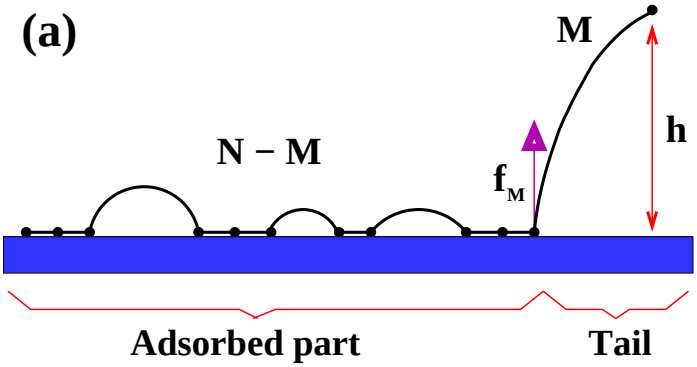

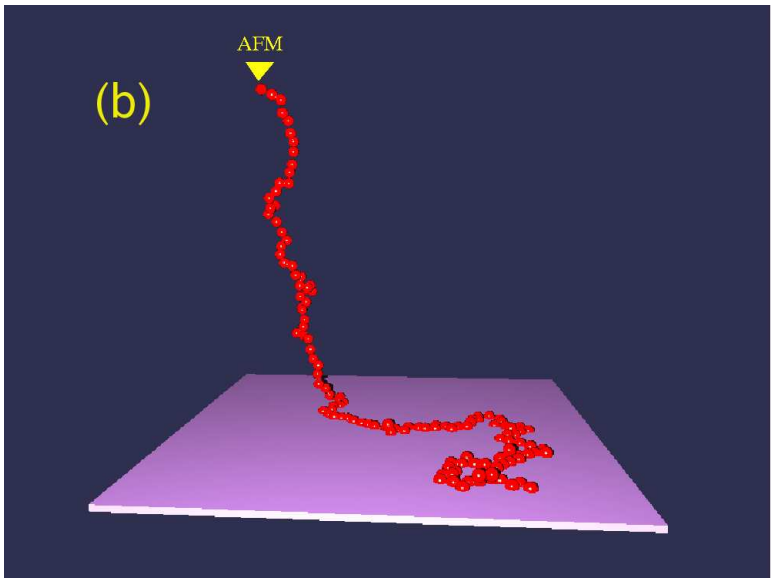

Figure 7.2: (a) Schematic graph of an adsorbed polymer chain, partially detached from the plane by an external force which keeps the last monomer at height h. The total chain is built up from a tail of length M and an adsorbed part of length $N - M$. The force f_M acting on the chain end is conjugated to h, i.e., $f_M = \partial F_{\text{tail}}/\partial h$. (b) A snapshot from the MC simulation: $N = 128$, $h = 25.0$, $\epsilon = 4.0$ and $\langle f \rangle = 6.1$.

As is evident from Fig. 7.2a, the system is built up from a tail of length M and an adsorbed portion of length $N-M$. The adsorbed part can be treated within the grand canonical ensemble approach as described in the previous Chapter. In ref.[7] it was shown that the free energy of the adsorbed portion is $F_{\rm ads} = k_B T(N-M)\ln z^*(\epsilon)$, where the fugacity per an adsorbed monomer $z^*(\epsilon)$ depends on ϵ and can be found from the basic equation (see Chapter 6 eq. 6.18)

$$\Phi(\alpha, \mu_3 z^*)\ \Phi(\lambda, \mu_2 w z^*) = 1 \tag{7.13}$$

As described earlier in Chapter 6 eq. 6.13 and in Appendix B, the so called *polylog function* in Eq. (7.13) is defined as $\Phi(\alpha, z) = \sum_{n=1}^{\infty} z^n/n^\alpha$ and the connective constants μ_3, μ_2 in three and two dimensional spaces are model dependent [90]. The exponents $\alpha = 1+\phi$ and $\lambda = 1-\gamma_{d=2}$ where $\phi \approx 0.5$ is the *crossover exponent* and $\gamma_{d=2} = 1.343$ [90]. Finally $w = \exp(\epsilon)$ is the additional statistical weight gained by each adsorbed segment.

In equilibrium, the force conjugated to h, that is, $f_M = \partial F_{\rm tail}/\partial h$, should be equal to the *chain resistance force to pulling* $f_{\rm p} = (k_B T/l_0)\mathcal{F}(\epsilon)$ (where $\mathcal{F}(\epsilon)$ is a scaling function depending only on ϵ), i.e.,

$$f_M = \begin{cases} \frac{k_B T}{R_M}\ \left[\delta D\left(\frac{h}{R_M}\right)^{\delta-1} - \zeta\left(\frac{R_M}{h}\right)\right] = f_{\rm p} & \text{, for BS-model} \\ \\ \frac{k_B T}{l_0}\ \mathcal{L}^{-1}\left(\frac{h}{l_0 M}\right) = f_{\rm p} & \text{, for FJBV-model} \end{cases} \tag{7.14}$$

The resisting force $f_{\rm p}$ holds the last adsorbed monomer in the adhesive plane (see again Fig.7.2a where the last adsorbed monomer experiences a force f_M). One should emphasize that the force $f_{\rm p}$ stays constant in the course of the pulling process (i.e., as long as one monomer, at least, is adsorbed on the surface), thus $f_{\rm p}$ corresponds to the *plateau* on the deformation curve (force f vs. chain end position h). The adsorbed monomer (see Fig. 7.2) has a chemical potential, $\mu_{\rm ads} = \ln z^*$, which in an equilibrium should be equal to the chemical potential of a desorbed monomer in the tail, $\mu_{\rm des} = \partial(F_{\rm tail}/k_B T)/\partial N$. The expression for $F_{\rm tail}$ depends on the model and is given either by eq. (7.10) for the BS-model or by eq.(7.12) in the case of FJBV-model. Taking this into account the condition $\mu_{\rm ads} = \mu_{\rm des}$ leads to the following "plateau law" relationship

$$\frac{l_0\, f_{\rm p}}{k_B T} = \begin{cases} |\ln[\mu_3 z^*(\epsilon)]|^\nu & \text{, for BS-model} \\ \\ \mathcal{G}^{-1}\left(|\ln[\mu_3 z^*(\varepsilon)]|\right) & \text{, for FJVB-model} \end{cases} \tag{7.15}$$

where $\mathcal{G}^{-1}(x)$ stands for the inversion of the function $\mathcal{G}(x) = x\coth(x) - 1$. One should note that Eq.(7.15) resembles Eq. 6.73 in Chapter 6 which determines the detachment

line in the pulling controlled by the applied force. Close to the critical point ϵ_c the plateau force $f_{\rm p}$ goes to zero. Namely, taking into account that in the vicinity of the critical point $\ln[\mu_3 z^*(\epsilon)] \propto -(\epsilon-\epsilon_c)^{1/\phi}$ (see ref.[7]) and $\mathcal{G}^{-1}(x) \approx (3x)^{1/2}$ we conclude that

$$f_p \;\propto\; \begin{cases} (\epsilon-\epsilon_c)^{\nu/\phi} & \text{, for BS-model} \\ \\ (\epsilon-\epsilon_c)^{1/2\phi} & \text{, for FJVB-model} \end{cases}$$

One can resolve Eq.(7.14) with respect to M (taking into account that $h \gg R_M$), and arrive at expression for the tail length

$$M(h,\epsilon) = \begin{cases} \frac{h}{l_0}\left(\frac{k_BT}{l_0 f_{\rm p}}\right)^{1/\nu-1} & \text{, for BS-model} \\ \\ \frac{h}{l_0}\left[\mathcal{L}\left(\frac{l_0 f_{\rm p}}{k_BT}\right)\right]^{-1} & \text{, for FJVB-model} \end{cases} \tag{7.16}$$

where the force at the plateau, $f_{\rm p}$, is described by the eq. (7.15). If, for the degree of adsorption we use the fraction of chain contacts with the plane, $n = N_s/N$, as an order parameter, where N_s is the number of monomers on the surface, we may write (as in Chapter 6)

$$n = -\frac{1}{k_BTN}\frac{\partial}{\partial\epsilon}\left(F_{\rm ads} + F_{\rm tail}\right) \tag{7.17}$$

where $F_{\rm ads}$ and $F_{\rm tail}$ are free energies of the adsorbed and desorbed portions of the chain respectively. The free energy $F_{\rm ads} = k_BT[N - M(h,\epsilon)]\ln z^*(\epsilon)$ whereas $F_{\rm tail} = k_BT\mu_{\rm des}M(h,\epsilon)$ (recall that $\mu_{\rm des}$ is the chemical potential of a desorbed monomer). After substitution these expressions in eq. (7.17) and taking into account that in equilibrium $\mu_{\rm ads} = \mu_{\rm des}$ (the sequence of operations is important: taking the derivative with respect to ϵ is to be followed by the condition $\mu_{\rm ads} = \mu_{\rm des}$) so one gets

$$n = -\left[1 - \frac{M(h,\epsilon)}{N}\right]\frac{\partial \ln z^*(\epsilon)}{\partial\epsilon} \tag{7.18}$$

i.e. the order parameter n is defined by the product of monomer fraction in the adsorbed portion, $1 - M/N$, and the fraction of surface contacts in this portion, $-\partial \ln z^*/\partial\epsilon$. The expressions for the order parameter can be recast in the form

$$n = \left|\frac{\partial \ln z^*(\epsilon)}{\partial\epsilon}\right| \times \begin{cases} 1 - \frac{h}{c_1 l_0 N}\left(\frac{k_BT}{l_0 f_{\rm p}}\right)^{1/\nu-1} & \text{, BS-model} \\ \\ 1 - \frac{h}{c_2 l_0 N}\left[\mathcal{L}\left(\frac{l_0 f_{\rm p}}{k_BT}\right)\right]^{-1} & \text{, FJVB-model} \end{cases} \tag{7.19}$$

Here c_1 and c_2 are some constants of the order of unity. As one can see from Eq. (7.19), the order parameter decreases linearly and steadily with h/N. This behavior is qualitatively different from the abrupt jump of n when the pulling force f is changed as a control parameter. In Section 7.4 we will show that this predictions is in a good agreement with our MC - findings. The transition point on the n vs. h curve corresponds to total detachment, $n = 0$. The corresponding distance h will be termed "detachment height" h_D. The dependence of h_D on the adsorption energy ϵ can be obtained from Eq.(7.19) where n is set to zero, i.e.

$$\frac{h_D}{l_0 N} = \begin{cases} \left(\frac{l_0 f_{\rm p}}{k_B T}\right)^{1/\nu - 1} & \text{, BS-model} \\ \\ \mathcal{L}\left(\frac{l_0 f_{\rm p}}{k_B T}\right) & \text{, FJVB-model} \end{cases} \tag{7.20}$$

where again $f_{\rm p}$ as a function of ϵ is given by Eq. (7.15).

The line given by Eq. (7.20), is named "detachment line". It corresponds to an adsorption - desorption polymer transition which appears as of *second order* since this order parameter n goes to zero continuously as h increases. One should emphasize, however, that this "detachment" transition has the same nature as the force-induced desorption transition [7] where the pulling force f, rather than the distance h, is fixed and used as a control parameter, and which is known to be of *first order*.

One can suggest a somewhat alternative way to define the detachment transition, namely, as a transition upon which the tail length M becomes equal to the total chain length N. Taking into account the eq. (7.16) for $M(h, \epsilon)$ we come to the following detachment line

$$\frac{h_D}{l_0 N} = \begin{cases} \left(\frac{l_0 f_{\rm p}}{k_B T}\right)^{1/\nu - 1} & \text{, for BS-model} \\ \\ \mathcal{L}\left(\frac{l_0 f_{\rm p}}{k_B T}\right) & \text{, for FJVB-model} \end{cases} \tag{7.21}$$

It is easy to understand that the condition $M(h, \varepsilon) = N$ corresponds to the force plateau termination and can be seen by the MC - simulation (see the next Section).

7.4 Results and Analysis

In order to verify the theoretical predictions, outlined in Section 7.3, we carried out extensive Monte Carlo simulations with the off-lattice model, described in Section 7.2. In these simulations we fixed the end monomer of the polymer chain at height h above the adsorbing surface, and measured the (fluctuating) force, needed to keep the last bead at distance h, as well as the corresponding fraction of adsorbed monomers n.

These computer experiments were performed at different strengths ϵ of the adsorption potential, Eq. (7.1).

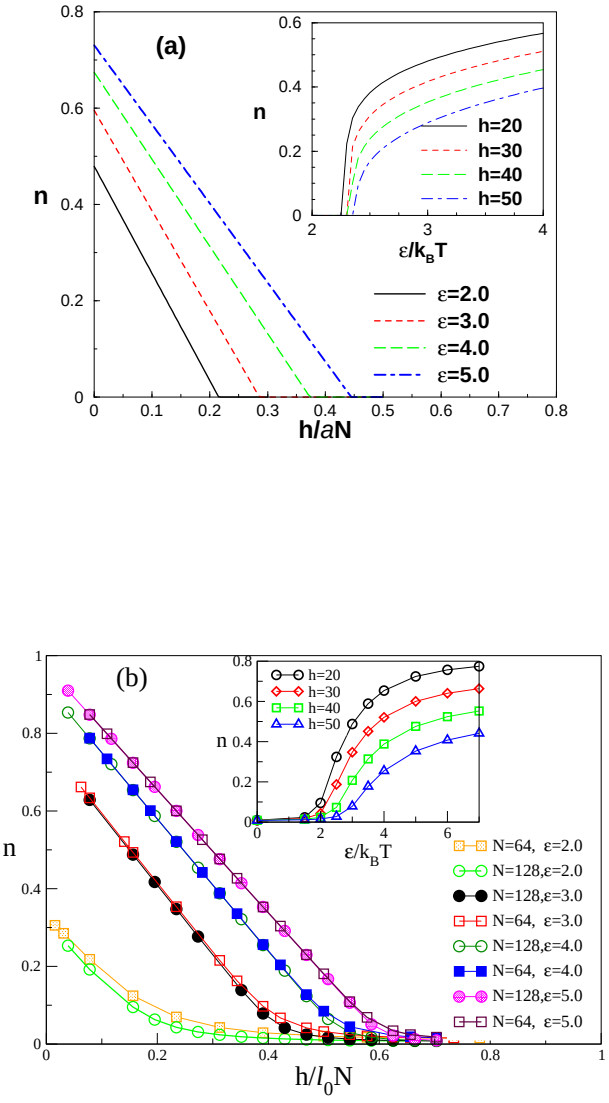

Figure 7.3: (a) Variation of order parameter (fraction of adsorbed monomers) n with changing height h/l_0N of the fixed chain-end for polymers of length $N = 64,\ 128$ and different adsorption strength ϵ/k_BT obtained analytically. (b) Variation of n with changing height of the chain end for different ϵ/k_BT from MC simulations. The insets show the resulting $n - \epsilon$ relationship for several fixed heights.

In Fig. 7.3a, 7.3b, we compare the predicted course of the order parameter n with changing reduced height h/l_0N for several values of $2.0 \leq \epsilon \leq 5.0$ with the results from MC simulations. Note, that the critical point of adsorption $\epsilon_c \approx 1.7$ (see Chapter 4 Section 4.6). We take our measurements outside the region of critical adsorption. Typically, both in the analytical results, plotted in Fig. 7.3a, which correspond to an infinitely-long chain $N \to \infty$, and in the MC-data, Fig. 7.3b, for $N = 128$, one recovers the predicted linear decrease of n with growing h.

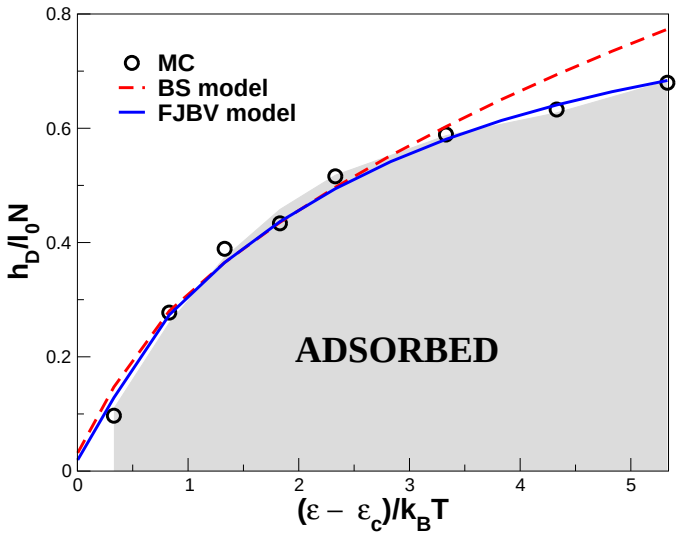

Figure 7.4: Phase diagram showing the dependence of the critical height of polymer detachment from the substrate, h_D/l_0N^ν, on the relative strength of adsorption $(\varepsilon - \varepsilon_c)$ where ε_c is the critical point of adsorption at zero force .

Finite-size effects lead to some rounding of the simulation data (in Fig. 7.3b these effects are seen to be larger for $N = 64$ than for $N = 128$) when $n \to 0$ so that the height of detachment h_D is determined from the intersection of the tangent to $n(h)$ and the $x-$axis where $n = 0$. Evidently, with growing adsorption strength, ϵ, larger height h_D is needed to detach the polymer from the substrate. Thus, one may construct a phase diagram for the desorption transition, which we show in Fig. 7.4. In the insets of Fig. 7.3a, 7.3b, we show the variation of the fraction of adsorbed segments with adsorption strengths ϵ for several heights $20 \leq h \leq 50$ of the $N = 128$ chain. It is evident that, apart from the rounding of the MC data for n at $n \to 0$, one finds very good agreement between the behavior, predicted by Eq. (7.18), and the simulation results. The gradual change of n in the whole interval of possible variation suggests a pseudo-continuous phase transition, as pointed out in the end of Section 7.3.

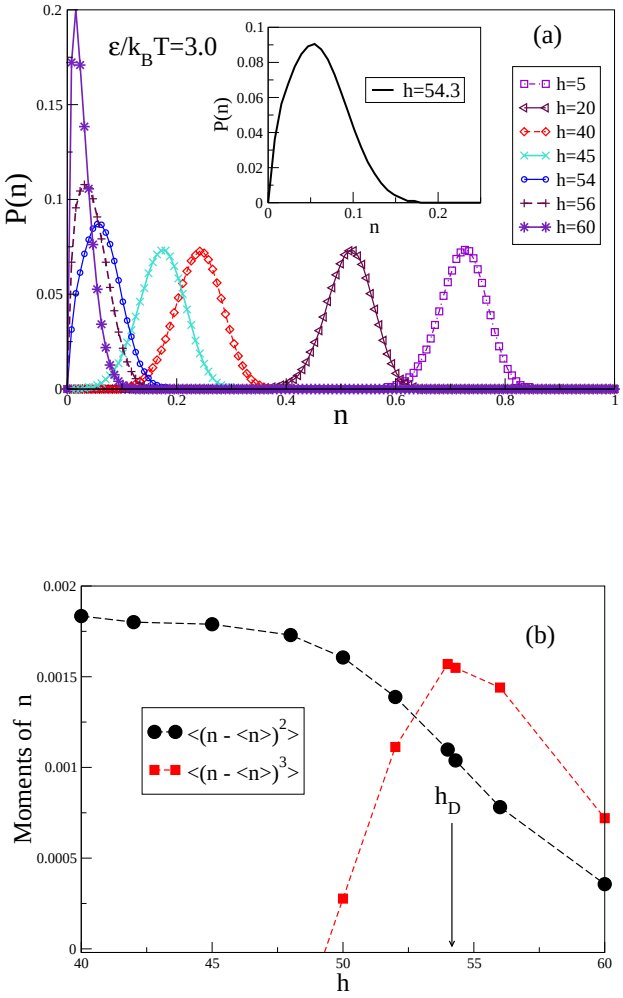

Figure 7.5: (a) Probability distribution $P(n)$ of the order parameter n (i.e., the fraction of adsorbed monomers) for $N = 128$ and $\epsilon = 3.0$ at different heights of the chain-end h over the grafting plane. In the inset we show $P(n)$ at the detachment line $h_D = 54.3$. (b) Variation of the second- and third central moments of $P(n)$ with h. The maximum of $\langle (n - \langle n \rangle)^3 \rangle$ is reached at $h = h_D$.

It has been pointed out earlier by Skvortsov et al.[81] that while both the fixed-force and the fixed-height ensembles are equivalent as far as the mean values of observables such as the fraction of adsorbed monomers and other related quantities are concerned, this does not apply to some more detailed properties like those involving fluctuations. Therefore, it is interesting to examine the fluctuations in the number of chain contacts with the surface, n, for different values of our control parameter h. First we consider the order parameter distribution $P(n)$ for zero force in Fig. 7.6 obtained from our computer experiment. For rather weak adsorption $\epsilon < \epsilon_c = 1.7$ in the subcritical regime, one can varify from Fig. 7.6 that $P(n)$ gradually transforms from nearly Gaussian into exponential distribution. For $\epsilon > \epsilon_c$ the distribution width grows and goes through a sharp maximum in the vicinity of ϵ_c, and then drops as ϵ increases further as displayed in the inset.

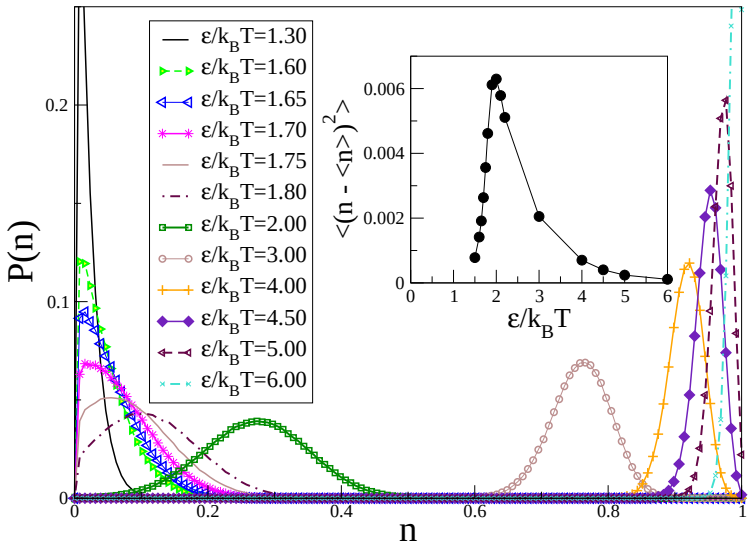

Figure 7.6: PDF of the order parameter (fraction of contacts with the plane) for different adsorption stregth ϵ at zero force. At the CAP one has $\epsilon_c \approx 1.7$. The change of the variance $\langle n^2 \rangle - \langle n \rangle^2$ with varying ϵ is displayed in the inset.

The theoretical analysis [81] for the fixed-height ensemble predicts a dispersion $\langle (\Delta n)^2 \rangle$ of the adsorbed fraction n is proportional to the chain length N while being independent of the value of h. The probability distribution $P(n)$ of the number of contacts is expected to be Gaussian. In Fig. 7.5a we display the distribution $P(n)$ measured in the MC simulations for different heights h at given adsorption energy $\epsilon = 3.0$. Indeed, one can readily verify from our results that far enough from the detachment line, $h < h_D$, the shape of $P(n)$ is Gaussian and the second moment, $\langle (\Delta n)^2 \rangle$, remains unchanged with varying height h. Of course, when $h \to h_D$ the maximum of $P(n)$ shifts to lower values of n. Only in the immediate vicinity of h_D

where $n \to 0$ and the fluctuations strongly decrease one observes a significant deviation from the Gaussian shape - cf. the inset in Fig. 7.5a. The latter is illustrated in more detail in Fig. 7.5b where we show the measured variation of the second moment, $\langle(\Delta n)^2\rangle$, and the third moment, $\langle(n-\langle n\rangle)^3\rangle$ with increasing height h. While the course of $\langle(\Delta n)^2\rangle$ closely follows that, predicted for Gaussian chains [81], the deviation from Gaussianity of $P(n)$, measured by the deviation of the third moment from zero, is localized in the vicinity of the detachment height h_D.

The force f, exerted by the chain on the end-monomer, when kept at height h above the surface, is one of the main properties which can be measured in experiments carried out within the fixed-height ensemble. Note that f has the same magnitude and opposite sign, $f = -\tilde{f}$, as the force, applied by the experimentalist. The variation of the force f with increasing height h is shown in Fig. 7.7a for several values of the adsorption potential $2.0 \leq \epsilon \leq 5.0$. In Fig. 7.7a we distinguish between the components of the total force f acting on the end bead. The total force consists of two contributions : the first stems from the quasi-elastic forces of the bonded interaction (FENE) whereas the second contribution is due to the short-range interactions between non-bonded monomers (in our model - the Morse potential). A typical feature of the $f-h$ relationship, namely, the existence of a broad interval of heights h where the force remains constant (a plateau in the force) is readily seen in Fig. 7.7a. With growing strength of adsorption ϵ the length of this plateau as well as the magnitude of the force increase. Note, that for $\epsilon = 0$ no plateau whatsoever is found. Upon further extension of the chain, the plateau ends and the measured force starts to grow rapidly in magnitude - an effect, caused by stretching of the individual bonds rather than the chain conformation itself.

A closer inspection of Fig. 7.7a reveals that the non-bonded contribution to f, which is generally much weaker than the bonded one, behaves differently, depending on whether the forces between non-nearest neighbors along the backbone of the chain are purely repulsive, or contain an attractive branch. While for strong adsorption, $\epsilon \geq 3.0$, a plateau is observed even for attractive non-bonded interactions, for weak adsorption, $\epsilon \leq 2.0$, an increase of the non-bonded contribution at $h/l_0N \approx 0.35$, (seen as a *minimum* in Fig. 7.7a) is observed.

This effect is entirely missing in the case of purely repulsive nonbonded interactions - see the inset in Fig. 7.7a where the contributions from bonded and non-bonded interactions are shown for a neutral surface $\epsilon = 0$. If one plots the magnitude of the measured force at the plateau against the corresponding value of the the adsorption potential, ϵ, one may check the theoretical result, Eq. (7.15)

The $f - h$ relationship, which gives the equation of state of the stretched poly-

mer, may be derived within one of the different theoretical modela, e.g., that of BS, Eq. (7.9), or FJBV, Eq. (7.11), as mentioned in Section 7.3. Which of these theoretical descriptions is the more adequate can be decided by comparison with experiment. In Fig. 7.8a, 7.8b, we present such comparison by plotting our simulation data using different scaling for the dimensionless height h. From Fig. 7.8a it becomes evident that the data for $N = 64$ and $N = 128$ from our computer experiment collapse on a single curve, albeit this collapse only holds as long as $h/l_0N^\nu \leq 3.0$ for the BS model while it fails for stronger stretching. In contrast, this collapse works well for all values of h, provided the height is scaled with the contour length of the chain N - Fig. 7.8b - regardless of whether a pure repulsive or the full Morse potential (which includes also an attractive part) of interactions are involved. The analytical expression, Eq. (6.37), is found to provide perfect agreement with the simulation data for strong stretching, $h/l_0N \geq 0.4$. From the simulation data on Fig. 7.8 one may verify that the force f goes through zero at some height h and even turns negative, provided one keeps the chain end very close to the grafting surface.

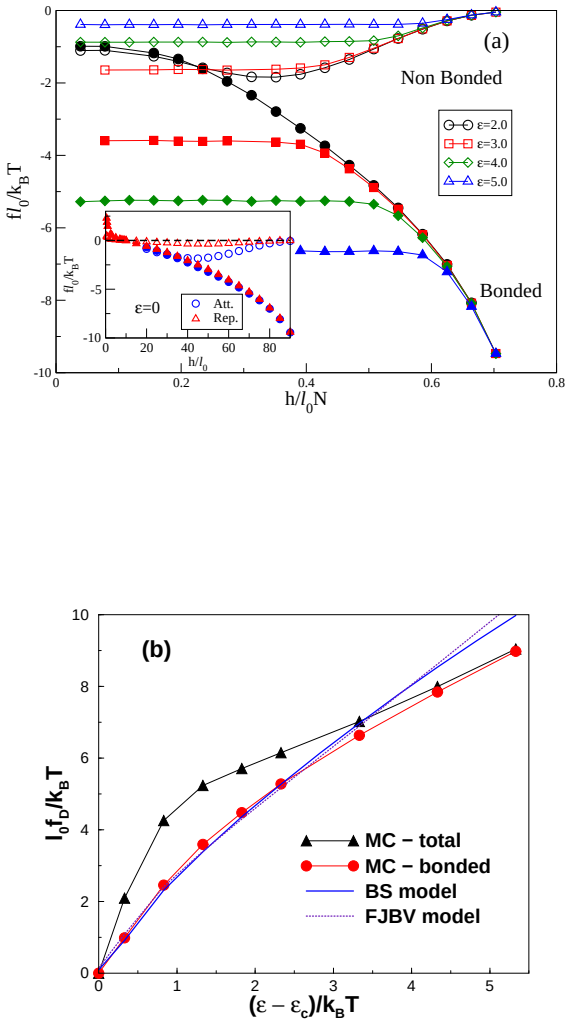

Figure 7.7: (a) Variation of the two components to the total force, exerted by the chain on the end-monomer which is fixed at (dimensionless) height h/l_0N for different adsorption potentials $2.0 \leq \epsilon/k_BT \leq 5.0$: bonding interactions (full symbols) and non-bonding Morse interactions (empty symbols). In the inset the same is shown for a neutral plane $\epsilon = 0.0$ for purely repulsive monomers (triangles) and for the usual Morse potential (circles). (b) Variation of the total force (plateau hight) exerted by the AFM tip on the chain-end for chain length $N = 128$ with adsorption strength ϵ.

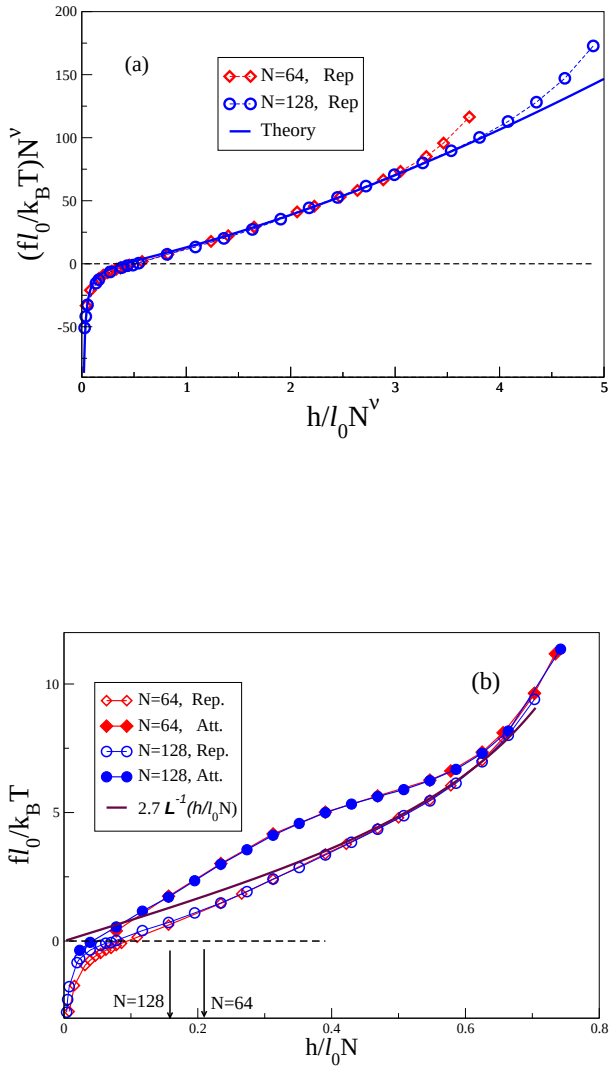

Figure 7.8: (a) Variation of the total applied force f with growing height of the end monomer in terms of Pincus reduced variables, fl_0N^ν/k_BT versus h/l_0N^ν, for a polymer with purely repulsive nonbonded forces for $N = 64,\ 128$. (b) The same as in (a) but in terms of reduced units fl_0/k_BT versus h/l_0N for purely repulsive (empty symbols) as well as for usual Morse potential (full symbols) of nonbonded interactions between monomers. The FJBV-model results, Eq. (7.14), is shown by a solid line. Arrows indicate the unperturbed gyration radius positions R_g/N for $N = 64,\ 128$

7.5 Discussion

This chapter is the concluding part of our discussion of the force induced desorption of a polymer from an attractive surface. We have treated the polymer in the so-called h-ensemble in which we consider the detachment of the polymer keeping the distance h between the chain end and the substrate as the control parameter. The motivation for this investigation has been the necessity to distinguish between results obtained in this ensemble and results, derived in the constant-force ensemble (described in the previous chapter), as far as both ensembles could in principle be used by experimentalists. We find that the observed behavior of the main quantity of interest, namely, the fraction of adsorbed beads n (i.e., the order parameter of the phase transition) with changing height h differs qualitatively from the variation of the order paremeter when the pulling force is varied. In the constant-height ensemble one observes a steady variation of n with changing h whereas in the constant-force ensemble one sees an abrupt jump of n at a particular value of f_D, termed a detachment force. However, this should not cast doubts on the genuine first-order nature of the phase transition which can be recovered within the constant-height ensemble too, provided one expresses the control parameter h in terms of the average force f. We have explored two different theoretical models for the basic force - extension relationship, namely, the bead-spring (BS) model as well as that of a Freely-Jointed Bond-Vectors (FJBV) model.

Our primary result is the phase diagram which gives the variation of the critical height of polymer detachment with the strength of adsorption. As expected, with growing adsorption strength, the height of detachment is found to increase. Another important consideration in this study was the measurement of the force on the end monomer. The equation of state i.e. the $f - h$ relationship was one of the foci of our investigations. An important feature is the plateau in the deformation curve which denotes the interval in which the force remains constant during the pulling process. The plateau was found to increase with growing strength of the adsorption potential. Our simulation results indicate a good agreement between theory and computer experiment. This concludes the present study of the pulling of an adsorbed polymer from a surface.

Chapter 8

Conclusions

This thesis is concerned with the adsorption of polymers at planar, rigid surfaces. Adsorption of polymers on surfaces plays a critical role in a host of technological applications such as adhesion, colloidal stabilization, and chromatography. Hence this subject has been the focus of research efforts for several decades. We have carried out a systematic investigation of adsorption of polymers using analytical techniques as well as Monte Carlo simulations with a coarse grained off-lattice bead spring model. The investigation was carried out in three stages :

- The adsorptive transition of regular multiblock and random copolymers was studied with particular focus on the critical behavior . Our main result was the phase diagram of regular multiblock copolymers which shows an increase in the critical adsorption potential of the substrate with decreasing size of blocks. The phase diagram for random copolymers with quenched disorder which gives the change in the critical adsorption potential, ϵ_c^p, with changing percentage of the sticking A-monomers, p, is also determined from computer simulations. We observe perfect agreement with the theoretically predicted result which has been derived by treating the adsorption transition in terms of the "annealed disorder" approximation. An important conclusion concerns the value of the universal crossover exponent $\phi = 0.5$ which is found to remain unchanged, regardless whether homo-, regular multiblock-, or random polymers are concerned. Thus the universality class of the adsorption transition of a a regular multi-block or a random copolymer is the same as that of a homopolymer.

- We studied the adsorption kinetics of a single polymer on a solid plane in the strong physisorption regime. We found a perfect agreement between the theoretical predictions and the simulation results for the PDF . From the numerical solution of the Master Equation, we have found that the growth of the adsorbed

fraction of monomers with time is governed by a power law

$$n(t) \propto t^{\frac{1}{1+\nu}},$$

while the typical time of adsorption τ scales with

$$\tau \propto N^{\alpha}$$

with $\alpha = 1 + \nu$. Our Monte Carlo results are in good agreement with these predictions if one takes into account the finite-size effects due to the finite length of the studied polymer chains. A deeper insight into the adsorption kinetics is provided by our detailed study of the relevant probability distributions of trains, loops and tails during the adsorption. The predicted exponential expression for the PDF of trains is in a very good agreement with our simulational findings. The loops in the strong physisorption regime are observed to reduce to occasional desorbed segments (vacancies) which play little role in the dominating picture of trains and tails. The PDFs of the latter are found from the simulation data to present a shape which is fully consistent with that of the theoretic treatment.

- We have studied force induced desorption of a polymer chain adsorbed on an attractive surface. This field has become topical due to the use of Atomic Force Microscopy (AFM) and optical tweezers which allow one to manipulate single polymer chains. We approached the problem within the framework of two different statistical ensembles; (i) by keeping the pulling force *fixed* while measuring the (fluctuating) position of the polymer chain end, and (ii) by measuring the (fluctuating) force necessary to keep the chain end at *fixed* distance above the adsorbing plane.

  - In the first case we treated the problem within the framework of the Grand Canonical Ensemble approach and derived analytic expressions for the various conformational building blocks, characterizing the structure of an adsorbed linear polymer chain, subject to pulling force of fixed strength. The main result was the phase diagram of a polymer chain under pulling. We demonstrated a novel first order phase transformation which is dichotomic i.e. phase coexistence is not possible. The primary result was the calculation of the crossover exponent, ϕ which provides insight into the background of the existing controversial reports about its numeric value. We demonstrated that the value of ϕ may vary within the interval $0.39 \leq \phi \leq 0.6$, depending on the possibility of a single loop to interact with the neighboring loops in the adsorbed polymer. Since this range is model-dependent, this accounts for the different estimates of ϕ in literature.

– In the second case, we carried out our study in the "fixed height" statistical ensemble where one measures the fluctuating force, exerted by the chain on the last monomer when a chain end is kept fixed at height h over the solid plane at different adsorption strength ϵ. The phase diagram in the $h - \epsilon$ plane was calculated both analytically and by Monte Carlo simulations. We demonstrated that in the vicinity of the polymer desorption transition a number of proprties like fluctuations and probability distribution of various quantities behave differently, if h rather than f is used as an independent control parameter.

For future considerations, it would be interesting to explore the dynamics of a polymer chain being pulled from an attractive surface. This can be achieved using kinetic Monte Carlo simulations by pulling one end of the chain at a constant rate . Another area for further studies would be to consider the pulling of heteropolymers from a surface. It would be interesting to find out how the sequence of monomers affect the force-extension curve.

Appendix A

Derivation of train distribution

The partition function of an one-dimensional array of $p+1$ trains, separated by p defects, has the following form

$$\begin{aligned}\Phi[n(t),p] &= \int\limits_{0<x_1<x_2\ldots x_p<n(t)}\ldots\int dx_1\ldots dx_p \\ &= \int\limits_0^{n(t)} dx_1 \int\limits_{x_1}^{n(t)} dx_2\ldots\int\limits_{x_{p-1}}^{n(t)} dx_p = \frac{1}{p!}\,[n(t)]^p \end{aligned} \tag{A.1}$$

where $n(t)$ is the total number of adsorbed monomers at time t.

Consider now the the distribution of an arbitrary train $h_{s+1}=x_{s+1}-x_s$. In order to find it, one should carry out the integration in Eq. (A.1) over all x-coordinates except x_s and x_{s+1}. In result of the integration one gets

$$\Phi_{x_s x_{s+1}}[n(t),p]\,dx_s dx_{s+1} = \frac{1}{(s-1)!(p-s-1)!}\,x_s^{s-1}\;[n(t)-x_{s+1}]^{p-s-1}\;dx_s dx_{s+1} \tag{A.2}$$

where Eq.(A.1) has been used separately for the intervals $[0,x_s]$ and $[x_{s+1},n(t)]$. The distribution of the train length, $h_{s+1}=x_{s+1}-x_s$, follows immediately from Eq.(A.2) after integrating over x_s, i.e.

$$\Phi_{h_{s+1}}[n(t),p] = \frac{1}{(s-1)!(p-s-1)!}\int\limits_0^{n(t)-h_{s+1}} x_s^{s-1}\;[n(t)-h_{s+1}-x_s]^{p-s-1}\;dx_s \tag{A.3}$$

By the substitution, $y=x_s/[n(t)-h_{s+1}]$, in the integral of Eq.(A.3) one arrives at the result

$$\begin{aligned}\Phi_{h_{s+1}}[n(t),p] &= \frac{[n(t)-h_{s+1}]^{p-1}}{(s-1)!(p-s-1)!}\int\limits_0^1 y^{s-1}(1-y)^{p-s-1}\,dy \\ &= \frac{1}{(p-1)!}\;[n(t)-h_{s+1}]^{p-1}\end{aligned} \tag{A.4}$$

where one has used $\int_0^1 y^{s-1}(1-y)^{p-s-1}dy = (s-1)!(p-s-1)!/(p-1)!$. The result in Eq. (A.4) does not depend on the consecutive number of the train, as expected. The normalized probability to find a train of the length h at time t is given by

$$\begin{aligned} D(h,t) &= \frac{\Phi_h[n(t),p]}{\Phi[n(t),p]} = \frac{p!}{(p-1)!}\,\frac{[n(t)-h]^{p-1}}{[n(t)]^p} \\ &= \frac{p}{n(t)}\,\left[1-\frac{h}{n(t)}\right]^{p-1} \simeq \frac{p}{n(t)}\,\exp\left[-h\frac{p}{n(t)}\right] \end{aligned} \tag{A.5}$$

where one uses Eqs.(A.1) and (A.4) as well as the conditions $p \gg 1$ and $h/n(t) \ll 1$. Taking into account that the average train length $h_{\rm av}(t) = n(t)/p$, the last expression results in Eq.(5.33).

Appendix B

Properties of the polylog function

The polylog function $\Phi(\alpha, z)$ is defined by the series

$$\Phi(\alpha, z) = \sum_{n=1}^{\infty} \frac{1}{n^{\alpha}}\, z^n \tag{B.1}$$

which converges at $|z| < 1$. From the definition, Eq. (B.1), one immediately obtains

$$z\,\frac{d}{dz}\,\Phi(\alpha, z) = \Phi(\alpha - 1, z) \tag{B.2}$$

The calculation of the series Eq. (B.1) (see Sec. 1.11 in ref. [30]) gives

$$\Phi(\alpha, z) = \Gamma(1-\alpha)\left[\ln\left(\frac{1}{z}\right)\right]^{\alpha-1} + \sum_{r=0}^{\infty} \zeta(\alpha - r)\frac{(\ln z)^r}{r!} \tag{B.3}$$

where $\Gamma(x)$ is the gamma-function, $\zeta(x)$ is the Riemann zeta-function, and the exponent α is noninteger, i.e. $\alpha \neq 1, 2, 3, \ldots$

Consider now the case of integer values of α. The gumma-function $\Gamma(x)$ has poles at all negative integer arguments whereas the pole of $\zeta(x)$ is placed at $x = 1$. One may write $\alpha = m + \delta$ where m is a positive integer and $\delta \to 0$. Then in the vicinity of the poles the gamma- and zeta-functions can be rewritten as

$$\begin{aligned} \Gamma(1 - m - \delta) &= \frac{(-1)^m}{(m-1)!}\,\left[\frac{1}{\delta} - \psi(m) + \mathcal{O}(\delta)\right] \\ \zeta(1+\delta) &= \left[\frac{1}{\delta} - \psi(1) + \mathcal{O}(\delta)\right] \end{aligned} \tag{B.4}$$

where $\psi(x)$ is the digamma function (or ψ-function) defined as the logarithmic derivative of the gamma-function, $\psi(x) = d\ln\Gamma(x)/dx$. One should also take into account that

$$\left[\ln\left(\frac{1}{z}\right)\right]^{\delta} = 1 + \delta \ln\left[\ln\left(\frac{1}{z}\right)\right] + \mathcal{O}(\delta) \tag{B.5}$$

After taking into account Eqs.(B.4) and (B.5) in Eq. (B.3) and due to the cancellation of poles in the gamma- and zeta-functions at small values of δ the polylog function, Eq.(B.1) becomes [30]

$$\Phi(m,z) = \frac{(\ln z)^{m-1}}{(m-1)!}\left[\psi(m) - \psi(1) - \ln\ln\left(\frac{1}{z}\right)\right] + \sum_{r=0}^{\infty}{}' \zeta(m-r)\,\frac{(\ln z))^r}{r!} \qquad \text{(B.6)}$$

where the prime indicates that the term $r = m-1$ is to be omitted.

We are interested in the behavior of $\Phi(\alpha, z)$ at $z \to 1$. In this case $\ln(1/z) = -\ln[1-(1-z)] \approx (1-z)$. At $\alpha < 1$, the main contribution comes from the first term in Eq. (B.3), i.e.

$$\Phi(\alpha, z) \approx \frac{\Gamma(1-\alpha)}{(1-z)^{1-\alpha}} \qquad \text{(B.7)}$$

At $\alpha = 1$ and $z \to 1$, and making use of Eq. (B.6), one obtains

$$\Phi(1, z) \approx -\ln\ln\left(\frac{1}{z}\right) \approx \ln\left(\frac{1}{1-z}\right) \qquad \text{(B.8)}$$

Finally, at $\alpha > 1$ the polylog function $\Phi(\alpha, z)$ has no singularity at $z \to 1$ and Eq.(B.3) results in the following expansion

$$\Phi(\alpha, z) \approx \zeta(\alpha) + \Gamma(1-\alpha)(1-z)^{\alpha-1} - \zeta(\alpha-1)(1-z) + \ldots \qquad \text{(B.9)}$$

In a bit more specific case when $1 < \alpha < 2$ we will use the well known relationship $\Gamma(1-\alpha) = -\pi/[\Gamma(\alpha)|\sin(\pi\alpha)|]$ so that

$$\Phi(\alpha, z) \approx \zeta(\alpha) - \frac{\pi}{\Gamma(\alpha)|\sin(\pi\alpha)|}(1-z)^{\alpha-1} - \zeta(\alpha-1)(1-z) + \ldots \qquad \text{(B.10)}$$

Taking into account the Eqs.(B.7), (B.8) and (B.10), the expression for the polylog function at $z \to 1$ reads

$$\Phi(\alpha, z) \approx \begin{cases} \frac{\Gamma(1-\alpha)}{(1-z)^{1-\alpha}}, & \text{at} \quad \alpha < 1 \\ \ln\left(\frac{1}{1-z}\right), & \text{at} \quad \alpha = 1 \\ \zeta(\alpha) - a_\alpha(1-z)^{\alpha-1} - b_\alpha(1-z) + \ldots, & \text{at} \quad 1 < \alpha < 2 \end{cases} \qquad \text{(B.11)}$$

where the coefficients $a_\alpha = \pi/\Gamma(\alpha)|\sin(\pi\alpha)|$ and $b_\alpha = \zeta(\alpha-1)$.

Appendix C

PDF of the end-to-end distance of a SAW chain.

Following McKenzie and Moore, we show that the probability that a SAW of n steps reaches a distance $\mathbf{r}$ from the origin has the form

$$p_n(\mathbf{r}) \sim R_n^{-d} \left(r/R_n\right)^t exp\left(-\left(r/R_n\right)^{1/(1-\nu)}\right) \tag{C.1}$$

where R_n is a scaling length which varies as n^ν and d is the dimensionality. We start with the analogy between the probability distribution $P_n(\mathbf{r})$ of a self avoiding walk of n steps that starts at the origin and ends at $\mathbf{r}$, and the high temperature series expansion of the spin-spin correlation of the Ising model. Consider the generating function

$$\Gamma(\mathbf{r}, v) = \sum_{n\geq 1} C_n(\mathbf{r}) v^n \tag{C.2}$$

where $C_n(\mathbf{r})$ is the number of SAW trajectories. The Fourier transform of $\Gamma(\mathbf{r}, \nu)$ close to the critical point has the following Ornstein-Zernicke form

$$\hat{\Gamma}(\mathbf{k}, v) = \frac{A\kappa^\eta}{\kappa^2 + k^2} \tag{C.3}$$

when k and κ are small and $k^2 = |\mathbf{k}^2|$. The parameter κ is the inverse correlation length ξ

$$\kappa \simeq \xi^{-1} = \kappa_0 \left(1 - v/v_c\right)^\nu$$

At $k \to 0$

$$\hat{\Gamma}(0.v) \simeq \frac{1}{(1 - v/v_c)^{(2-\eta)\nu}} = \frac{1}{(1 - v/v_c)^{\gamma_1}} = \chi/T \tag{C.4}$$

where $\gamma_1 = (2 - \eta)\nu$.

Now consider the polymer generating function

$$\Gamma(\mathbf{r}, v) = \sum_{n\geq 1}^{\infty} C_n P_n(\mathbf{r}) v^n \tag{C.5}$$

which is analogous to the spin-spin correlation function mentioned above. Here $C_n \sim \mu_3^n n^{\gamma_1 - 1}$. The Fourier transformation of $\Gamma(\mathbf{r}, \theta)$ is

$$\hat{\Gamma}(\mathbf{k}, v) = \sum_{n \geq 1} n^{\gamma_1 - 1} (\mu_3 v)^n \int P_n(\mathbf{r}) e^{i\mathbf{k}.\mathbf{r}} d^3\mathbf{r} \tag{C.6}$$

Now, $\int P_n \mathbf{r} d^3\mathbf{r} = 0$ and

$$\sum_{n \geq 1}^{\infty} \frac{(\mu_3 v)^n}{n^{1-\gamma}} = \frac{\Gamma(\gamma)}{(1 - \mu_3 v)^\gamma}$$

for $1 - \gamma < 0$. As a result , at $\mathbf{k} \to 0$

$$\hat{\Gamma}(\mathbf{0}, v) \simeq \frac{\Gamma(\gamma)}{(1 - \mu_3 v)^\gamma} \tag{C.7}$$

Comparing with Equation C.4, we see that $v_c = 1/\mu_3$. Let $v = v_c e^{-\theta}$. With this change of variable, in the limit $\theta \to 0$, the generating functional has the form

$$\Gamma(\mathbf{r}, \theta) = \sum_{n \geq 1} v_c^n C_n P_n(\mathbf{r}) e^{-n\theta}$$

and we assume that the Fourier Transform of $\Gamma(\mathbf{r}, \theta)$ *i.e* $\Gamma(\mathbf{k}, \theta)$ also has the Ornstein Zernicke form

$$\hat{\Gamma}(\mathbf{k}, \theta) \sim \frac{A\kappa^\eta}{\kappa^2 + k^2} \tag{C.8}$$

where $\kappa = \kappa_0 \theta^\nu$.

The inverse of Equation C.8 is

$$\Gamma(\mathbf{r}, \theta) = A\kappa^\eta \int_0^\infty d^d k \frac{e^{i\mathbf{k}.\mathbf{r}}}{\kappa^2 + k^2} \int_0^\pi d\phi \sin^{d-2}\phi \int_0^\infty dk k^{d-1} \frac{e^{ikr\cos\phi}}{\kappa^2 + k^2}$$

After a little algebra and simplification , we get

$$\Gamma(\mathbf{r}, \theta) \sim \kappa^{\eta - \frac{3-d}{2}} r^{-(d-1)/2} e^{-\kappa r} \tag{C.9}$$

for $\kappa r \gg 1$ and $\theta \to 0$. Now, since

$$\Gamma(\mathbf{r}, \theta) = \sum_{n > ge1}^{\infty} \mu^{-n} C_n P_n(\mathbf{r}) e^{-n\theta}$$

using Cauchy's theorem, we have

$$\mu^{-n} C_n P_n(\mathbf{r}) = \frac{1}{2\pi i} \oint \frac{dv}{v^{n+1}} \Gamma(\mathbf{r}, v)$$

or

$$\mu^{-n} C_n P_n(\mathbf{r}) = \frac{1}{2\pi i} \int_{c-i\pi}^{c+i\pi} \Gamma(\mathbf{r}, \theta) e^{n\theta} d\theta$$

where c is larger than the real part of any singularity of $\Gamma(\mathbf{r}, \theta)$. Using the method of steepest descent to perform the integral, we finally get

$$C_n P_n(\mathbf{r}) \propto \mu^n n^{\gamma-1-\nu d} \left[\frac{r\kappa_0\nu}{n^\nu}\right]^{\frac{1-\gamma+\nu d-d/2}{1-\nu}} \exp\left(-(1/\nu-1)\left(\frac{r\kappa_0\nu}{n^\nu}\right)^{1/(1-\nu)}\right) \tag{C.10}$$

But we know that $C_n \sim \mu^n n^{\gamma-1}$. Therefore , the PDF for the end-to-end distance has the form

$$P_n(r) \propto \left(\frac{1}{n^{\nu d}}\right)\left[\frac{r\kappa_0\nu}{n^\nu}\right]^t \exp\left(-D\left(\frac{r\kappa_0\nu}{n^\nu}\right)^\delta\right) \tag{C.11}$$

with

$$t = \frac{1-\gamma_1+\nu d-d/2}{1-\nu} \tag{C.12}$$

$$\delta = \frac{1}{1-\nu} \tag{C.13}$$

Appendix D

Freely jointed bond vectors model

The deformation law in the overstretched regime (when the chain deformation is close to its saturation) could be treated better within the FJBV model. Let us consider a tethered chain of the length N with one end anchored at the origin of the coordinates and the external force f_N acting on the free end. The corresponding deformation energy reads

$$U_{\rm ext} = -f_N \, r_N^{\perp} = -f_N \, \sum_{i=1}^{N} b_i \cos\theta_i \tag{D.1}$$

where $r_N^{\perp}$ is the z-coorditate (directed perpendicular to the surf ace) of the chain end, b_i and θ_i are the length and the polar angle of the i-th bond vector respectively. The corresponding partition function of the FJBV model is given by

$$\begin{aligned} Z_N(f_N) &= \int \prod_{i=1}^{N} d\phi_i \sin\theta_i d\theta_i \exp\left(\frac{f_N}{T}\sum_{i=1}^{N} b_i\cos\theta_i\right) \\ &= (4\pi)^N \prod_{i=1}^{N}\left(\frac{T}{b_i f_N}\right)\cosh\left(\frac{b_i f_N}{T}\right) \end{aligned} \tag{D.2}$$

The average orientation of the i-th bond vector can be calculated as

$$< \cos\theta_i >= \left(\frac{T}{f_N}\right)\frac{\partial}{\partial b_i}\ln Z_N(f_N) = \coth\left(\frac{b_i f_N}{T}\right) - \left(\frac{T}{b_i f_N}\right) \tag{D.3}$$

From eq.(D.3) the chain end mean distance h is given by

$$h = \sum_{i=1}^{N} b_i < \cos\theta_i >= bN\mathcal{L}\left(\frac{bf_N}{T}\right) \tag{D.4}$$

where we have took into account that the lengths of all bond vectors are the same, $b_i = b$, and where $\mathcal{L}(x) = \coth(x) - 1/x$ is the Langevin function. This leads to the

force - distance relationship

$$\frac{bf_N}{T} = \mathcal{L}^{-1}\left(\frac{h}{bN}\right) = \begin{cases} \frac{1}{1-h/bN} & \text{, at } h/bN \leq 1 \\ \frac{2h}{bN} & \text{, at } h/bN \ll 1 \end{cases} \tag{D.5}$$

which we use in Sec.II. The notation $\mathcal{L}^{-1}(x)$ stands for the inverce Langevin function.

Bibliography

[1] A. Milchev, V. Yamakov, and K. Binder. Escape transition of a compressed polymer mushroom under good solvent conditions. *Europhysics Letters*, 47(6):675–680, sep 1999.

[2] A. Serr and R.R. Netz. Pulling adsorbed polymers from surfaces with the afm: stick vs. slip, peeling vs. gliding. *Europhysics Letters*, 73(2):292–298, jan 2006.

[3] B. Alberts, D. Bray, J. Lewis, M. Raff, K. Roberts, and J.D. Watson.

[4] A. Ashkin. Optical trapping and manipulation of neutral particles using lasers. *PNAS*, 94:4853–4860, May 1997.

[5] B. O'Shaughnessy and D. Vavylonis. Irreversible adsorption from dilute polymer solutions. *The European Physical Journal E*, 11(3):213–230, jul 2003.

[6] S. Bhattacharya, H.-P. Hsu, A. Milchev, V. G. Rostiashvili, and T. A. Vilgis. Adsorption of multiblock and random copolymer on a solid surface: Critical behavior and phase diagram. *Macromolecules*, 41(8):2920–2930, 2008.

[7] S. Bhattacharya, V.G. Rostiashvili, A. Milchev, and T.A. Vilgis. Forced-induced desorption of a polymer chain adsorbed on an attractive surface - theory and computer experiment. *Macromolecules*, 42(6):2236–2250, 2009.

[8] K. Binder. Theory of first-order phase transitions. *Reports on Progress in Physics*, 50(7):783–859, 1987.

[9] K. Binder and A. Milchev. Off-lattice monte carlo methods for coarse-grained models of polymeric materials and selected applications. *Journal of Computer-Aided Material Design*, 9:33–74, 2002.

[10] F. Brochard-Wyart. Polymer chains under strong flows: Stems and flowers. *EPL (Europhysics Letters)*, 30(7):387–392, 1995.

[11] Theodore W. Burkhardt, Erich Eisenriegler, and Ihnsouk Guim. Conformal theory of energy correlations in the semi-infinite two-dimensional o(n) model. *Nuclear Physics B*, 316(3):559 – 572, 1989.

[12] F. Celestini, T. Frisch, and X. Oyharcabal. Stretching an adsorbed polymer globule. *Phys. Rev. E*, 70(1):012801, Jul 2004.

[13] A. Corsi, A. Milchev, V. G. Rostiashvili, and T. A. Vilgis. Localization of a multiblock copolymer at a selective interface: Scaling predictions and monte carlo verification. *The Journal of Chemical Physics*, 122(9):094907, 2005.

[14] P. G. de Gennes. *Scaling Concepts in Polymer Physics*. Cornell Univ. Press, Ithaca, 1979.

[15] P. G. de Gennes. Conformations of polymers attached to an interface. *Macromolecules*, 13(5):1069–1075, 1980.

[16] P. G. de Gennes. Polymer solutions near an interface. adsorption and depletion layers. *Macromolecules*, 14(6):1637–1644, 1981.

[17] P.G. de Gennes. Polymers at an interface; a simplified view. *Advances in Colloid and Interface Science*, 27(3-4):189 – 209, 1987.

[18] P.G. de Gennes and P. Pincus. Scaling theory of polymer adsorption : proximal exponent. *Journal de Physique Lettres*, 44(7):241–246, 1983.

[19] J. des Cloizeaux and G. Jannink. *Polymers in Solution*. Clarendon Press, Oxford, 1990.

[20] R. Descas, J.-U. Sommer, and A. Blumen. Static and dynamic properties of tethered chains at adsorbing surfaces: A monte carlo study. *The Journal of Chemical Physics*, 120(18):8831–8840, 2004.

[21] R. Descas, J.-U. Sommer, and A. Blumen. Irreversible adsorption of tethered chains at substrates: Monte carlo study. *The Journal of Chemical Physics*, 124(9):094701, 2006.

[22] H. W. Diehl. *Phase Transition and Critical Phenomena. ed Domb, C. and Lebowitz, J.L.*, volume 10. London Academic Press, London, 1986.

[23] H. W. Diehl and S. Dietrich. Field-theoretical approach to multicritical behavior near free surfaces. *Phys. Rev. B*, 24(5):2878–2880, Sep 1981.

[24] H. W. Diehl and M. Shpot. Surface critical behavior in fixed dimensions : Nonanalyticity of critical surface enhancement and massive field theory approach. *Phys. Rev. Lett.*, 73(25):3431–3434, Dec 1994.

[25] H. W. Diehl and M. Shpot. Massive field-theory approach to surface critical behavior in three-dimensional systems. *Nuclear Physics B*, 528(3):595 – 647, 1998.

[26] M. Doi and S.F. Edwards. *The theory of polymer dynamics.* Clarendon Press, Oxford, 1986.

[27] B. Duplantier. Statistical mechanics of polymer networks of any topology. *Journal of Statistical Physics*, 54(3):581–680.

[28] E. Eisenriegler. *Polymers Near Surfaces.* World Scientific, London, 1993.

[29] E. Eisenriegler, K. Kremer, and K. Binder. Adsorption of polymer chains at surfaces: Scaling and monte carlo analyses. *The Journal of Chemical Physics*, 77(12):6296–6320, 1982.

[30] A. Erdélyi. *Higher transcendental functions.* McGraw-Hill, New York, 1953.

[31] O. A. Evers, J. M. H. M. Scheutjens, and G. J. Fleer. Statistical thermodynamics of block copolymer adsorption. 1. formulation of the model and results for the adsorbed layer structure. *Macromolecules*, 23(25):5221–5233, 1990.

[32] F. Hanke, L. Livadaru, and H. J. Kreuzer. Adsorption forces on a single polymer molecule in contact with a solid surface. *Europhysics Letters*, 69(2):242–248, jan 2005.

[33] G.J. Fleer, M.A. Cohen Stuart, J.M.H.M Scheutjens, T. Cosgrove, and B. Vincent. *Polymers at Interfaces.* Chapman and Hall, London, 1993.

[34] Karl F. Freed. *Renormalization Group Theory of Macromolecules.* Wiley, New York, 1987.

[35] A. A. Gorbunov and A. M. Skvortsov. Adsorbed chain-stretched coil: An unusual phase transition. *The Journal of Chemical Physics*, 98(7):5961–5970, 1993.

[36] A. A. Gorbunov, A. M. Skvortsov, J. van Male, and G. J. Fleer. Mapping of continuum and lattice models for describing the adsorption of an ideal chain anchored to a planar surface. *The Journal of Chemical Physics*, 114(12):5366–5375, 2001.

[37] P. Grassberger. Simulations of grafted polymers in a good solvent. *Journal of Physics A: Mathematical and General*, 38(2):323–331, 2005.

[38] S. C. Greer. Reversible polymerizations and aggregations. *Annual Review of Physical Chemistry*, 53(1):173–200, 2002. PMID: 11972006.

[39] A. Yu. Grosberg and A.R. Khokhlov. *Statistical Physics of Macromolecules*. AIP Press, New York, 1994.

[40] A. Yu. Grosberg and E. I. Shakhnovich. Theory of phase transitions of the coil-globule type in a het- eropolymer chain with disordered sequence of links. *Sov. Phys. JETP*, 1986.

[41] H. G. Hansma. Atomic force microscopy of biomolecules. volume 14, pages 1390–1394. AVS, 1996.

[42] B. J. Haupt, J. Ennis, and E. M. Sevick. The detachment of a polymer chain from a weakly adsorbing surface using an afm tip. *Langmuir*, 15(11):3886–3892, 1999.

[43] R. Hegger and P. Grassberger. Chain polymers near an adsorbing surface. *Journal of Physics A: Mathematical and General*, 27(12):4069–4081, 1994.

[44] C. A. J. Hoeve, E. A. DiMarzio, and P. Peyser. Adsorption of polymer molecules at low surface coverage. *The Journal of Chemical Physics*, 42(7):2558–2563, 1965.

[45] H. Kikuchi, N. Yokoyama, and T. Kajiyama. Direct measurements of stretching force-chain ends elongation relationships of a single polystyrene chain in dilute solution. *Chemistry Letters*, 26(11):1107–1108, 1997.

[46] S. M. King and T. Cosgrove. A dynamical monte carlo model of polymer adsorption. *Macromolecules*, 26(20):5414–5422, 1993.

[47] A. Kishino and T. Yanagida. FORCE MEASUREMENTS BY MICROMANIPULATION OF A SINGLE ACTIN FILAMENT BY GLASS NEEDLES. *Nature*, 334(6177):74–76, JUL 7 1988.

[48] L. I. Klushin, A. M. Skvortsov, and F. A. M. Leermakers. Partition function, metastability, and kinetics of the escape transition for an ideal chain. *Phys. Rev. E*, 69(6):061101, Jun 2004.

[49] K. Konstadinidis, S. Prager, and M. Tirrell. Monte carlo simulation of irreversible polymer adsorption: Single chains. *The Journal of Chemical Physics*, 97(10):7777–7780, 1992.

[50] J. Krawczyk, T. Prellberg, A. L. Owczarek, and A. Rechnitzer. Stretching of a chain polymer adsorbed at a surface. *Journal of Statistical Mechanics: Theory and Experiment*, 2004(10):P10004, 2004.

[51] T. Kreer, S. Metzger, M. Müller, K. Binder, and J. Baschnagel. Static properties of end-tethered polymers in good solution: A comparison between different models. *The Journal of Chemical Physics*, 120(8):4012–4023, 2004.

[52] M. LAL. Monte carlo computer simulation of chain molecules .i. *Molecular physics*, 17(1):57–, 1969.

[53] D. P. Landau and K. Binder. *A Guide to Monte Carlo Simulations in Statistical Physics*. Cambridge University Press, Cambridge, 2000.

[54] J. C. Le Guillou and J. Zinn-Justin. Critical exponents for the n-vector model in three dimensions from field theory. *Phys. Rev. Lett.*, 39(2):95–98, Jul 1977.

[55] D. Marenduzzo, A. Trovato, and A. Maritan. Phase diagram of force-induced dna unzipping in exactly solvable models. *Phys. Rev. E*, 64(3):031901, Aug 2001.

[56] H. Meirovitch and S. Livne. Computer simulation of long polymers adsorbed on a surface. ii. critical behavior of a single self-avoiding walk. *The Journal of Chemical Physics*, 88(7):4507–4515, 1988.

[57] S. Metzger, M. Mller, K. Binder, and J. Baschnagel. Adsorption transition of a polymer chain at a weakly attractive surface: Monte carlo simulation of off-lattice models. *Macromolecular Theory and Simulations*, 11(9):985–995, 2002.

[58] A. Milchev and K. Binder. Static and dynamic properties of adsorbed chains at surfaces: Monte carlo simulation of a bead-spring model. *Macromolecules*, 29(1):343–354, 1996.

[59] A. Milchev, V. Yamakov, and K. Binder. Escape transition of a polymer chain: Phenomenological theory and monte carlo simulations. *Physical Chemistry Chemical Physics*, 1:2083 – 2091, 1999.

[60] M. S. Moghaddam. A monte carlo study of adsorption of random copolymers on random surfaces. *Journal of Physics A: Mathematical and General*, 36(4):939–949, 2003.

[61] M. S. Moghaddam and S. G. Whittington. A monte carlo study of polymer adsorption: random copolymers and random surfaces. *Journal of Physics A: Mathematical and General*, 35(1):33–42, 2002.

[62] E. A. Mukamel and E. I. Shakhnovich. Phase diagram for unzipping dna with long-range interactions. *Phys. Rev. E*, 66(3):032901, Sep 2002.

[63] D.H. Napper. *Polymeric stabilization of colloidal dispersions.* Academic Press, London, 1989.

[64] G. Odian. *Principles of Polymerization.* Wiley, New York, 1981.

[65] E. Orlandini, S. M. Bhattacharjee, D. Marenduzzo, A. Maritan, and F. Seno. Mechanical denaturation of dna: existence of a low-temperature denaturation. *Journal of Physics A: Mathematical and General*, 34(50):L751–L758, 2001.

[66] B. O'Shaughnessy and D. Vavylonis. Non-equilibrium in adsorbed polymer layers. *Journal of Physics: Condensed Matter*, 17(2):R63–R99, 2005.

[67] P. K. Mishra, S. Kumar, and Y. Singh. Force-induced desorption of a linear polymer chain adsorbed on an attractive surface. *Europhysics Letters*, 69(1):102–108, jan 2005.

[68] D. Poland and H. A. Scheraga. Phase transitions in one dimension and the helix—coil transition in polyamino acids. *The Journal of Chemical Physics*, 45(5):1456–1463, 1966.

[69] A. Polotsky, F. Schmid, and A. Degenhard. Polymer adsorption onto random planar surfaces: Interplay of polymer and surface correlations. *The Journal of Chemical Physics*, 121(10):4853–4864, 2004.

[70] A. L. Ponomarev, T. D. Sewell, and C. J. Durning. Adsorption of isolated, flexible polymers onto a strongly attracting surface. *Macromolecules*, 33(7):2662–2669, 2000.

[71] M. Rief, F. Oesterhelt, B. Heymann, and H. E. Gaub. Single Molecule Force Spectroscopy on Polysaccharides by Atomic Force Microscopy. *Science*, 275(5304):1295–1297, 1997.

[72] M. Rubinstein and R.H. Colby. *Polymer Physics.* Oxford University Press, Oxford, 1986.

[73] J.A. Rudnick and G.D. Gaspari. *Elements of the random walk: an introduction for advanced students and researchers.* Cambridge University Press, Cambridge, 2004.

[74] T. Sakaue. Nonequilibrium dynamics of polymer translocation and straightening. *Physical Review E (Statistical, Nonlinear, and Soft Matter Physics)*, 76(2):021803, 2007.

[75] I. Sanchez. *Physics of polymer surfaces and interfaces.* Butterwort-Heinemann, Boston, 1992.

[76] J. Michael Schurr and Steven B. Smith. Theory for the extension of a linear polyelectrolyte attached at one end in an electric field. *Biopolymers*, 29(8-9):1161–1165, 1990.

[77] J. S. Shaffer. Computer simulation of homopolymer and copolymer adsorption dynamics. *Macromolecules*, 27(11):2987–2995, 1994.

[78] Y.-J. Sheng, P.-Y. Lai, and H.-K. Tsao. Nonequilibrium relaxation of a stretched polymer chain. *Phys. Rev. E*, 56(2):1900–1909, Aug 1997.

[79] A. M. Skvortsov, A. A. Gorbunov, and L. I. Klushin. Adsorption-stretching analogy for a polymer chain on a plane. symmetry property of the phase diagram. *The Journal of Chemical Physics*, 100(3):2325–2334, 1994.

[80] A. M. Skvortsov, A. A. Gorbunov, and L. I. Klushin. Adsorption-stretching analogy for a polymer chain on a plane. symmetry property of the phase diagram. *The Journal of Chemical Physics*, 100(3):2325–2334, 1994.

[81] A.M. Skvortsov, L. I. Klushin, and T. M. Birshtein. *Polymer Science A (Moscow)*, 2009 (in press).

[82] S. B. Smith, Y. Cui, and C. Bustamante. Overstretching B-DNA: The Elastic Response of Individual Double-Stranded and Single-Stranded DNA Molecules. *Science*, 271(5250):795–799, 1996.

[83] C. E. Soteros and S. G. Whittington. The statistical mechanics of random copolymers. *Journal of Physics A: Mathematical and General*, 37(41):R279–R325, 2004.

[84] T. Strick, J.-F. Allemand, V. Croquette, and D. Bensimon. The manipulation of single biomolecules. *Physics Today*, 54(10):46–51, 2001.

[85] G. Subramanian, D. R. M. Williams, and P. A. Pincus. Escape transitions and force laws for compressed polymer mushrooms. *EPL (Europhysics Letters)*, 29(4):285–290, 1995.

[86] G. Subramanian, D. R. M. Williams, and P. A. Pincus. Interaction between finite-sized particles and end grafted polymers. *Macromolecules*, 29(11):4045–4050, 1996.

[87] K. Sumithra and A. Baumgaertner. Adsorption of random copolymers: A scaling analysis. *The Journal of Chemical Physics*, 110(5):2727–2731, 1999.

[88] K. Svoboda and S. M. Block. Biological applications of optical forces. *Annual Review of Biophysics and Biomolecular Structure*, 23(1):247–285, 1994. PMID: 7919782.

[89] N.G. van Kampen. *Stochastic Processes in Physics and Chemistry*. North - Holland, Amsterdam, 1992.

[90] C. Vanderzande. *Lattice Models of Polymers*. Cambridge University Press, Cambridge, 1998.

[91] F. T. Wall, L. A. Hiller Jr., and D. J. Wheeler. Statistical computation of mean dimensions of macromolecules. i. *The Journal of Chemical Physics*, 22(6):1036–1041, 1954.

[92] T. A. Weber and E. Helfand. Molecular dynamics simulation of polymers. i. structure. *The Journal of Chemical Physics*, 71(11):4760–4762, 1979.

[93] M. Wittkop, J.-U. Sommer, S. Kreitmeier, and D. Göritz. Monte carlo simulations of a single polymer chain under an external force in two and three dimensions. *Phys. Rev. E*, 49(6):5472–5476, Jun 1994.

[94] Y. Kafri, D. Mukamel, and L. Peliti. Melting and unzipping of dna. *The European Physical Journal B*, 27(1):135–146, May 2002.

[95] J. D. Ziebarth, Y. Wang, A. Polotsky, and M. Luo. Dependence of the critical adsorption point on surface and sequence disorders for self-avoiding walks interacting with a planar surface. *Macromolecules*, 40(9):3498–3504, 2007.